Experimental Verification for the Design of a Doubly-fed Permanent Magnet Generator

by

Bin Lu

B.S., Tsinghua University (July 2006)

Submitted to the Department of Electrical Engineering and Computer Science in partial
fulfillment of the requirements for the degree of

Master of Science

At the

MASSACHUSETTS INSTITUTE OF TECHNOLOGY

September 2007

Author…………………………………………………………………………………………
Department of Electrical Engineering and Computer Science
August 31, 2007

Certified by………………………………………………………………………………….
Professor James L. Kirtley Jr.
Professor of Electrical Engineering
Thesis Supervisor

Accepted by…………………………………………………………………………………...
Terry P. Orlando
Chairman, Department Committee on Graduate Students

Experimental Verification for the Design of a Doubly-fed Permanent Magnet Generator

By
Bin Lu

Submitted to the Department of Electrical Engineering and Computer Science
On August 31, 2007, in partial fulfillment of the
requirements for the degree of
Master of Science

Abstract

This is a continuous work on the project of a doubly-fed permanent magnet (DFPM) generator for wind turbines. The construction of a prototype machine was finally finished and experiments were conducted to verify the design of the DFPM machine and to establish a basis for designing more powerful machines in industry usage.

In the thesis, a finite element model of the machine is established, from which the parameters of the prototype machine are estimated. Then the experiment data are compared with the estimated values to verify the model of the machine. At last a vector control method is proposed with the stability analysis using the parameters developed from the model. Moreover, the damping effect of the permanent magnet (PM) rotor plate is explored.

Keywords: doubly-fed induction, permanent magnet, finite element, open circuit, v-curve, damping coil, vector control, sensorless.

Thesis Supervisor: James L. Kirtley, Jr.
Title: Professor of Electrical Engineering

Acknowledgement

I would like to thank Professor Kirtley for his supervision on the project. I gained invaluable experience from his ways of solving problems and hands on skills. I would also like to thank technician Wayne Ryan and senior undergraduate student Matt Angle for their help of the construction of the prototype machine. I am grateful to the lab secretary Vivian Mizuno, who gave me lot of assistant and encouragement in the lab. I would also like to express my gratitude to Professor Dave Perreault and Professor Steve Leeb who provided many advices and support during the process of the exepriement. Finally, thanks to fellow graduate students Steve Englebretson, Yehui Han, Anthony Sagneri, Juan Rivas and many other graduate students in the Laboratory for Electromagnetic and Electronic System (LEES) for their support of my experiment.

Contents

List of Figures

List of Tables

Chapter 1

1 Introduction

1.1 Motivation

Wind energy is clean, renewable and widely distributed. In the recent years the global wind energy market is experiencing a rapid growth from 59,091 MW in 2005 up to 74,233 MW in 2006, according to the report from the Global Wind Energy Council. This rapid growth drives researchers to improve the efficiency and lower the costs of the wind energy production.

Variable speed operation is preferable for winding turbine systems, for maximizing the energy capture from the wind [1]. There are several different configurations that have been used [2], among which the system of variable-speed doubly-fed induction generator combined with pitch control is superior for large turbines where the output power is more than 1MW. This system has many advantages with reduced costs and improved efficiency [3].

Professor Kirtley proposed a novel Doubly-fed Permanent Magnet generator for wind turbines, which is an enhancement of TORUS generator [4]. In the design of this generator, the TORUS basic geometry is kept with two more rotors mounted to the generator's main shaft outside of the permanent magnet rotors which are designed to rotate freely on the main shaft. Figure 1.1 shows the structure of the generator.

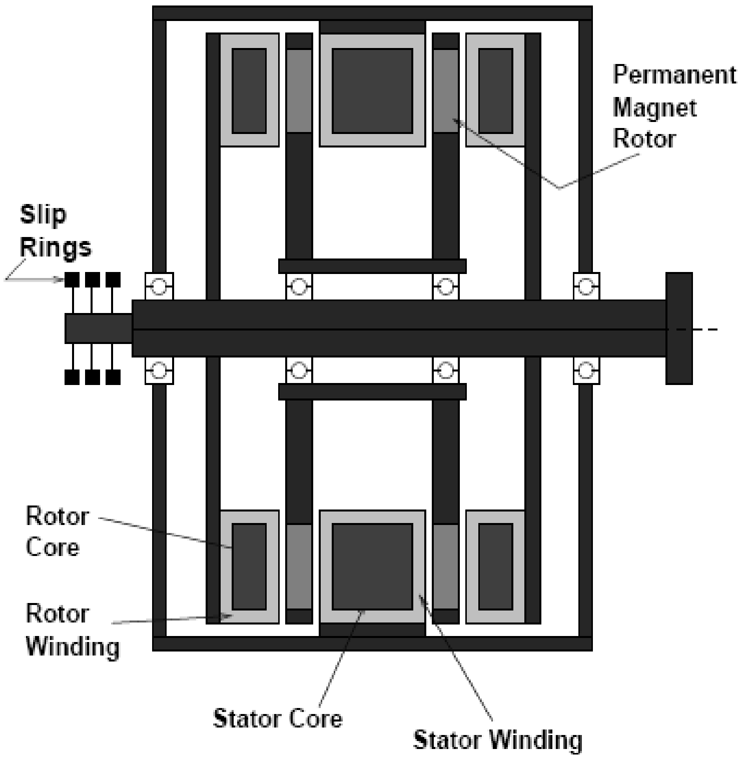

Figure 1.1 Schematic illustration of Doubly-fed Permanent Magnet generator

The concept of this design is to incorporate the merits of the TORUS generator into the doubly-fed induction generator (DFIG). High air-gap magnetic axial flux density is achieved using Neodymium-Iron-Boron for the magnets to employ a large air gap and a small number of winding turns to generate the required EMF with reduced winding weight, resistances and inductance. The slotless windings also make the generator easy to manufacture. Thus, we present a cost effective, compact generator for variable speed wind turbines.

1.2 Thesis organization

Chapter 2 describes the remaining the prototype machine construction work including a new case and system resonant frequency tuning with potential mechanical problems of the prototype. Chapter 3 establishes a finite element model of the machine and estimates the parameters of the machine. Chapter 4 presents the experiment results with comparison to the estimated values from Chapter 3. Chapter 5 develops a vector control scheme for the machine and analyzes its stability. Chapter 6 is a conclusion and a recommendation to the future work.

Chapter 2

2 Machine Construction

After a large amount of efforts of previous graduate students Andrew Thomas and Sivananda Reddy, a 10kW prototype machine was built in LEES. However, the prototype experienced a severe vibration [6] and was only able to run at most one third of the rating speed. Therefore, the experimental verification of the new design of the machine was unable to be performed until these mechanical problems were overcome. It was suspected that the rotors were not balanced well so the prototype machine was disassembled and the rotors were shipped to a factory to be balanced again. Moreover a new housing was manufactured for the prototype.

2.1 New housing

An aluminum cylinder case is manufactured to replace the old skeleton frame which provides extra stiffness for the system. The drawing of the new housing is shown in Figure A.1 and Figure A.2. The new housing is actually a revision of the original housing in Andrew Thomas's thesis [5], but has a larger diameter so that it can accommodate the power rotor end turns. The space between the housing cylinder and the stator mounting ring provides space for the transverse turns between coils of the stator winding.

2.2 Assembly

The stator is bolted in the center of the housing by 20 pairs of evenly spaced socked-head screws with 20 aluminum blocks in between the housing cylinder wall and the stator mounting ring.

Due to the new housing, it becomes more difficult to deal with the extreme strong magnetic force during assembly to place the PM rotor into position in a controlled manner. This was done by three screw-jacks lowering the PM rotors one by one down to the stator from the either side of the housing. 10 plastic spacers, each about 3mm thick, were inserted from the 10 slots around the housing body into keep the air gap between the

PM rotor and the stator. However, they didn't work in practical. The PM rotor always got stuck to the surface of the stator.

Positioning of the two pair of rotors with respect to the stator is by two pieces of steel sleeves which sit on either ends of the shaft between the power rotor and the end plate bearing. However, the length of the sleeves is tricky. Oversized sleeves were used, which can then produce enough pressure to keep the PM rotor from sticking to the stator.

The same test bed [6] was used to mount the machine. Before any run of the machine, it is very important to tune the resonant frequency of the test bed system so that in the entire speed range of the machine, there cannot be any resonant frequency. There are mainly three points to be considered. First, the larger the spring constant of the main rails where the machine is mount onto, the higher the resonant frequency. To increase the stiffness, two more short steel bars are attached to the main rails; Second, the mass center of the machine is also important. Because the machine is mounted on the rails off the solid drive bed, the closer the machine to the bed, the higher the resonant frequency. This can be adjusted by the turnbuckles at the corners of the machine. Tightening the turnbuckle at the back of the machine will move the mass center towards the solid base of the drive and the transmission belt loosened. Third, the transmission belt is the most important part. It was found that the periodic unbalanced force is mainly from the transmission belt. It is suspected that the belt is not uniform and may be stretched so that the belt slips on the sheaves every revolution until the belt is tight enough. This is adjusted by the turnbuckles. Originally, there are only three turnbuckles at three corners of the machine. A forth one was mounted at the fringe of the housing and to the solid drive bed. By the above configuration and tuning, the mounting system is now very firm and there is no resonant observed during the entire speed range of the prototype machine.

2.3 Remaining problem

Although the prototype can now run stably at the rating speed, 360RPM, there are several potential problems that were spotted during the assembly and for the long time run, these problems should be eliminated.

First, it is observed that when positioning the rotors, the PM rotor constantly skewed and got stuck to the stator. This is probably due to the fact that the end bearing cap is about 3mm larger than the bearing in diameter so that whenever an unbalanced force is experienced by the PM rotor, the bearing will shift in the cap causing the shaft skew. Moreover, it is also suspected that the stator may be not well centered in the housing and may also a little skew. Besides, it is also possible that the end plates are not well aligned to each other.

Second, there is a short point found in phase A of the stator winding. The spot of the shortage was determined by measuring the potential distribution on the housing and the stator ring when DC current was injected to the body of the machine. Luckily enough, the shortage is at the edge of the stator ring close to the stator output terminals and can be reached from one of the slots in the housing. This shortage was fixed temporarily with tapes making insulation at the contact point. But it is highly recommended that all the wires should be taped again when there is opportunity to disassembly the prototype.

At last, because the belt is a main source of the vibration, A shorter belt of high quality is desirable.

Chapter 3

3 Machine modeling and parameters derivation

3.1 Magnetic flux density distribution of Permanent Magnets

There are 20 permanent magnets for either of the PM rotors. The dimension of the trapezoidal shape permanent magnet is shown in the Firgure 3.1, producing axial magnetic flux.

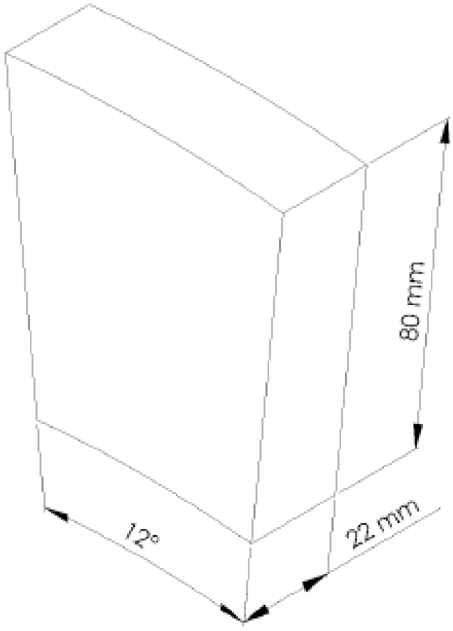

Figure 3.1 Dimension of permanent magnet

At a distance of 270mm from the center of the PM rotor plate, there are 20 evenly spaced pockets for the 20 permanent magnets. Therefore, the shorter side of the permanent magnet is about $\frac{12\pi}{180}\times 270=56.55mm$ wide and the longer side is about $\frac{12\pi}{180}\times 350=73.3mm$. The distribution of the residual magnetic field of the permanent magnets is shown in Figure 3.2.

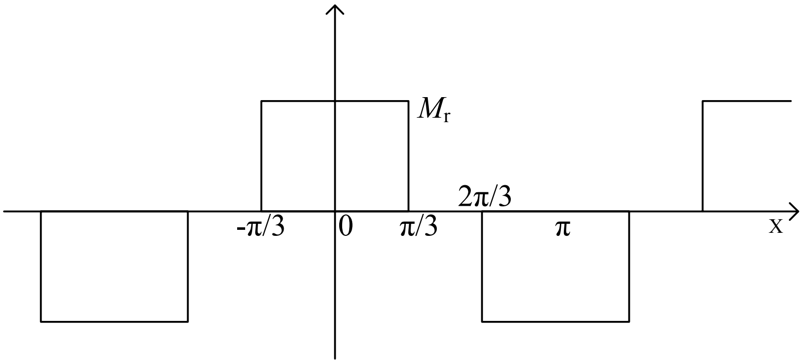

Figure 3.2 Residual flux density distribution of the PMs in electric angle

By Fourier series expansion, this wave form only has odd harmonics.

$$M_{2n+1} = \frac{2M_r}{\pi}\left(\int_0^{\pi/3} dx\cos(2n+1)x - \int_{2\pi/3}^{\pi} dx\cos(2n+1)x\right)$$
$$= \frac{2M_r}{\pi}\frac{\sin((2n+1)\pi/3)+\sin(2(2n+1)\pi/3)}{2n+1}$$

where n = 0, 1, 2, 3 …

If n = 3k, k = 0, 1, 2, 3…

$$M_{2n+1} = M_{6k+1} = \frac{2\sqrt{3}M_r}{\pi(6k+1)}$$

If n = 3k+1, k = 0,1,2,3…

$$M_{2n+1} = 0$$

If n = 3k+2, k = 0,1,2,3…

$$M_{2n+1} = M_{6k+5} = -\frac{2\sqrt{3}M_r}{\pi(6k+5)}$$

Only the 1, 7, 13, 19, … and 5, 11, 17, 23, … orders are not zero.

The first order amplitude is $M_1 = \frac{2\sqrt{3}}{\pi}M_r \approx 1.1M_r$.

The fifth order amplitude is $M_5 \approx -0.22M_r$.

The seventh order amplitude is $M_7 \approx 0.157M_r$.

3.1.1 Exact solution of the fundamental magnetic flux density

In the model of the machine, the change of the magnetic field in radial direction is compensation by taking the magnetic field at the middle of the inner and outer radius to be the average, which is at a distance of 310mm from the center of the PM rotor. The poles of the 20 magnets in the PM rotor alternates therefore have a wavelength of $310\times 2\pi/10=194.78mm$ and the total distance between the stator iron and power rotor iron core of the prototype is 59.87mm. The permanent magnet material is Neodymium-Iron-Boron, with residual flux density of B_r about 1.3T and recoil permeability of 1.05. Ignoring the radial dimension, the model is shown in Figure 3.3.

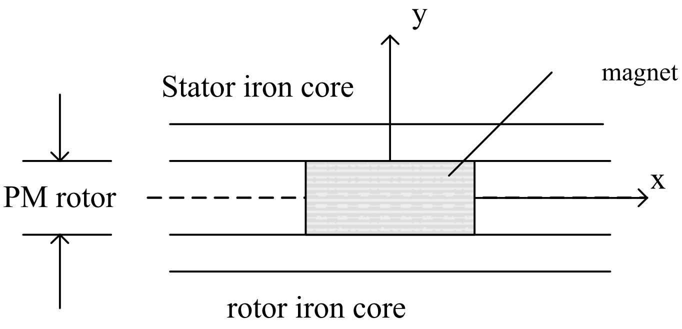

Figure 3.3 Schematic illustration of the model for FEM calculation

Establishing Equations

In the air gap, which is denoted by subscript 1, the magnetic field satisfies

$$\nabla\times H_1=0$$

Using scalar potential, then

$$H_1=-\nabla\varphi_1 .$$

Because $\nabla\bullet B_1=\nabla\bullet(\mu_0 H_1)=0$,

$$\nabla^2\varphi_1=0$$

In the area of PM rotor, which is denoted by subscript 2, the fundamental component is

$$\bar{M}=i_y 1.1 M_r\cos kx .$$

The magnetic field still satisfies $\nabla\times H_2=0$ and thus $H_2=-\nabla\varphi_2$.

From $\nabla \bullet B_2 = \mu \nabla \bullet (H_2 + M) = 0$,and $\nabla \bullet \overline{M} = 0$,

Then

$$\nabla^2 \varphi_2 = 0 .$$

Therefore, in the area of both PM and the air gap, magnetic scalar potential satisfies the Laplace's equations. The generic solution of Laplace's equation is

$$\varphi(x, y) = X(x)Y(y)$$

Where

$$X(x) = A \cos kx + B \sin kx$$

$$Y(y) = Ce^{ky} + De^{-ky}$$

Therefore, the magnetic field can be expressed.

$$H_x = -Y(y)\frac{dX(x)}{dx} = -Y(y)(-Ak \sin kx + Bk \cos kx),$$

$$H_y = -X(x)\frac{dY(y)}{dy} = -X(x)(Cke^{ky} - Dke^{-ky})$$

Because of symmetric geometry shown in Figure 3.3, at $x = 0$, $H_x(x = 0) = 0$, then

$$H_x = (Ce^{ky} + De^{-ky})k \sin kx$$

$$H_y = -(Ce^{ky} - De^{-ky})k \cos kx$$

(A is included in C and D)

Boundary Condition

At the surface of the stator iron core, where $y = 0.02994m$

$$H_{x1} = 0$$

$$\text{So, } H_{x1}(y = 0.029935) = (C_1 e^{ky} + D_1 e^{-ky})|_{y=0.029935}\, k \sin kx = 0$$

$$(C_1 e^{ky} + D_1 e^{-ky})|_{y=0.029935} = 0 \qquad \textbf{Equation 3.1}$$

At the center of PM rotor, where $y = 0$

$$H_{x2} = 0 .$$

$$Y_2(y = 0) = C_2 + D_2 = 0 \qquad \textbf{Equation 3.2}$$

At the interface of permanent magnet and air gap, where $y = 0.011m$, H_x and B_y are continuous.

$$H_{x1} = H_{x2},$$

$$B_{y1} = \mu_0 H_{y1} = B_{y2} = \mu(H_{y2} + M\cos kx)$$

Thus,

$$(C_1 e^{ky} + D_1 e^{-ky})\,|_{y=0.011} = (C_2 e^{ky} + D_2 e^{-ky})\,|_{y=0.011} \qquad \textbf{Equation 3.3}$$

$$(C_1 k e^{ky} - D_1 k e^{-ky})\,|_{y=0.011} = \mu_r (k(C_2 e^{ky} - D_2 e^{-ky})\,|_{y=0.011} + M) \qquad \textbf{Equation 3.4}$$

From Equation 3.1 to 3.4, we have

$$C_1 = -2.1023 \times 10^3,\ D_1 = 1.4503 \times 10^4$$

$$C_2 = 9.8983 \times 10^3,\ D_2 = -9.8983 \times 10^3$$

Therefore,

In the air gap:

$$B_{x1} = \mu_0 (C_1 e^{ky} + D_1 e^{-ky}) k \sin kx = (-0.0852 e^{ky} + 0.5879 e^{-ky}) \sin kx$$

$$B_{y1} = -\mu_0 k \cos kx (C_1 e^{ky} - D_1 e^{-ky}) = (0.0852 e^{ky} + 0.5879 e^{-ky}) \cos kx$$

In the area of PM rotor:

$$B_{x2} = \mu (C_2 e^{ky} + D_2 e^{-ky}) k \sin kx = 0.4213 (e^{ky} - e^{-ky}) \sin kx$$

$$\begin{aligned} B_{y2} &= -\mu k \cos kx (C_2 e^{ky} - D_2 e^{-ky}) + 1.1 B_r \cos kx \\ &= (1.43 - 0.4213 (e^{ky} + e^{-ky})) \cos kx \end{aligned}$$

The magnetic flux density at x = 0 is plotted in the Figure 3.4.

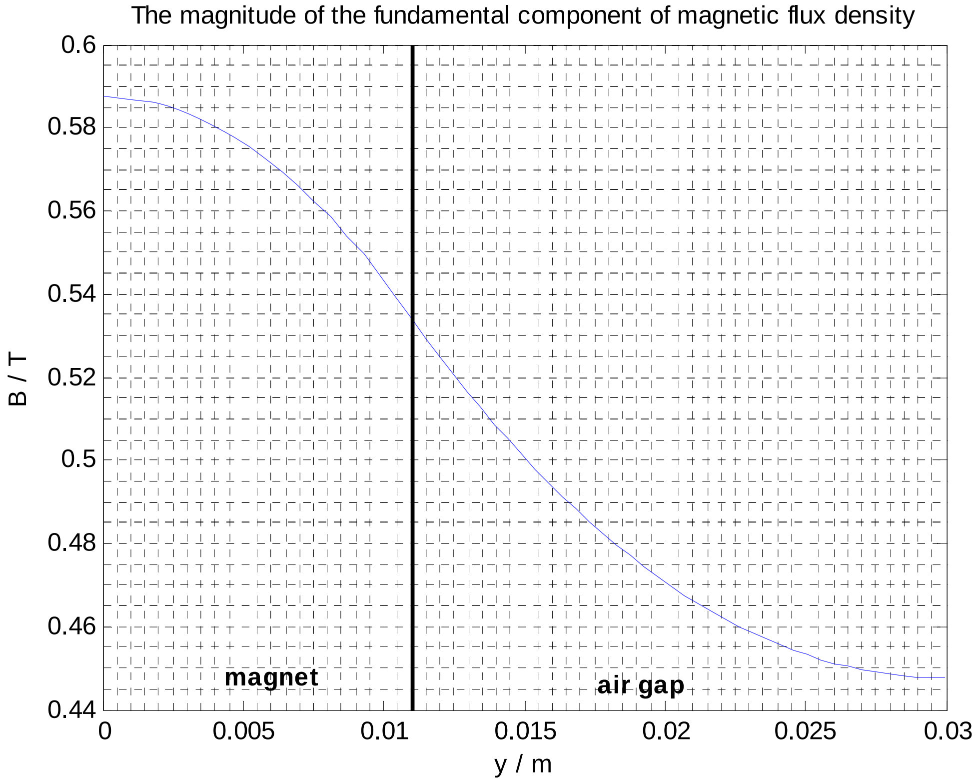

Figure 3.4Fundamental component of magnetic flux density at x = 0

From the exact solution, at the surface of stator iron core, the magnitude of the fundamental component of magnetic flux density is 0.4476T.

3.1.2 Solutions by finite element method (FEM)

For more complicated geometry, computer simulation using FEM is widely used to solve the PDEs. In the thesis, the MATLAB PDE toolbox is used to calculate the electromagnetic field. In this section, the FEM results are compared with the solutions of section 3.1.2 to examine the reliability of the FEM of the MATLAB PDE toolbox.

Establishing Equation

Using vector potential, $\overline{B} = \nabla \times A = i_x \dfrac{\partial A}{\partial y} - i_y \dfrac{\partial A}{\partial x}$

In the air gap, $\nabla \times H = 0$,

So, $\nabla \times H = \nabla \times \frac{1}{\mu_0} \nabla \times A = -\frac{1}{\mu_0} \nabla^2 A = 0$, where $\nabla \bullet A = 0$ is applied.

In the area of permanent magnet,

$$\nabla \times H = 0$$

$$B = \mu(H + M_r)$$

Considering the fundamental component of the residual flux density, we have

$$B = \mu(H + 1.1M_r \cos kx),$$

where wave vector is 32.258m^{-1}.

Therefore, $\frac{1}{\mu} \nabla \times \overline{B} = \nabla \times (i_y 1.1M_r \cos(kx)) = -i_z 1.1M_r k \sin(kx)$

Thus, in the magnet, $-\frac{1}{\mu} \nabla^2 A = -1.1M_r k \sin(kx)$.

Using the matlab PDE tool box to calculate the flux distribution, this is an elliptic problem with Neunmann boundary condition. Simulation result is shown in Figure 3.5.

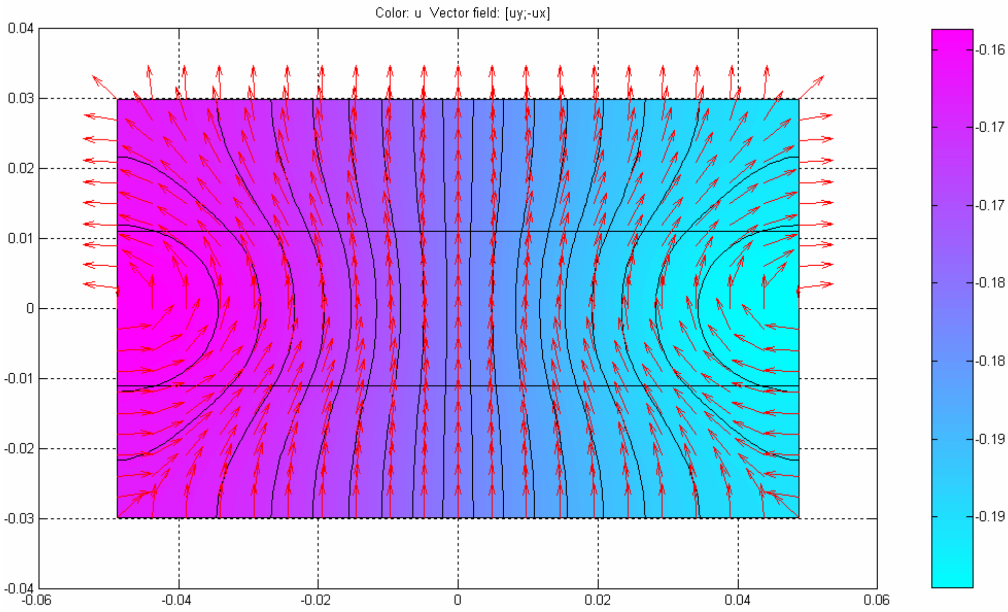

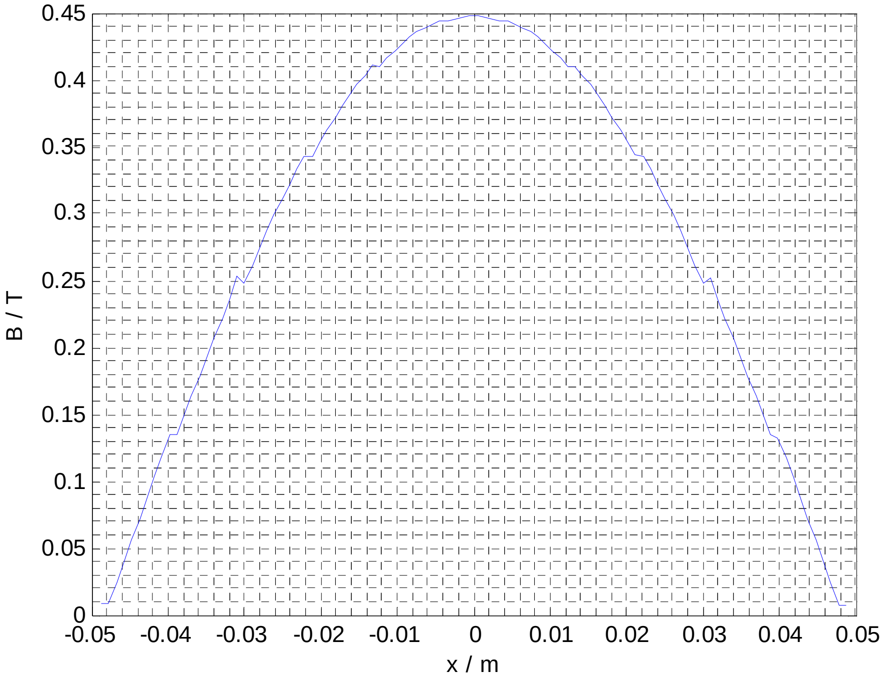

Figure 3.5 Fundamental magnetic field distribution (upper picture) and flux density distribution at the stator surface (lower picture)

From the simulation, the magnitude of fundamental flux density at the stator iron surface is 0.4476 tesla, which is equal to the result in Section 3.1.1. Note that the curve of the flux density distribution can be smoothened by refining the mesh for the FEM. The 5th order and 7th order magnetic flux density distribution are shown in Figure 3.6 and Figure 3.7. The magnitude of their flux density at the stator iron surface is 0.013T and 0.003T respectively.

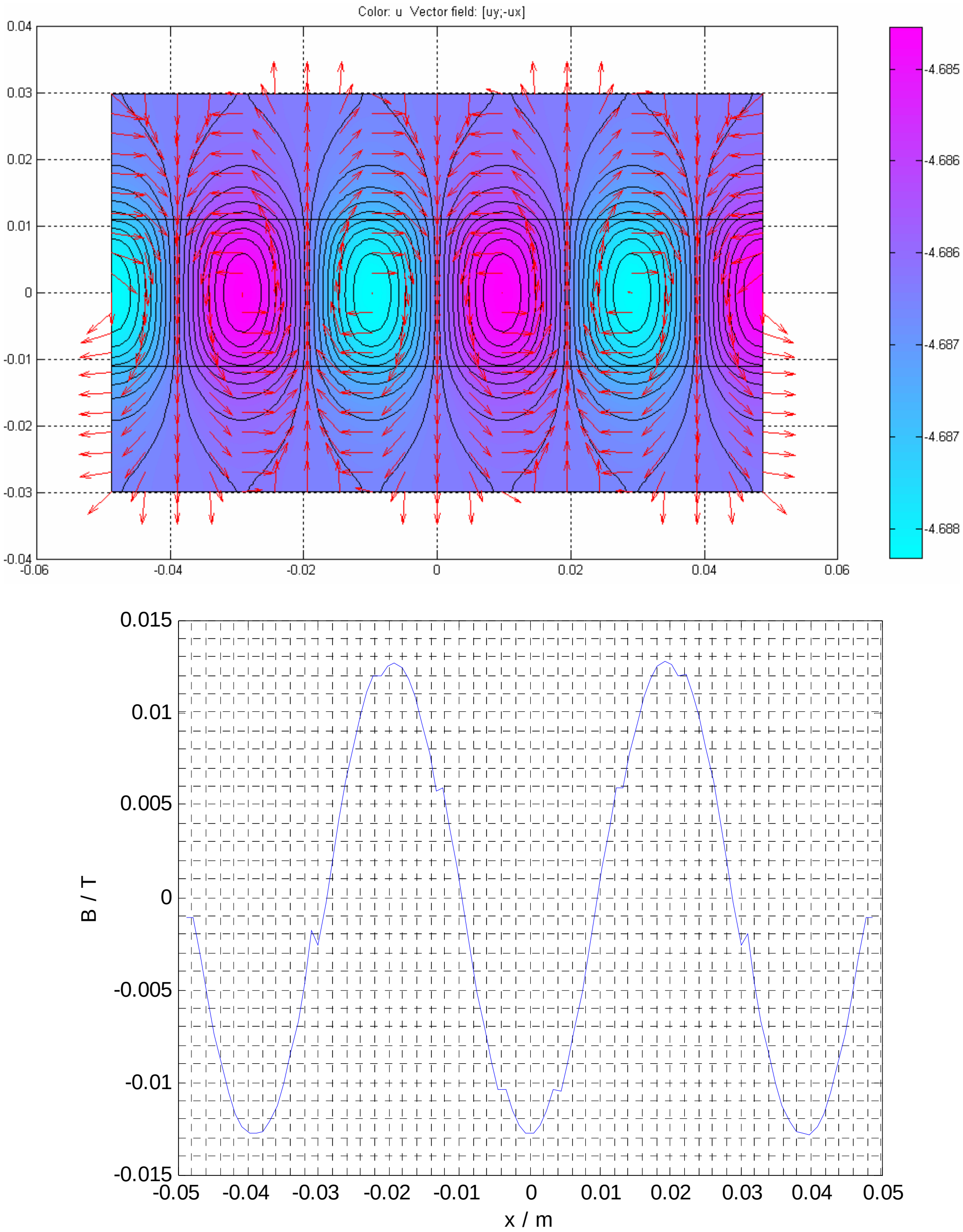

Figure 3.6 5th order magnetic field distribution (upper picture) and flux density distribution at the stator surface (low picture)

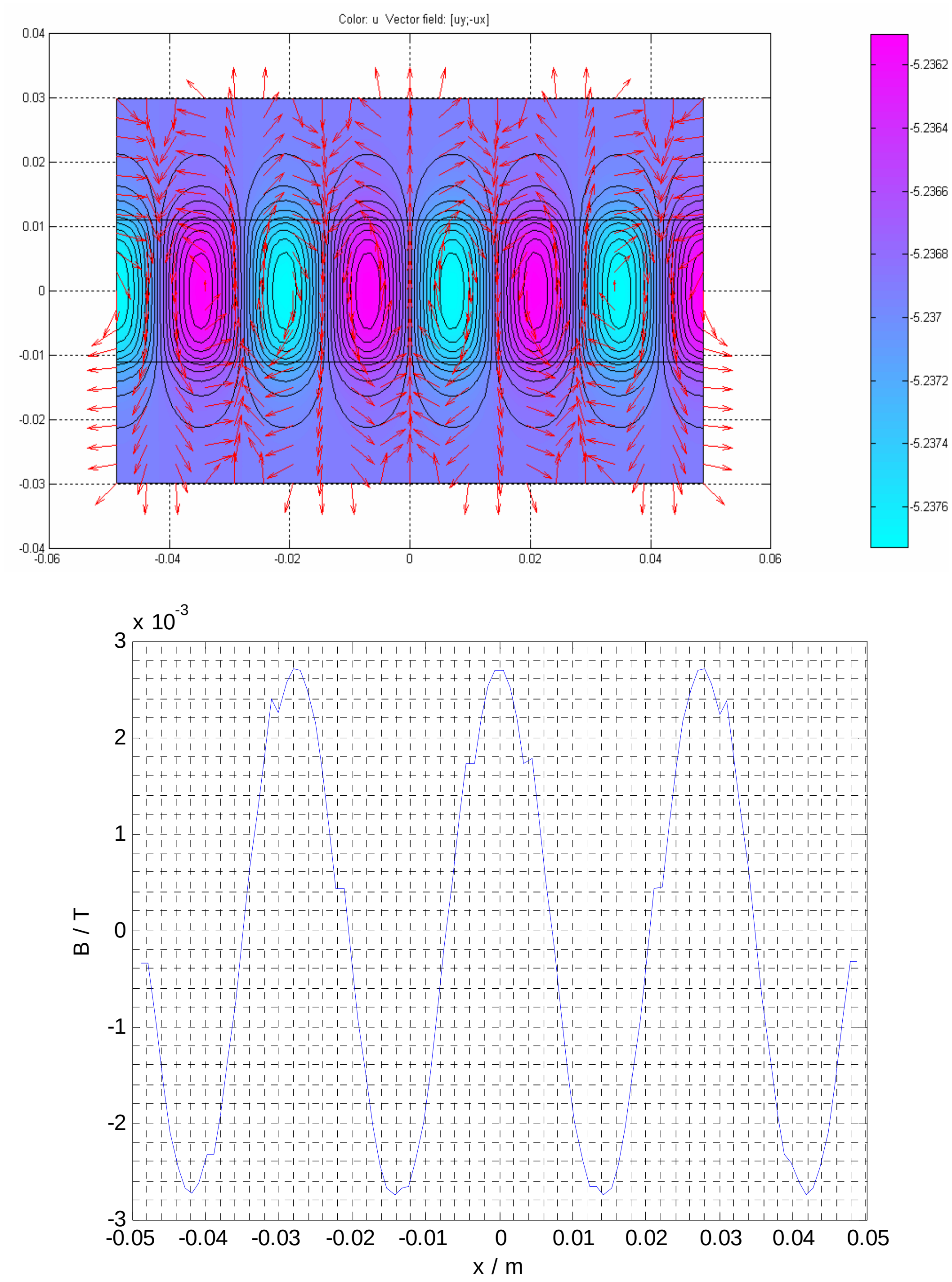

Figure 3.7 7th order magnetic field distribution (upper picture) and flux density distribution at the stator surface (lower picture)

Combining the 1st, 5th and 7th order components yields the flux density distribution at the stator iron surface shown in the Figure 3.8, which is rather flat between x = -0.01m and 0.01m.

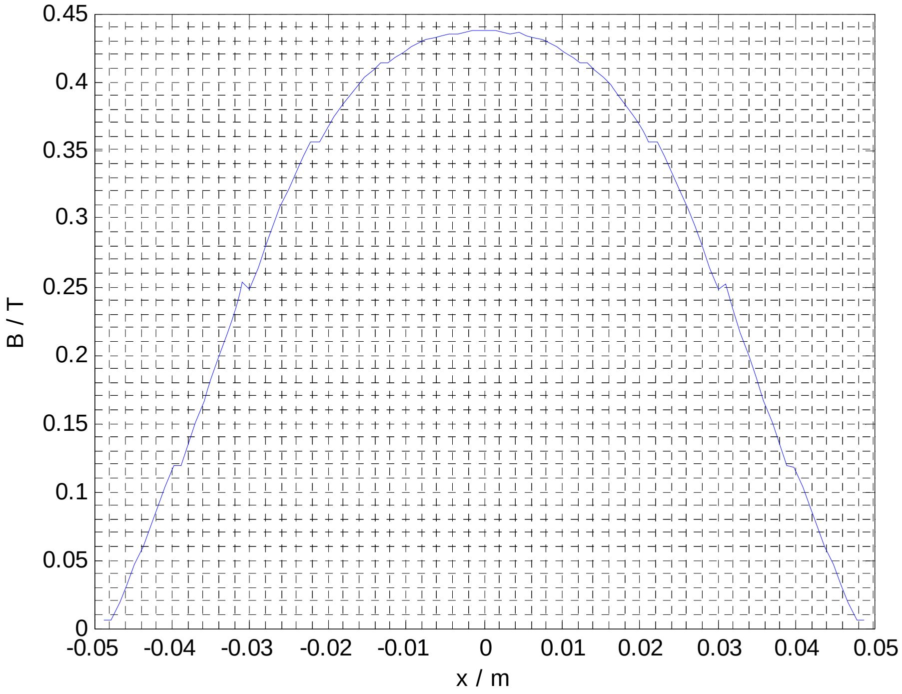

Figure 3.8 The combined 1st, 5th and 7th order magnetic flux density distribution at the stator iron surface

3.1.3 Estimation of stator internal voltage

Using the value of the fundamental magnetic flux density at the surface of the stator iron core, the internal voltage of the stator winding can be calculated, which is the stator open circuit voltage at the rating speed, 360RPM. The result is then compared with the experiment value in Section 4.1.

Stator winding factor

Stator winding has 20 coils for each phase. Each coil has 10 turns with 2 layers thick and 5 wide. The stator winding wire is composed of 7 strands of transposed #16.5 AWG litz wire, which is 5.3mm wide and 2.5mm thick. As shown in Figure 3.9, the electrical angle of each turn is $\theta_{ws} = \frac{5.3}{270} = 0.0196 rad = 1.12^0$.

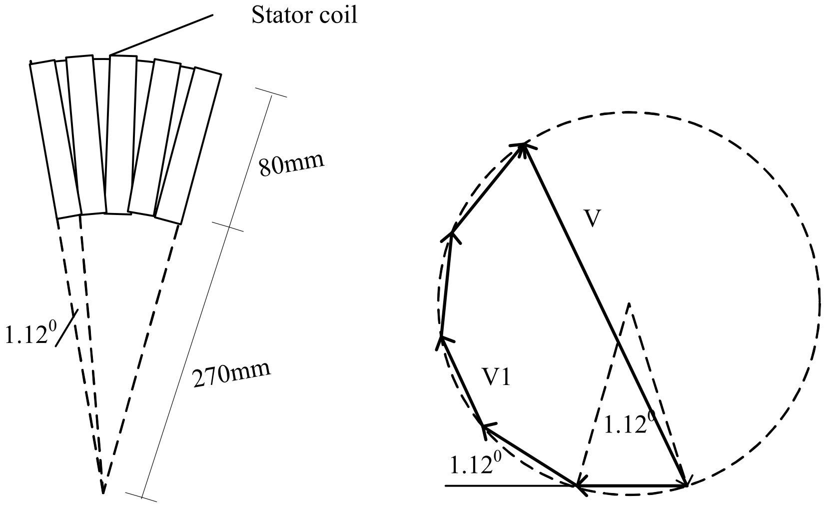

Figure 3.9 Stator winding angle and voltage phaser diagram

Therefore, the fundamental stator winding factor is

$$k_{\mathrm{ws1}} = \frac{\sin\frac{5p\theta_{ws}}{2}}{5\sin\frac{p\theta_{ws}}{2}} \approx 0.96$$

The 5th order and 7th order stator winding factor are

$$k_{\mathrm{ws5}} = \frac{\sin\dfrac{5p\theta_{ws}\times 5}{2}}{5\sin\dfrac{p\theta_{ws}\times 5}{2}} \approx 0.27$$

$$k_{\mathrm{ws7}} = \frac{\sin\dfrac{5p\theta_{ws}\times 7}{2}}{5\sin\dfrac{p\theta_{ws}\times 7}{2}} \approx -0.09$$

Then the amplitude of stator voltage of each phase is

$$V_n = Nk_{wsn}B_n l_m \omega(r_o + r_i)/2 \qquad \textbf{Equation 3.5}$$

Where l_m is the radial length of the magnet which is 80mm; r_o is outer radius of the magnet, 350mm, r_i is inner radius, 270mm; ω is the mechanical angular speed,12π; N is total turns which is 400 (Note that the stator winding has two sides).

Using the result in the Section 3.1.2, and taking account of the thickness of the stator winding (the average magnetic flux density through the thickness of the stator winding is about 0.45T), the result is shown in Table 3.1.

Table 3.1 Estimated stator open circuit voltage

	Voltage amplitude (V)	**RMS Voltage (V)**	**Stator winding factor**	**Flux density amplitude at stator surface (T)**
1st order component	161.6	114.2	0.96	0.446
5th order component	1.5	1.1	0.27	0.013
7th order component	0.12	0.08	-0.09	0.003

3.2 Stator winding

This section is to estimate the stator resistance and its self inductance at the synchronous state of the machine. The 60Hz subtransient inductance is also estimated in order to compare with the static experiment in Section 4.3, which is also helpful in understanding how the PM rotor plate affects the stator inductance.

3.2.1 Stator winding DC resistance

The stator winding has 20 coils per phase and 10 turns per coil with 2 layer thick and 5 turns wide. The wire bundle of the coil is composed of 7 transposed #16 ½ litz wire. Each wire bundle is about 2.5mm thick and 5.3mm wide. Therefore each coil is 5mm thick and 26.5mm wide. The stator coil is wounded around the iron core of 33mm thick.

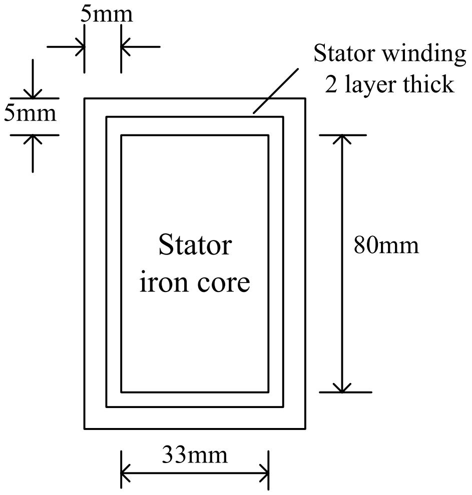

Figure 3.10 Cross section view of stator iron core and winding

As shown in Figure 3.10, the total length of the stator coil per phase is proximately $49.2m$. Because the resistance of #16 ½ AWG wire is about 0.014ohm/m, the estimated resistance of one phase of stator coil is about 0.1 ohm.

3.2.2 Stator inductance

The calculation of the stator winding inductance is separated by the inductance of the active winding and the inductance of the end turns. The active winding is the one of 80mm shown in Figure 3.10, interacting with the air gap flux. The end turns are the 33mm parts of the winding shown in Figure 3.10.

Inductance of the active winding

At steady state, the PM rotor is synchronous with the air gap flux so that there is no induced current in its aluminum plate. Therefore the PM rotor can be eliminated when calculating the synchronous inductance. Figure 3.11 is a cross section of the model for estimating the inductance of the active stator winding, containing one coil.

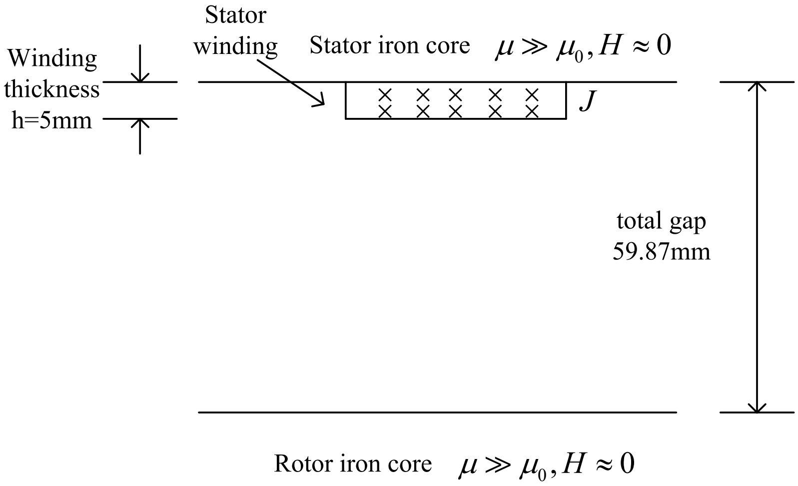

Figure 3.11 Stator inductance calculation model

The 20 coils of each phase are spaced evenly on the stator iron core with a period of 18 degrees. Applying the periodicity of the stator winding, the model in Figure 3.11 only is of half wavelength wide which is 97.39mm. The total gap between the stator iron and the power rotor iron is 59.87mm. As shown in Figure 3.9, the stator coil is 26.5mm wide at the inner radius of the stator iron core while 34.35mm at the outer radius. In the model the width of the coil is taken at the middle value, (26.5+34.35)/2 = 30.43mm. The thickness of the two layer coil is 5mm. The following is to establish the equations for the simulation.

Applying vector potential, then

$$\overline{B} = \nabla \times \overline{A} = i_x \frac{\partial A_z}{\partial y} - i_y \frac{\partial A_z}{\partial x} .$$

In the coil, $\nabla \times H = J$. Thus

$$-\frac{1}{\mu_0} \nabla^2 A = J \qquad \textbf{Equation 3.6}$$

In the air gap, $\nabla \times H = 0$. Thus

$$-\frac{1}{\mu_0}\nabla^2 A = 0$$ **Equation 3.7**

At the boundary of iron core, $H_x = 0$. So $B_x = \frac{\partial A_z}{\partial y} = 0$, which is the Neumann boundary condition. At the edge of the model, $H_x = 0$ due to the symmetric geometry. Thus $\frac{\partial A_z}{\partial y} = 0$ and A_z is constant at the two edges which is the Dirichlet boundary condition.

Because the inductance does not depend on the current in the coil, injecting 1A DC current in the coil as a trial current, the current density is thus 65724.6A/m^2. Then equation 3.6 and 3.7 can be solved using Matlab PDE toolbox. Figure 3.12 is the simulation result.

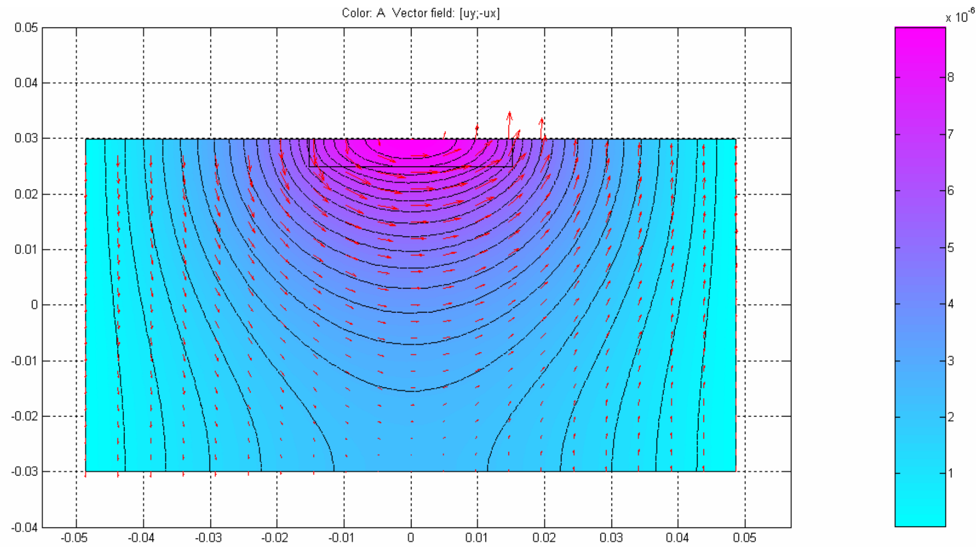

Figure 3.12 Magnetic field strength vector distribution by 1A DC current in the coil wire.

The inductance can be calculated by equation 3.8.

$$L = \frac{n\phi}{I} = \frac{n\iint \bar{B} \bullet d\bar{S}}{I} = \frac{n\oint \bar{A}_z \bullet d\bar{l}}{I}$$ **Equation 3.8**

In the problem, A_z is considered uniform along the length of the active winding. Therefore, the integration in equation 3.8 can be replaced by summation over the 10 turns of each coil. From the simulation, the estimated inductance for the stator active winding is 0.2566mH.

End turn inductance

The end turn inductance is from the wires wound around the outer and inner peripherals of the stator iron-core. The outer end turn faces the aluminum stator mounting ring and the housing which is different from inner end turn. The following is the calculation for the two parts of the end turn.

Outer end turn

The outer end turn is 350mm from the center of the stator. The diameter of the stator aluminum ring is 800mm and of 19.05mm thick. The diameter of housing is 889mm with 6.35mm thick. Each stator coil is 0.561 degree wide. Also because of the periodicity of the stator winding, the model is an 18 degree section with outer boundary at the infinity. However, the FEM can only calculate finite areas, so the outer boundary is set at the radius of 0.6m, which is far away enough for the vector potential to be zero. The model is shown in Figure 3.13. The following is to establish simulation equations.

Considering 60Hz AC current in the coil, $I = I_0 \sin \omega t$, In the region of stator coil

$$\nabla \times H = J + \varepsilon_0 \frac{\partial E}{\partial t}$$

$$\nabla \times E = -\mu_0 \frac{\partial H}{\partial t}$$

Because the frequency is very low, $\varepsilon_0 \frac{\partial E}{\partial t}$ can be ignored. Using vector potential, $\overline{B} = \nabla \times \overline{A} = i_x \frac{\partial A_z}{\partial y} - i_y \frac{\partial A_z}{\partial x}$, equation $\nabla \times H = J + \varepsilon_0 \frac{\partial E}{\partial t}$ can be rewritten as

$$-\frac{1}{\mu_0} \nabla^2 A = J \qquad \textbf{Equation 3.9}$$

In the air gap,

$$\nabla \times H = \varepsilon_0 \frac{\partial E}{\partial t}$$

$$\nabla \times E = -\mu_0 \frac{\partial H}{\partial t}$$

Applying vector potential, we have Laplace's equation

$$-\frac{1}{\mu_0}\nabla^2 A = 0 \qquad \textbf{Equation 3.10}$$

In the aluminum PM rotor plate,

$$\nabla \times H = \sigma E + \varepsilon_0 \frac{\partial E}{\partial t}$$

$$\nabla \times E = -\mu_0 \frac{\partial H}{\partial t}$$

Where σ is the conductivity of aluminum which is $37.8 \times 10^6 Sm^{-1}$. Applying vector potential to the pair of equations, we have

$$-\frac{1}{\mu_0}\nabla^2 A = \sigma E \qquad \textbf{Equation 3.11}$$

$$\nabla \times E = -\nabla \times \frac{\partial A}{\partial t} \qquad \textbf{Equation 3.12}$$

From Equation 3.12, $E = -\frac{\partial A}{\partial t}$. Applying it to Equation 3.11,

$$\sigma \frac{\partial A}{\partial t} - \frac{1}{\mu_0}\nabla^2 A = 0 \qquad \textbf{Equation 3.13}$$

By the separation of variables, one part in $e^{i\omega t}$, the parabolic Equation 3.13 can be written as

$$i\sigma\omega A - \frac{1}{\mu_0}\nabla^2 A = 0 \qquad \textbf{Equation 3.14}$$

Which is an elliptic equation.

Injecting 1A sinusoidal current into the coil as a trial current, the amplitude of current density is $5.822 \times 10^4 Am^{-2}$. At the surface of the iron core, it is Neumann boundary condition. At the other boundaries, it is the Dirichlet boundary condition. Figure 3.13 is the simulation result. It can be seen that the magnetic field is shielded by the aluminum stator mounting ring and the housing.

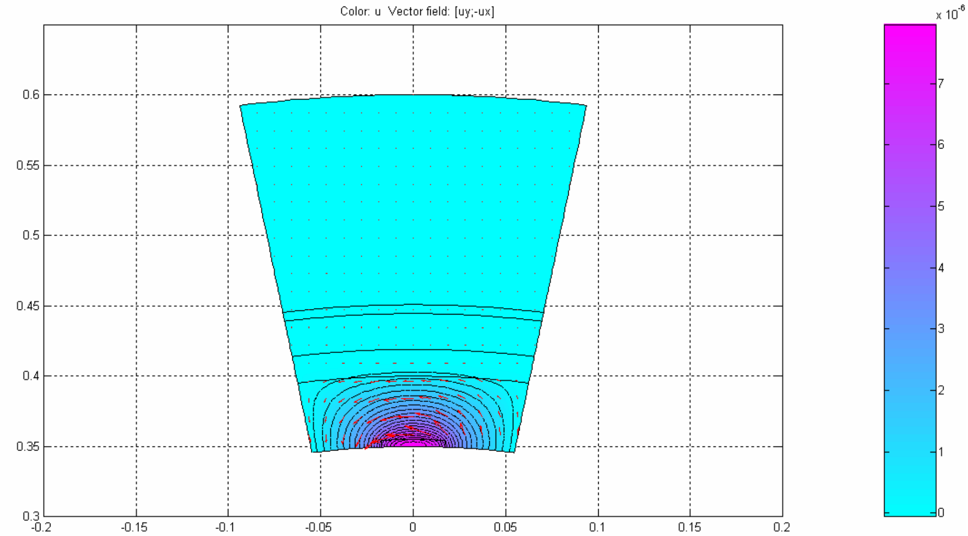

Figure 3.13 Plot of the real part of the magnetic field distribution for the model of the stator winding inductance of the outer end turn

By the equation $Z = \frac{j\omega\phi}{I}$, the impedance is $z = 0.0354 - j0.0009$ ohm. The end turn inductance for this wire is therefore $L \approx -2.4\mu H$, which is capacitive.

Inner end turn

The inner end turn is 270mm from the center of the stator iron core. The coil is also 0.561 degree wide. Figure 3.14 shows the simulation model of an 18 degree section. Injecting 1A DC current into stator coil as a trial current, the current density is $7.547 \times 10^4 A/m^2$. At the surface of the iron core, it is Neumann boundary condition. At the other boundaries, it is the Dirichlet boundary condition. The simulation result is shown in Figure 3.14.

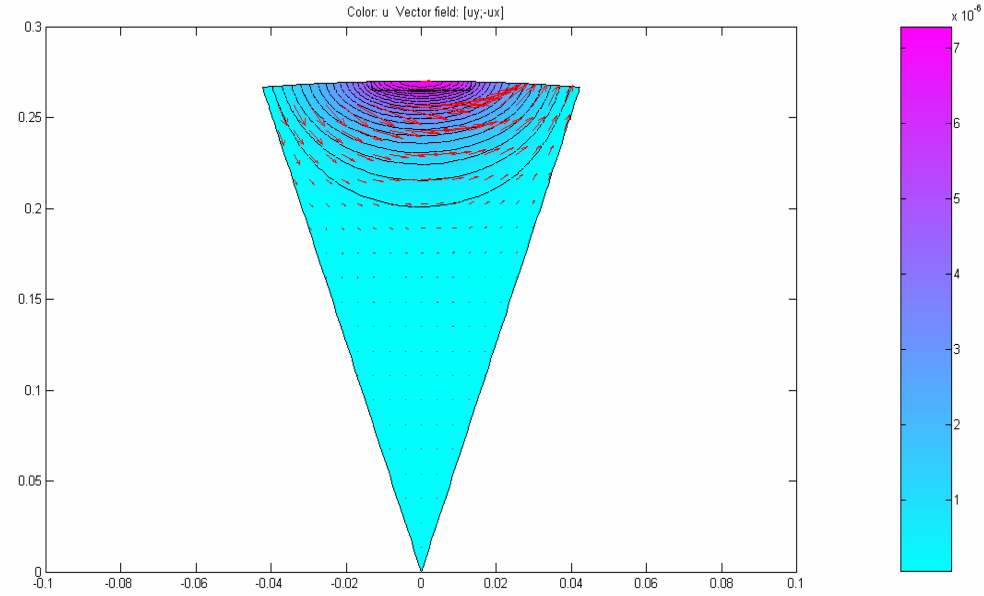

Figure 3.14 Plot of the real part of the magnetic field distribution for the model of the stator winding inductance of the inner end turn

By equation 3.8, the inner end turn inductance is 0.049mH. Therefore, the total end turn inductance is 0.047mH with a resistance of 0.035ohm.

3.2.3 Stator Subtransient inductance at 60Hz

When the PM rotor is not at the synchronous speed, the alternating current in the stator coil will induce current in the aluminum PM rotor plate which reacts with the stator winding. In this section, a model is established to simulate the situation that the PM rotor is at still while a 60Hz current is injected into the stator winding. It is to examine how the PM rotor plate reacts to the stator winding current the result of the simulation is compared with the static experiment in Section 4.4.

The simulation model is the same as in Section 3.2.2. Using 1A 60Hz current as the trial current, the current density in the coil is $6.572\times10^{4}\,A/m^{2}$. Figure 3.13 plots the real part of the magnetic field strength vector.

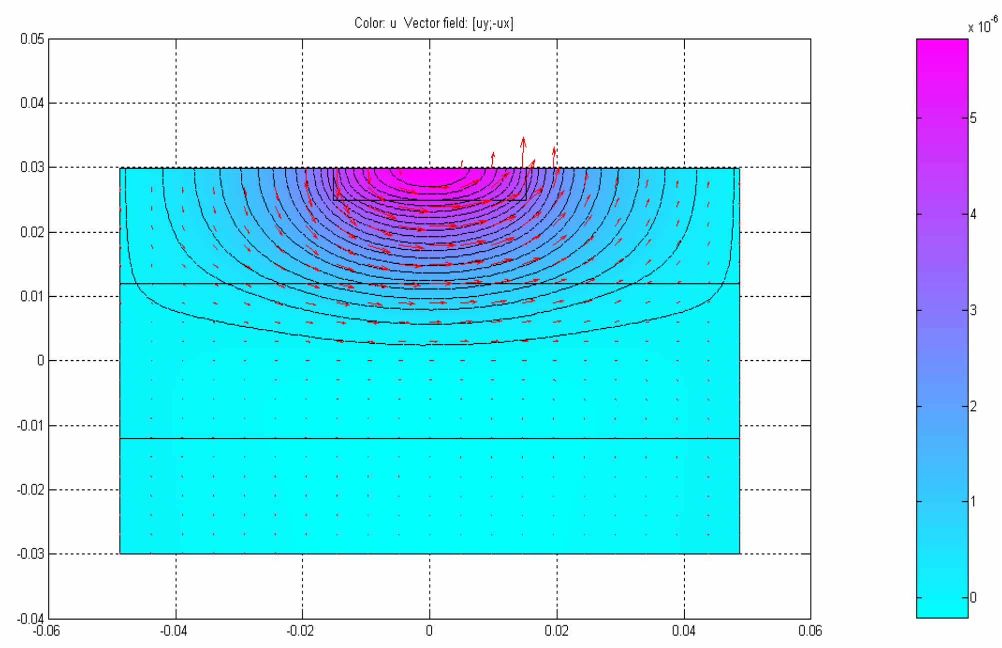

Figure 3.15 Plot of magnetic field distribution of the real part with coil current of 1A at 60Hz

From the simulation, the impedance of the active stator winding in this situation is $z = 0.00909 + j0.0609$ ohm. The inductance is therefore 0.162mH which is reduced compared with the result in Section 3.2.2.

3.2.4 Summary

Table 3.2 summarizes the estimated parameters of stator winding.

Table 3.2 Stator winding estimated parameters

Stator winding parameters

DC resistance	Active winding inductance	End turn winding inductance	End turn induced resistance
0.1ohm	0.257mH	0.047mH	0.035ohm

Total resistance:	0.135ohm
Total self-inductance:	0.304mH

At 60Hz subtransient condition:

Active winding inductance	Induced resistance
0.162mH	0.0609ohm

Total resistance	0.144ohm
Total self-inductance	0.209mH

3.3 rotor winding

This section estimates the resistance and inductance of rotor winding using the same method in Section 3.2. The simulation result in 60Hz subtransient condition is compared with the rotor static experiment in Section 4.3.

3.3.1 Rotor winding DC resistance

The power rotor winding has 20 coils per phase. Each coil is composed of 24-turn 16AWG wire, which is of 2-layer thick and 12-turn wide. Each coil is of the diamond shape, with the bending angle of 35 and 65 degrees at the inner and outer side respectively.

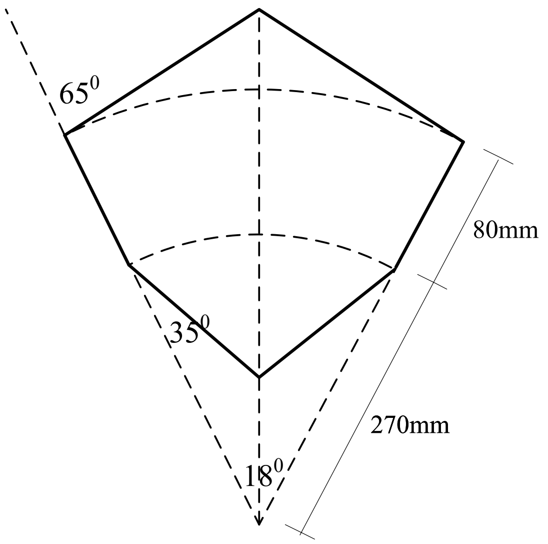

Figure 3.16 Shape of the power rotor coil

As shown in Figure 3.16, the total length of the 20 coils of each phase of the power rotor winding is about 198.57m. Because the #16 AWG wire has a resistance of 0.01318 ohms per unit meter, the estimated resistance of one phase stator coil is 2.6ohm.

3.3.2 Rotor inductance

Each rotor coil is 12 turn wide and 2 turn thick. Because the diameter of the #16 AWG wire is 1.291mm, the coil is 15.49mm wide and 2mm thick. The inductance of the rotor winding is also composed of two parts, the active winding and the end turns. The active winding is the 80mm long side of the coil and the end turn is the bent side of the coil, as shown in Figure 3.16

Inductance of the active side of rotor winding

As shown in Figure 3.17, every active side of the winding has two layers of coils. Therefore, the thickness of each active side is 5mm. For 1A current, the current density in the coil area is $6.198\times10^{5} A/m^{2}$. Using the same method in Section 3.2.2, the simulation is shown in Figure 3.18

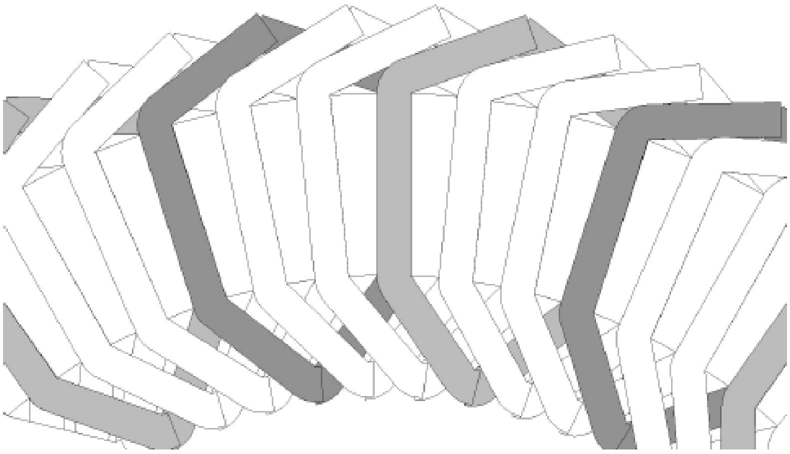

Figure 3.17 Schematic representation of rotor end-turn configuration (Source: A. Thomas)

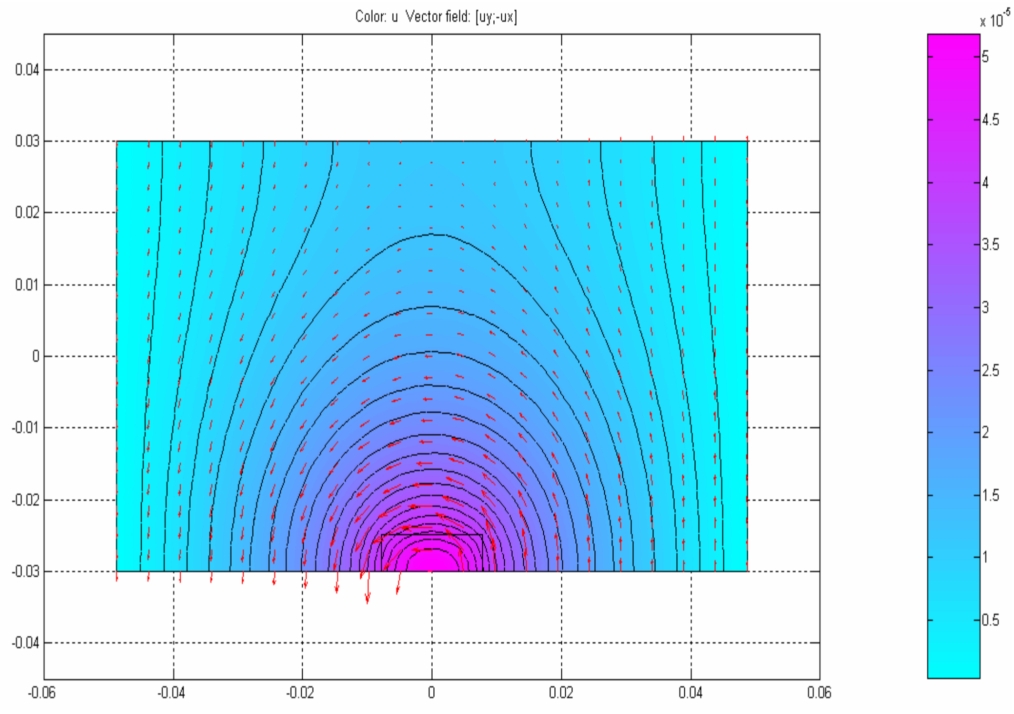

Figure 3.18 Magnetic field distribution for 1A current in rotor coil

From the simulation, the inductance of active rotor winding is 3.57mH.

End turn inductance

As shown in Figure 3.16, it is difficult to estimate the inductance of the end turn exactly. So the diamond shape rotor coil is approximated with trapezoid, replacing the end turns with straight lines. Cutting the machine through its diameter, the cross section is shown in Figure 3.19. The end turns are perpendicular to the cross section and they are placed at the corners of the rotor iron core. The cross section of each end turn is 2 turn by 12 turn, which is $2.5mm \times 15.49mm$. The rotor iron core is attached to the power rotor aluminum plate with a radius of 370mm and 45mm thick. Surrounding the rotor is the housing, whose diameter is 889mm with an axial dimension of 308mm. The thickness of the housing aluminum is about 6.35mm. Because the machine is symmetric about the center of the stator iron core in axial direction, the model contains only a half of the machine.

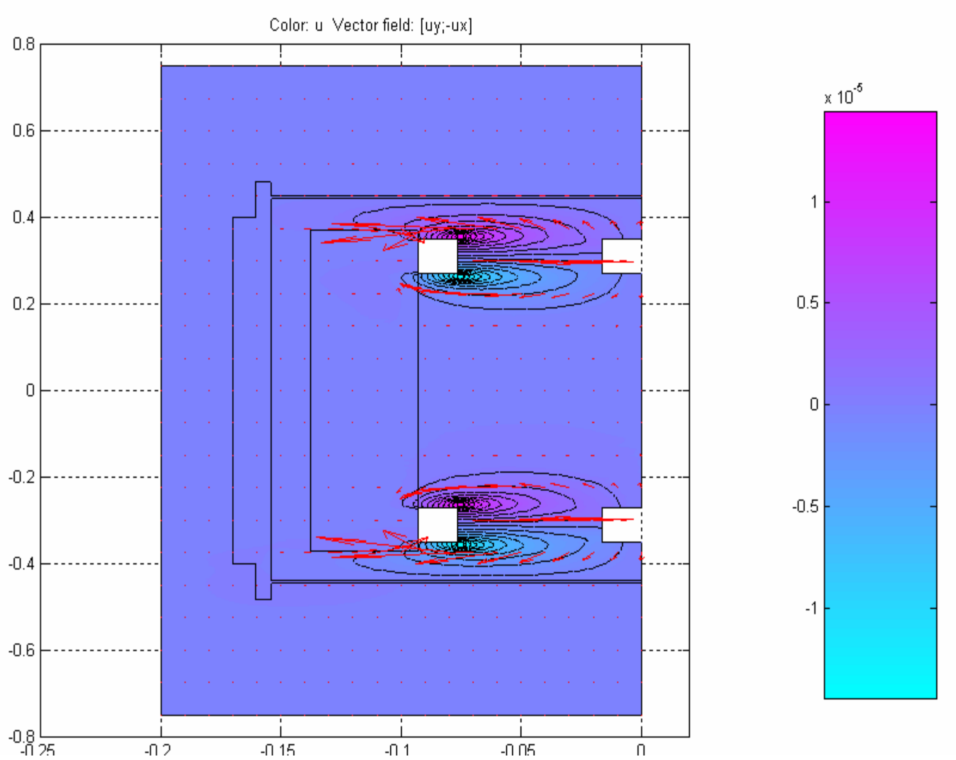

Figure 3.19 Model of rotor inductance

By the same method used in Section 3.2.2, the end turn inductance is about 1.202mH with an induced resistance of 0.0324ohm.

3.3.3 Power rotor subtransient inductance at 60Hz

Considering the effect of aluminum PM rotor plate, the 60Hz subtransient inductance of the active side of the rotor winding can be calculated the same way as in Section 3.2.3. The result of the simulation is compared with the rotor static experiment in Section 4.4. Using 1A 60Hz current as a trial current, the simulation result as shown in Figure 3.20.

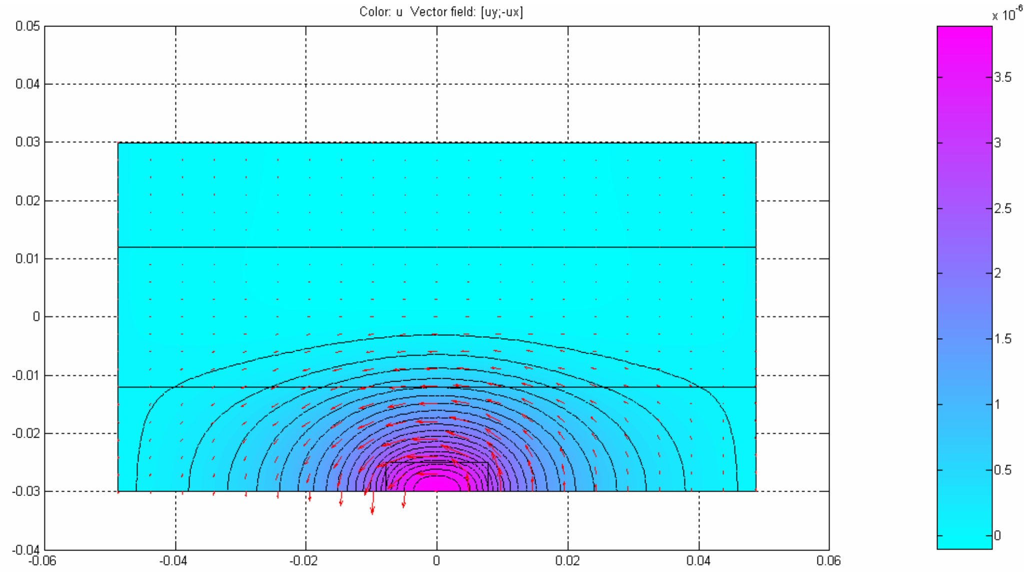

Figure 3.20 Magnetic field strength vector distribution for rotor subtransient inductance calculation

The impedance is $z = 0.113 + j0.909$ ohm and the subtransient inductance of the active rotor winding at 60Hz is 2.4mH.

3.3.4 Summary

Table 3.3 Rotor winding estimated parameters

Rotor winding parameters

DC resistance	**Active winding inductance**	**End turn winding inductance**	**End turn induced resistance**
2.6ohm	3.57mH	1.202mH	0.0324ohm

Total resistance: 2.63ohm

Total self-inductance: 4.77mH

At 60Hz subtransient condition:

Active winding inductance	**Induced resistance**
2.4mH	0.113ohm

Total resistance 2.74ohm

Total self-inductance 3.60mH

3.4 Mutual inductance

The mutual inductance between the stator winding and the rotor winding can be estimated using the simulation result in Section 3.2.2 and 3.3.2. The mutual inductance can be calculated by Equation 3.8. The integration is replaced by summation over the 48 rotor winding turns.

Therefore, the mutual inductance between the stator and power rotor winding is $M_{sr} = 0.175mH$. At 60Hz subtransient condition, the mutual inductance is -0.0157mH, which is rather small, because the PM rotor plate shields the electromagnetic field produced by the stator winding.

3.5 Damping coil estimation

When the PM rotor is not at synchronous speed, current will be induced in the aluminum plate of PM rotor, which is therefore acting as a damping coil. This section is to estimate the parameters of the damping coil. The mutual inductance between the stator winding and the damping coil is different from the mutual inductance between the rotor winding and the damping coil. Therefore, it is analyzed separately.

At the stator side

Using the same method for calculating the 60Hz subtransient inductance in Section 3.2 and 3.3, a subtransient impedance-frequency curve is generated. This will reveal the frequency response of the PM rotor plate. The curves of inductance and resistance are shown in Figure 3.21.

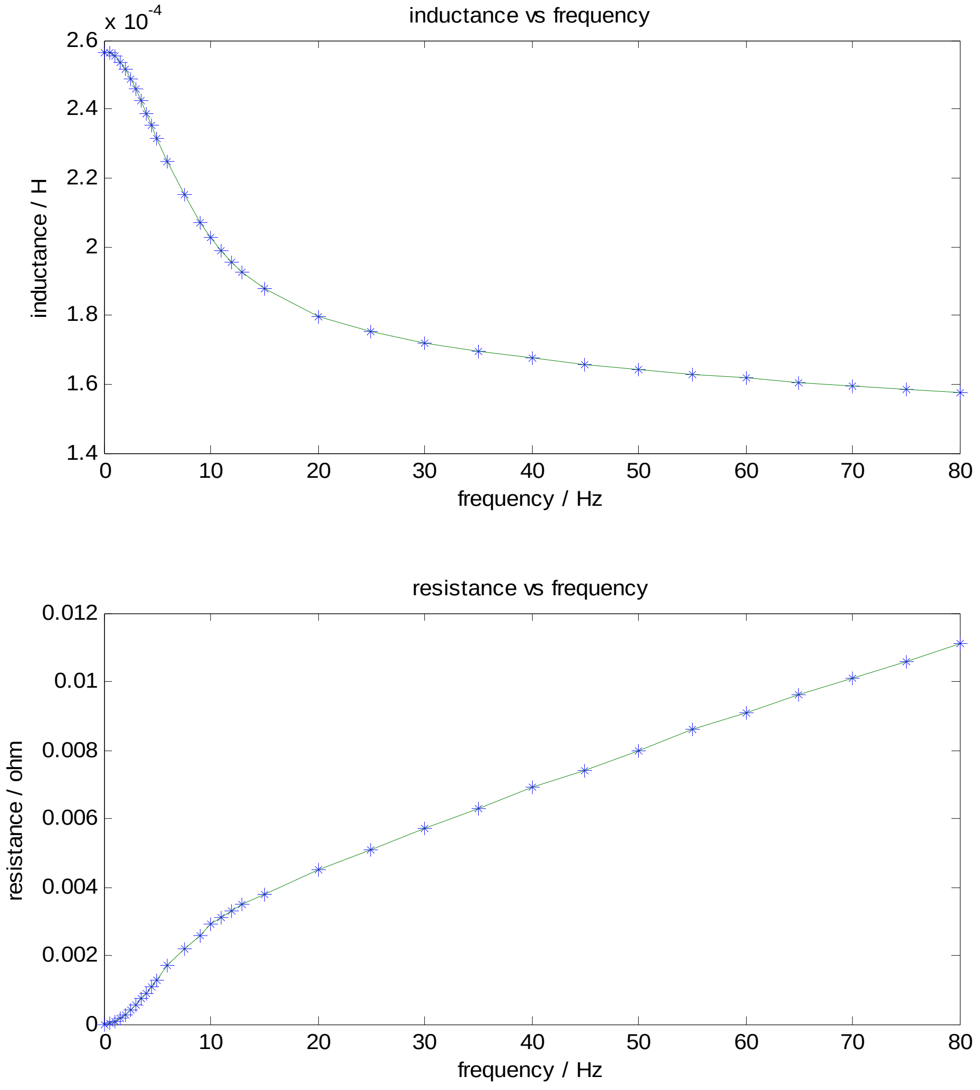

Figure 3.21 Inductance and resistance frequency response measured from the stator

The interaction between the stator winding and the PM rotor aluminum plate can be modeled in Figure 3.22 with the PM rotor plate represented by a damping coil.

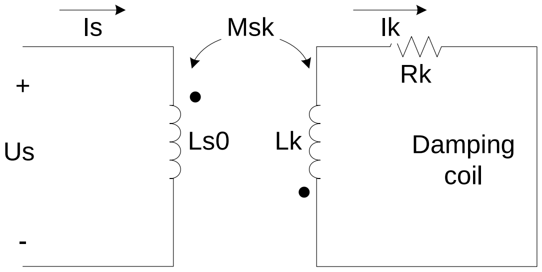

Figure 3.22 Equivalent circuit of damping coil

From the equivalent circuit, we have

$$U_s = j\omega(I_s L_{s0} + I_k M_{sk})$$

$$j\omega(I_s M_{sk} + I_k L_k) + I_k R_k = 0$$

Then the impedance measured from the stator winding is

$$Z_s = \frac{U_s}{I_s} = j\omega(L_{s0} + I_k M_{sk} / I_s)$$

$$= j\omega(L_{s0} - \frac{j\omega M_{sk}^2}{R_k + j\omega L_k})$$

$$= \frac{\omega^2 M_{sk}^2 R_k}{R_k^2 + \omega^2 L_k^2} + j(\omega L_{s0} - \frac{\omega^3 M_{sk}^2 L_k}{R_k^2 + \omega^2 L_k^2})$$

So the measured resistance and inductance are

$$R = \frac{\omega^2 M_{sk}^2 R_k}{R_k^2 + \omega^2 L_k^2}$$ **Equation 3.15**

$$L = L_{s0} - \frac{\omega^2 M_{sk}^2 L_k}{R_k^2 + \omega^2 L_k^2}$$ **Equation 3.16**

Where L_{s0} is the inductance of the stator active winding at zero frequency which is 0.257mH.

It is expected that the simulation result deviates from the equivalent circuit model, which can be illustrated from the resistance curve. In Equation 3.15, the resistance tends towards a constant value as the frequency increasing. However in Figure 3.21, there is no sign of this tendency. This is because the resistance and inductance of the equivalent circuit of the PM aluminum plate actually depend on the frequency. Due to the skin effect, the current circulating in the PM rotor aluminum plate will be rejected to the surface and peripheral of the PM rotor plate as the frequency increasing, resulting an increasing resistance, as shown in Figure 3.21.

Moreover, using Equation 3.15 and 3.16, the time constant of the damping coil can be expressed as

$$\tau = \frac{L_k}{R_k} = \frac{L_{s0} - L}{R}$$

Which is plotted as in Figure

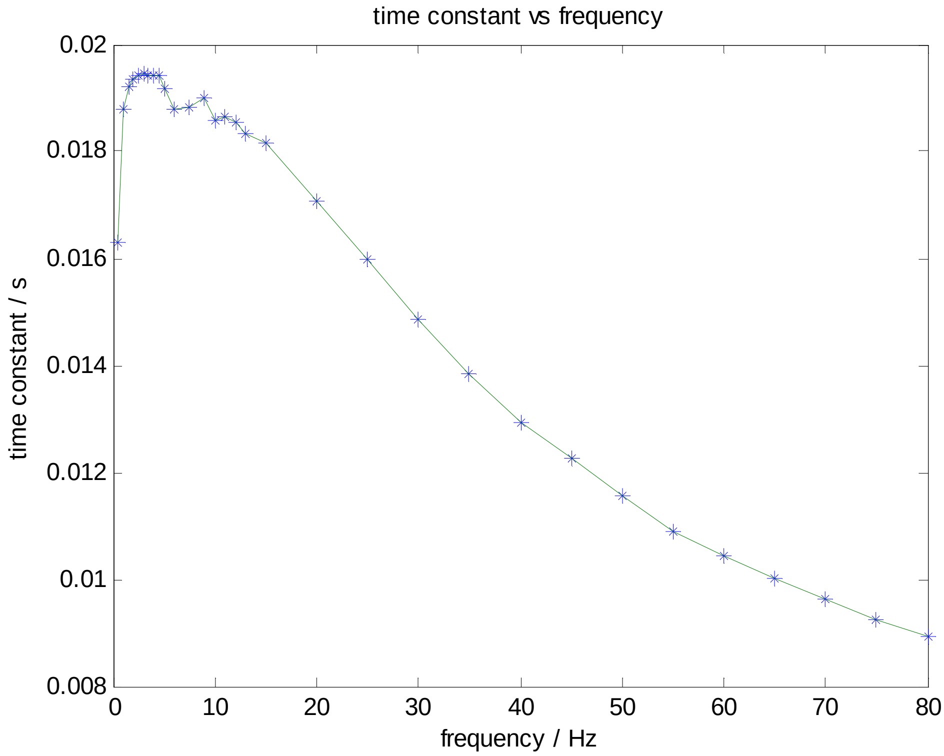

Figure 3.23 Time constant of the damping coil vs frequency simulated at the stator side

The time constant decreases as the frequency increases. However, in low frequency range from 0~15Hz, the time constant is close to a constant value, which means that the equivalent circuit model can be used at this frequency range to derive the parameters of the damping coil. Moreover, this frequency range is also a reasonable range for the transient response of the machine.

Therefore, Equation 3.15 and 3.16 are used to fit the inductance and resistance curve at 0~15Hz range to generate the equivalent damping circuit parameters. The optimization fitting curves are shown in Figure 3.24 and Figure 3.25

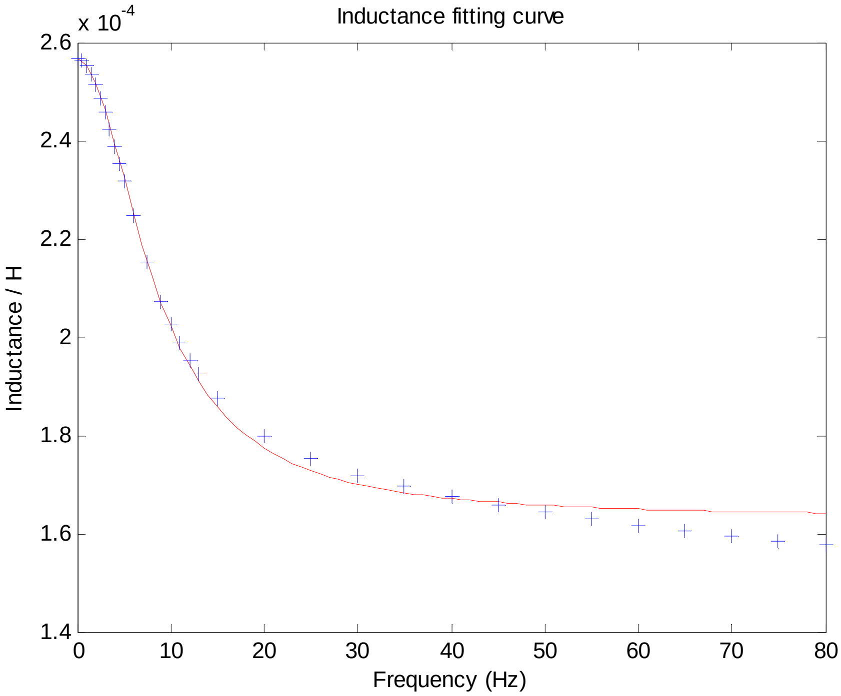

Figure 3.24 Stator inductance-frequency fitting curve

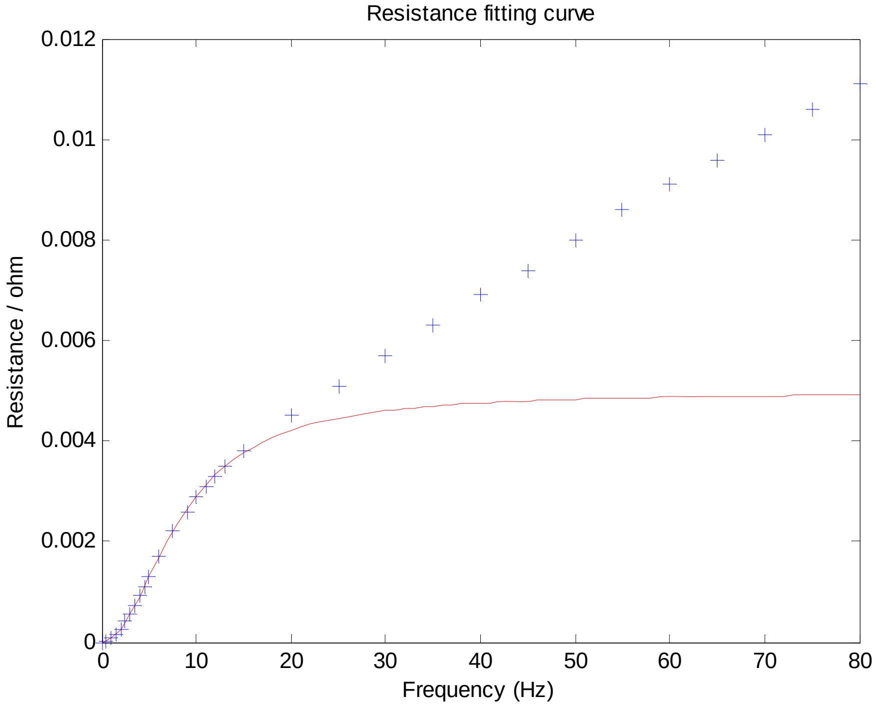

Figure 3.25 Stator resistance-frequency fitting curve

Note that in Equation 3.15 and 3.16, there are only two independent variables, the damping coil time constant $\frac{L_k}{R_k}$ and $\frac{M_{sk}^2}{R_k}$. From the fitting of the curve, we know

$$\tau_k = \frac{L_k}{R_k} \approx 0.0188s$$

$$\frac{M_{sk}^2}{R_k} \approx 1.76 \times 10^{-6} H \bullet s$$

At the rotor side

Following the same procedure, the damping coil seen from the rotor side can be estimated. The damping coil time constant curve is shown in Figure 3.26.

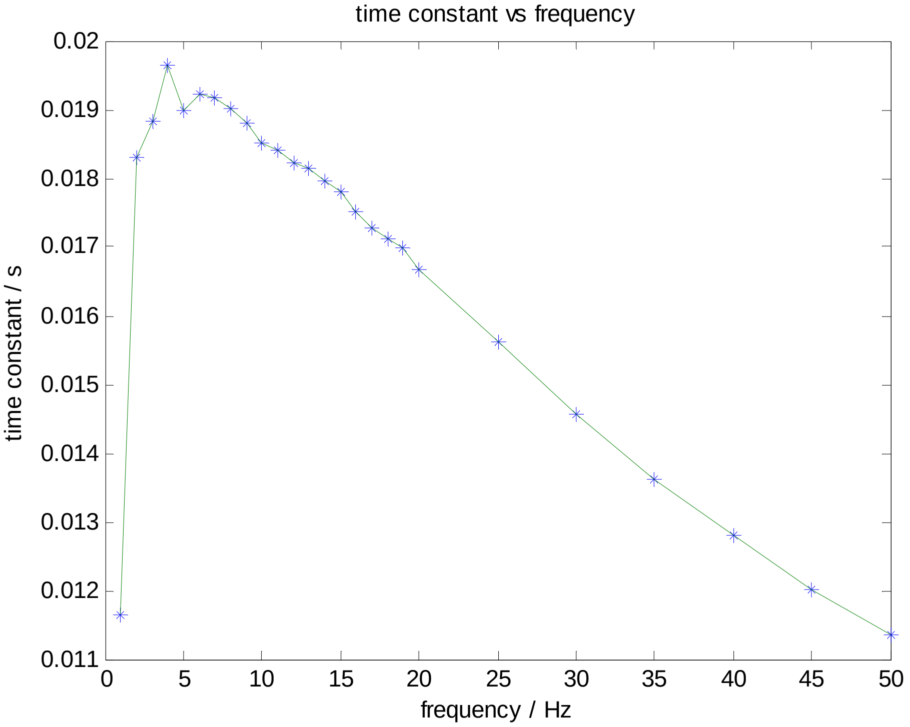

Figure 3.26 Time constant of the damping coil vs frequency simulated at the stator side

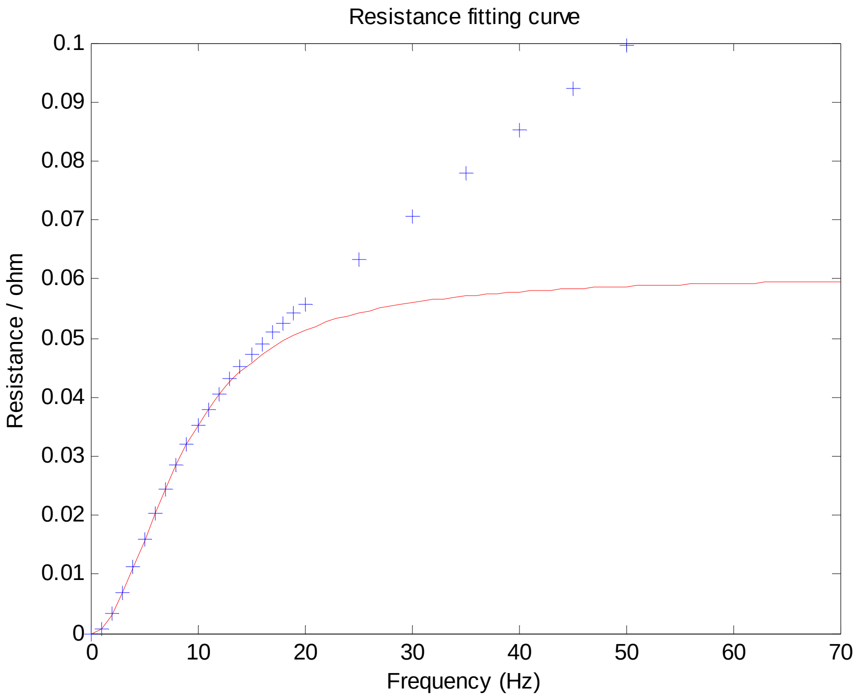

Figure 3.27 Rotor resistance-frequency fitting curve

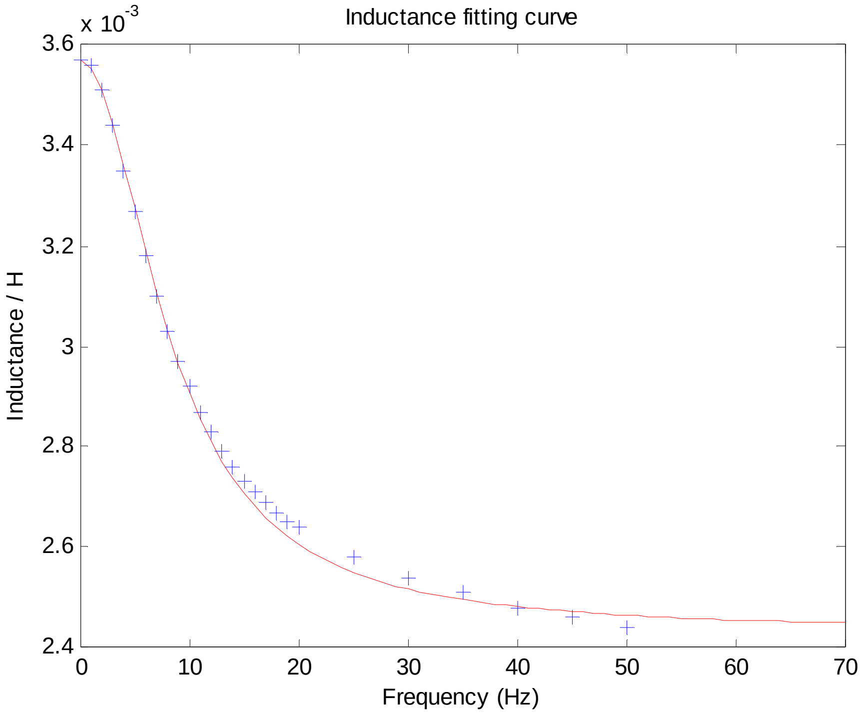

Figure 3.28 Rotor inductance-frequency fitting curve

In Figure 3.26, it can be seen that at the frequency range of 0~12Hz, the time constant of the damping coil changes slowly with the frequency. Therefore, fitting the data at this frequency range, shown in Figure 3.27 and Figure 3.28, the time constant of the damping coil is

$$\tau_k = \frac{L_k}{R_k} \approx 0.0188s$$

Which is the same as the result from the stator side, because it is the same damping coil. The other parameter is

$$\frac{M_{rk}^2}{R_k} \approx 2.14\times10^{-5} H\bullet s$$

As expected, it is different from the result from the stator side, showing that the mutual inductance between the rotor winding and the damping coil is different from the one between stator winding and the damping coil.

The parameters developed in this section will be used in the stability analysis of the machine.

Chapter 4

4 Experiment result and analysis

4.1 Stator open circuit experiment

The machine is driven by the slave sheave on the shaft with the transmission of torque through the belt connecting the two sheaves. The drive sheave has 40 teeth while the slave sheave has 144 teeth. So the speed ratio of the angular velocity of the drive and the slave is 3.6. Shorting the power rotor winding, the machine is driven at the rating speed 360RPM with the drive speed of 1298RPM. The result is shown in Figure 4.1.

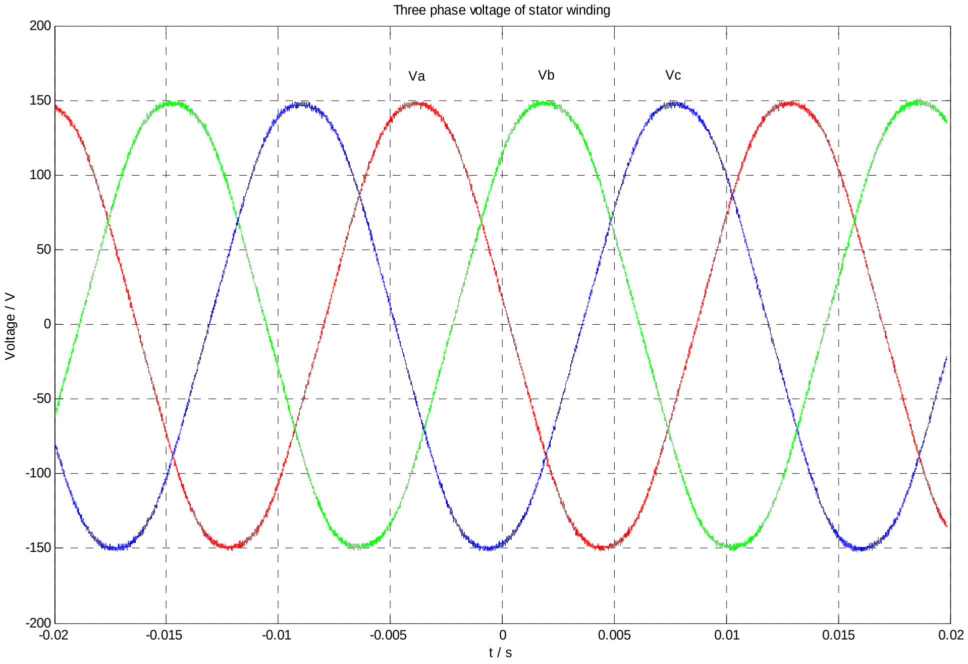

Figure 4.1 Stator open circuit three phase voltage at rating speed.

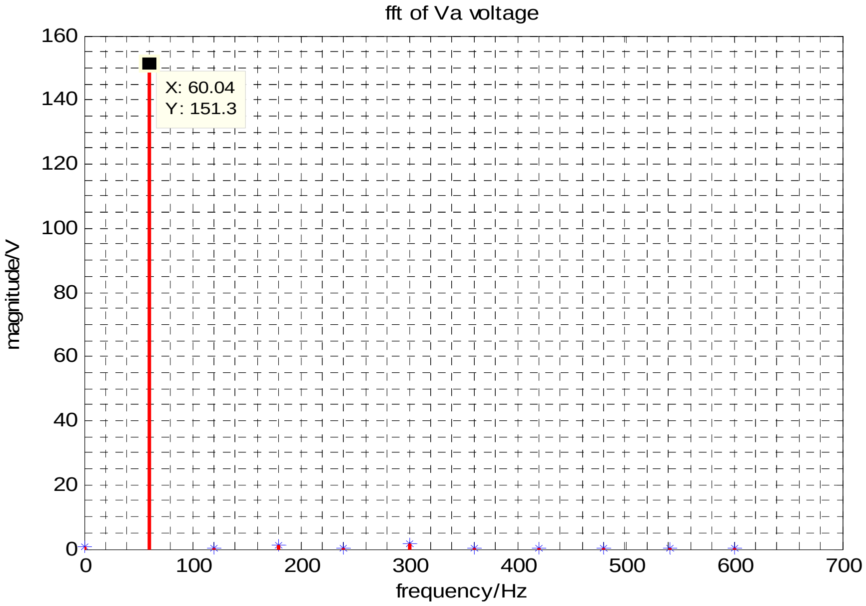
fft of Va voltage
X: 60.04
Y: 151.3
magnitude/V
0
20
40
60
80
100
120
140
160
0
100
200
300
400
500
600
700
frequency/Hz

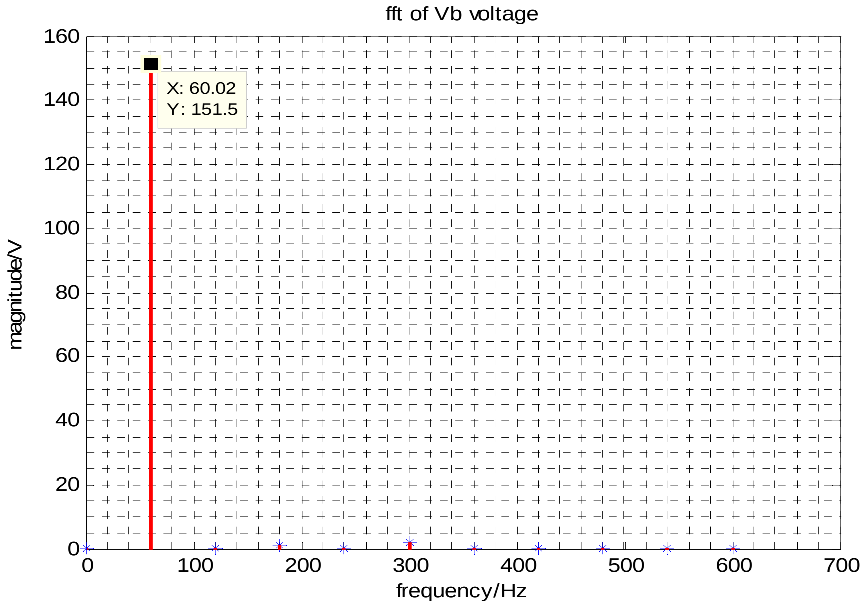
fft of Vb voltage
X: 60.02
Y: 151.5
magnitude/V
0
20
40
60
80
100
120
140
160
0
100
200
300
400
500
600
700
frequency/Hz

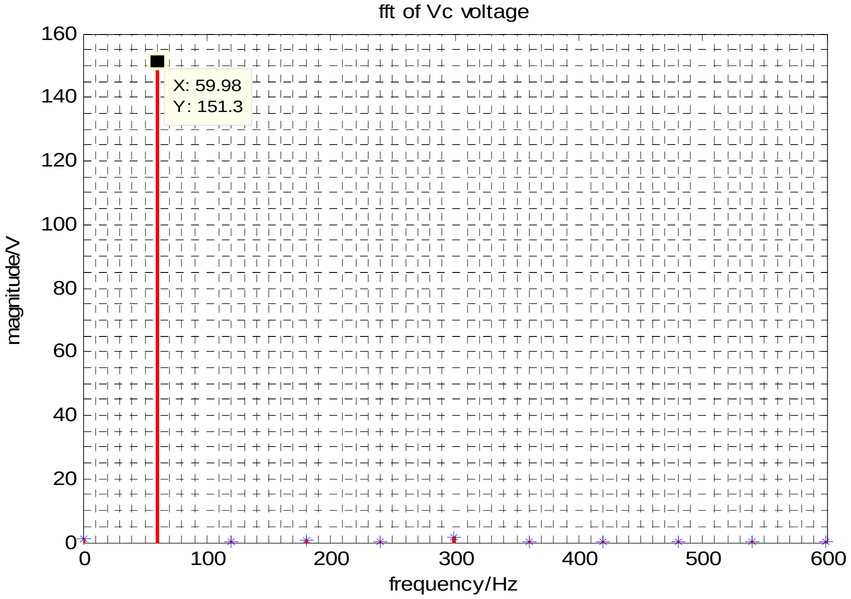

Figure 4.2 FFT of Va, Vb and Vc.

From the frequency analysis shown in Figure 4.2, the magnitude of the fundamental voltage is $151.3V$ and the 5^{th} order harmonic is the main harmonic which is about 1.8V. Compared with the estimated fundamental voltage in Section 3.1.3, the actual voltage is smaller than the theoretical estimated value. From the measured voltage, the actual magnetic flux density at the stator coil is $0.421 tesla$. The permanent magnets won't be the same as the rated value. The lower air gap magnetic flux density is probably due to the weaker magnets than rating value.

Moreover, the phase differences among the three phase voltage are not 120 degrees. Phase difference between A and B is about 124.6^0. Phase difference between B and C is about 124.8^0. Phase difference between C and A is about 110.6^0. The phase problem is strongly suspected to be the problem of the stator winding distribution.

As shown in the photo in [5], the peripheral of the stator iron core is divided uniformly into 20 sections. In each of the 20 sections, the three phase coils of the stator are wounded side by side. This will cause the unbalanced phases. Because each coil is 26.5mm wide, which is about 56 degrees of electric angle, the phase difference between three phases will be of the condition shown in Figure 4.3, which is close to the measured values.

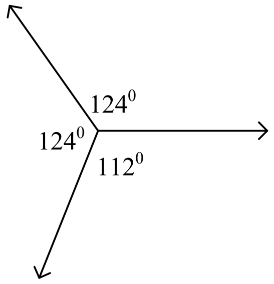

Figure 4.3 Phase differences of the three phases for the current stator winding arrangement

V-f curve

Running the machine at different frequency, the stator open circuit voltage response is shown in Figure 4.4.

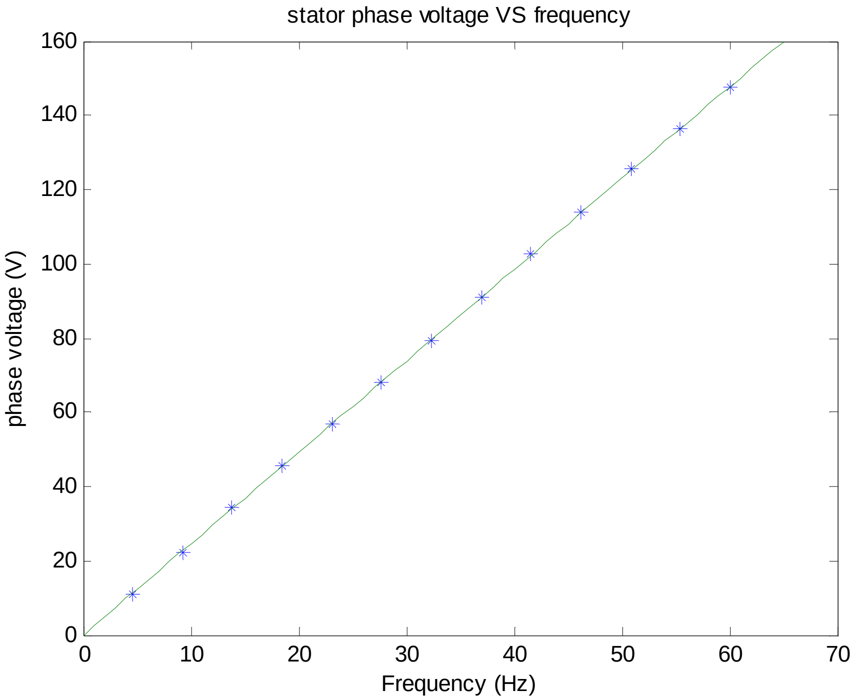

Figure 4.4 Stator V-f curve

The slope is 2.5V/Hz. Therefore, the flux linkage is $0.389\mathrm{Vrad}^{-1}\mathrm{s}$.

4.2 Rotor open circuit experiment

There are two power rotors. In this thesis, the one near the slip-ring end of the shaft of the machine is named power rotor I. The other one is named power rotor II. Both of the two power rotor windings are "Y" connected and two sets of the A, B and C winding terminals are brought out through the shaft in connection of 6 slip rings, which is shown in Figure 4.5.

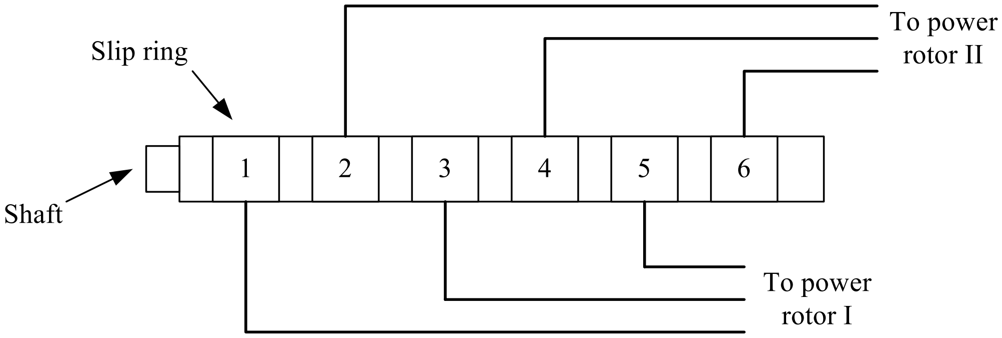

Figure 4.5 Schematic representation of the connection of slip rings to power rotors.

The experiment was done by injecting DC current into one phase of the stator winding to "hold" the PM rotor from spinning while the power rotor was driven by the drive. Then the terminal voltage of the two sets power rotor were recorded.

Power rotor side I

The three phase voltages of power rotor I is shown in the Figure 4.6

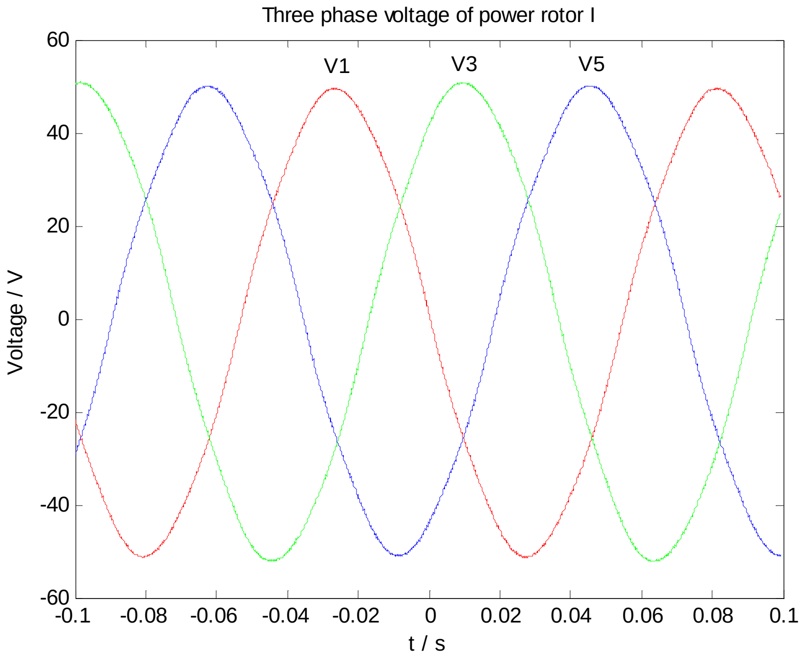

Figure 4.6 Power rotor I open circuit voltage, V1, V3 and V5.

V1 is in advance of V3 by 120.7 degrees and V5 is in advance of V1 by 121.9 degrees. The frequency of the experiment is 9.26Hz. Fourier analysis of the voltage wave forms are shown in the Figure 4.7

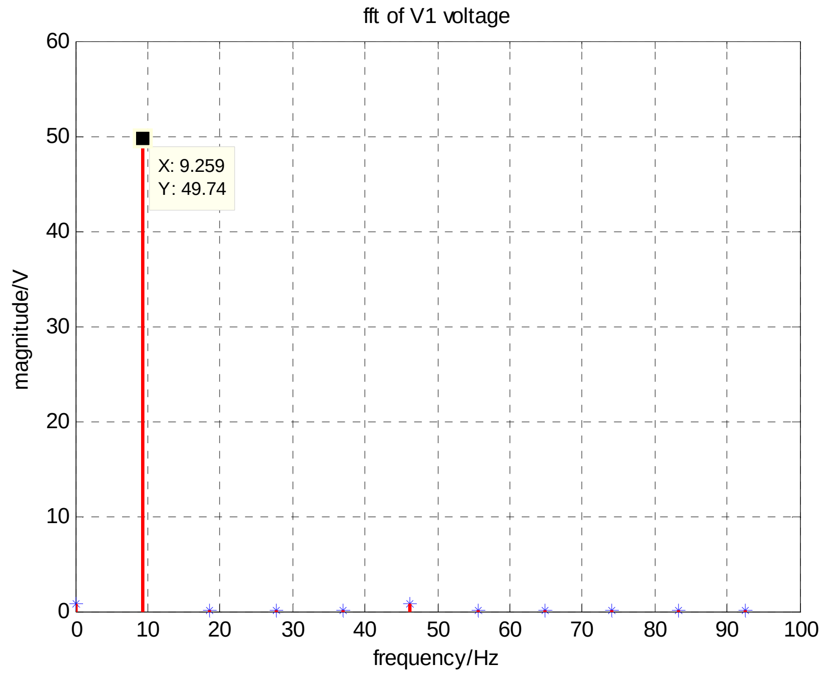
fft of V1 voltage
magnitude/V
frequency/Hz
X: 9.259
Y: 49.74
0
10
20
30
40
50
60
0
10
20
30
40
50
60
70
80
90
100

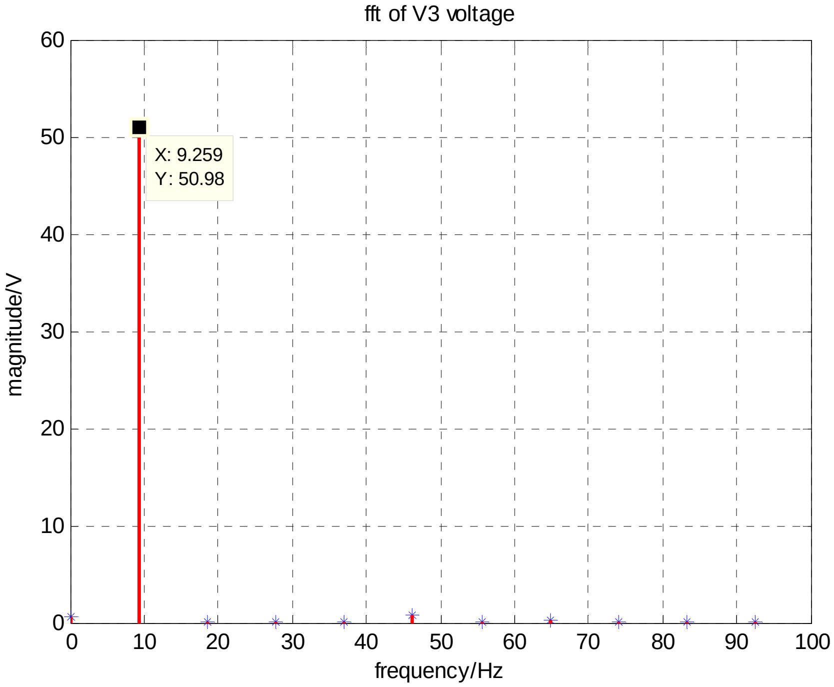
fft of V3 voltage
magnitude/V
frequency/Hz
X: 9.259
Y: 50.98
0
10
20
30
40
50
60
0
10
20
30
40
50
60
70
80
90
100

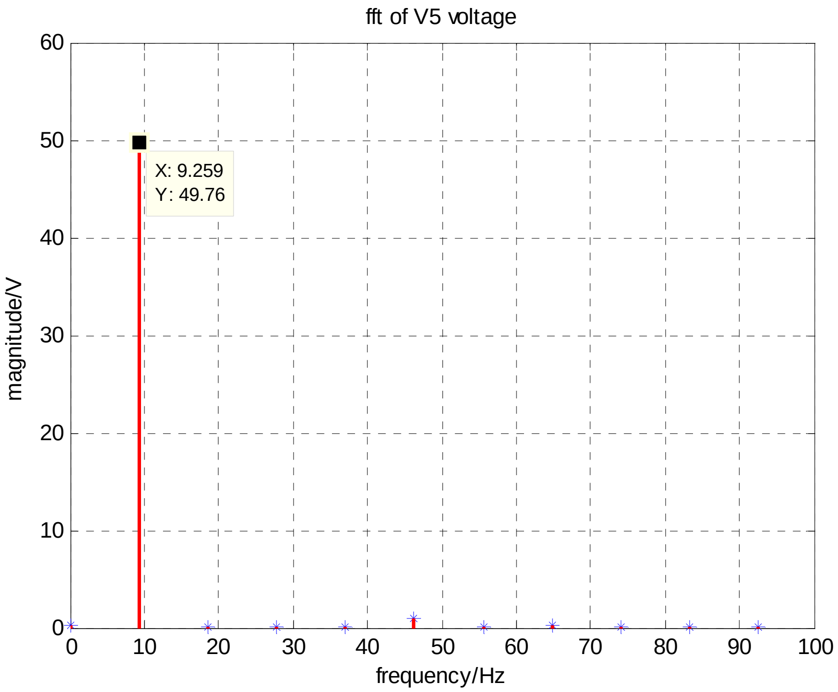

Figure 4.7 fft of rotor I open circuit

From the Fourier analysis, the amplitude of the fundamental component phase voltage of power rotor I is about 50.2V at 9.26Hz. The largest harmonics is the 5th harmonic component, whose amplitude is only about 0.9V, 1.8% of the fundamental voltage.

Power rotor side II

The open circuit voltage of power rotor II is shown in Figure 4.8

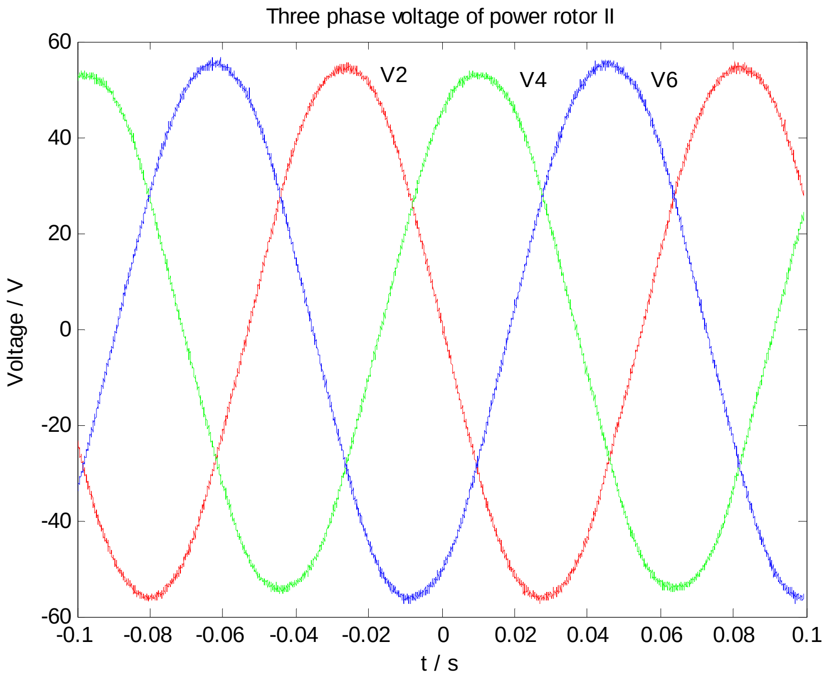

Figure 4.8 Open circuit voltage of power rotor II

V6 is in advance of V2 by 120.7 degrees and V2 is in advance of V4 by 121.5 degrees. Fourier analysis of the open circuit voltages is shown in Figure 4.9

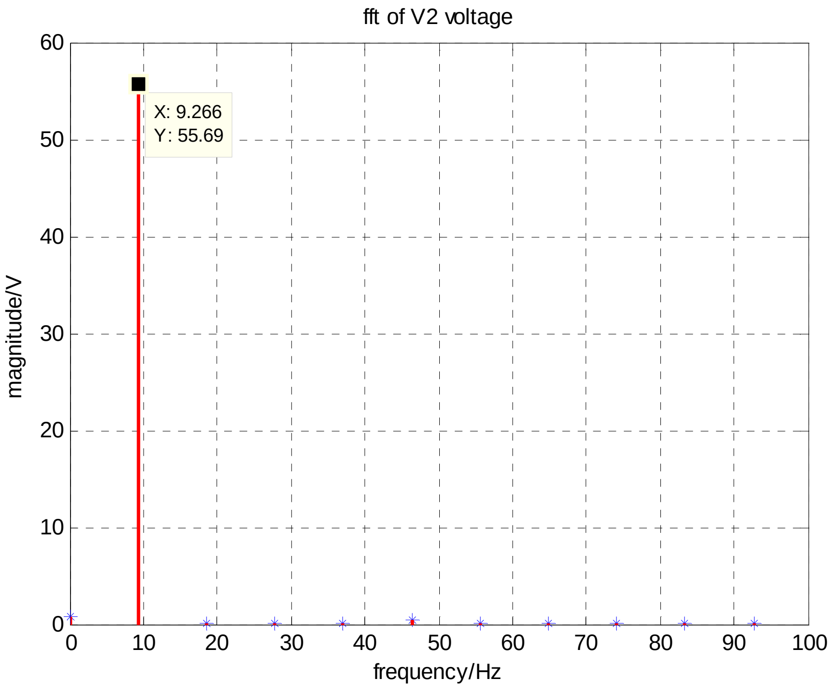

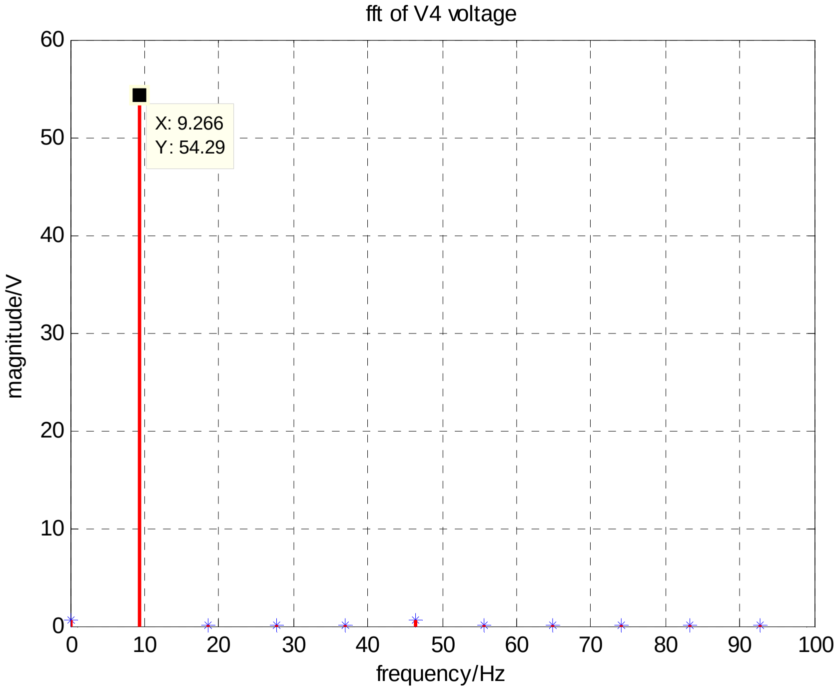

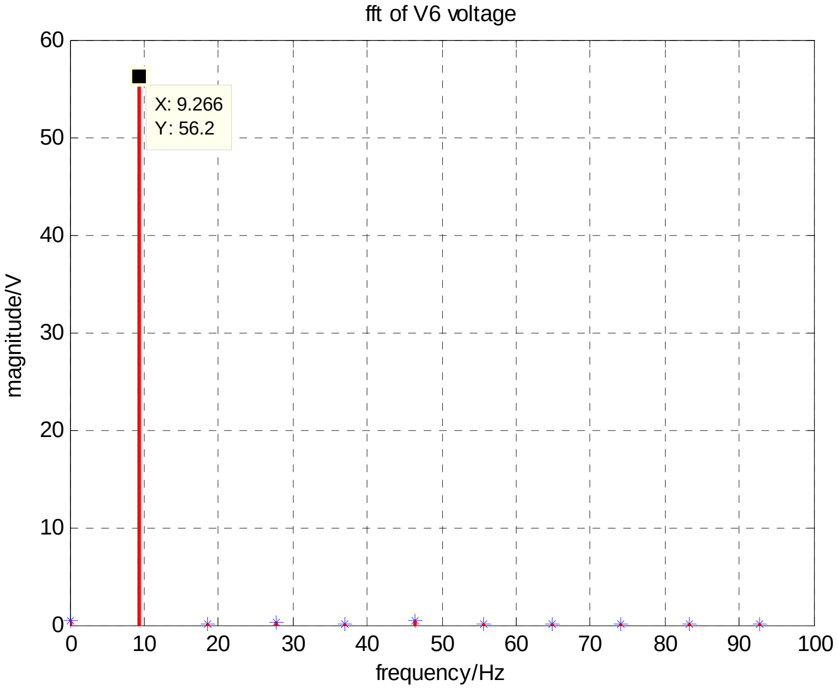

Figure 4.9 fft of the rotor II open circuit voltage

From the Fourier analysis, the amplitude of the fundamental component phase voltage of power rotor II is 55.4 V at 9.26Hz. The 5th harmonic is the biggest harmonic which is smaller than 1.2% of the fundamental voltage.

Comparison of power rotor I and II

The relative position of the voltage wave forms of the two power rotors is compared to determine the alignment of the rotors. V1 and V2 are compared in Figure 4.10, where V2 is in advance of V1 by 152.8 degrees.

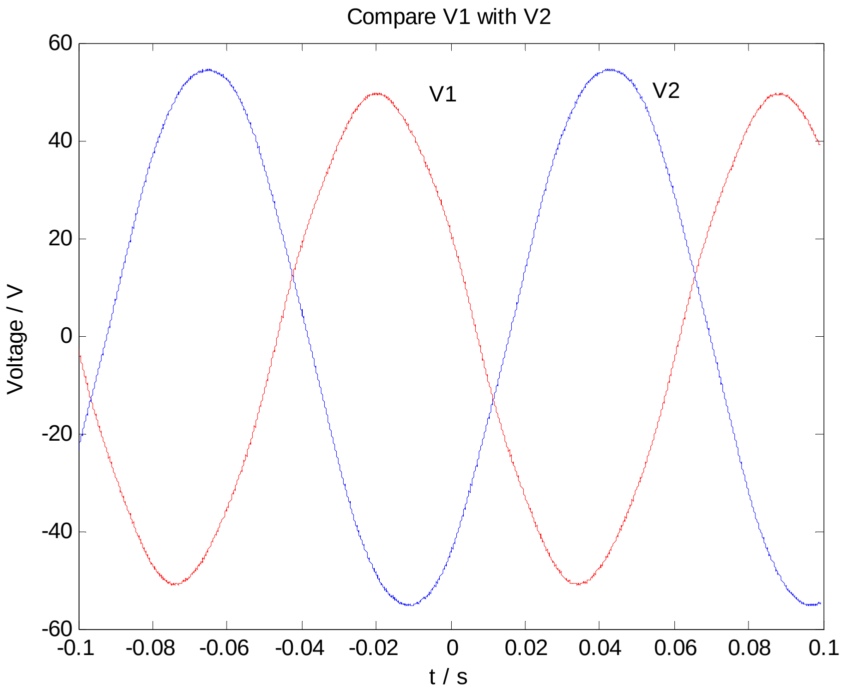

Figure 4.10 Comparison of V1 with V2

So the phaser diagram of the six phases of the two power rotors can be determined, as shown in Figure 4.11.

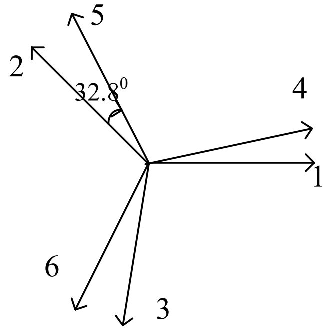

Figure 4.11 Phaser diagram of the 6 phase voltages of the two power rotors

Analysis

The phase difference between the two sets of the power rotor windings corresponds to only 3.28 degree mechanical angles. This is due to the misalignment of either the two power rotors or the two PM rotors.

The open circuit voltage of the two power rotors are not the same either. The voltage of power rotor II is 1.10 times the voltage of power rotor I, which means that the air gap at the side of power rotor II may smaller. The active side of rotor winding coil is 12 turns' wide, which corresponds to 3.288 degrees of mechanical angle. Thus the winding factor of power rotor is 0.986 for the fundamental frequency. Using the voltage data, the magnetic flux density at the rotor winding can be estimated by equation $V_n = Nk_{wsn}B_n l_m \omega(r_o + r_i)/2$.

At winding of power rotor I, the magnitude of magnetic flux density is 0.370T.
At winding of power rotor II, the magnitude of magnetic flux density is 0.408T.
The estimated flux density at the rotor winding is smaller than the flux density at the stator winding which is about 0.421T.

V-f curve

The rotor open circuit voltage versus frequency is shown in Figure 4.12.

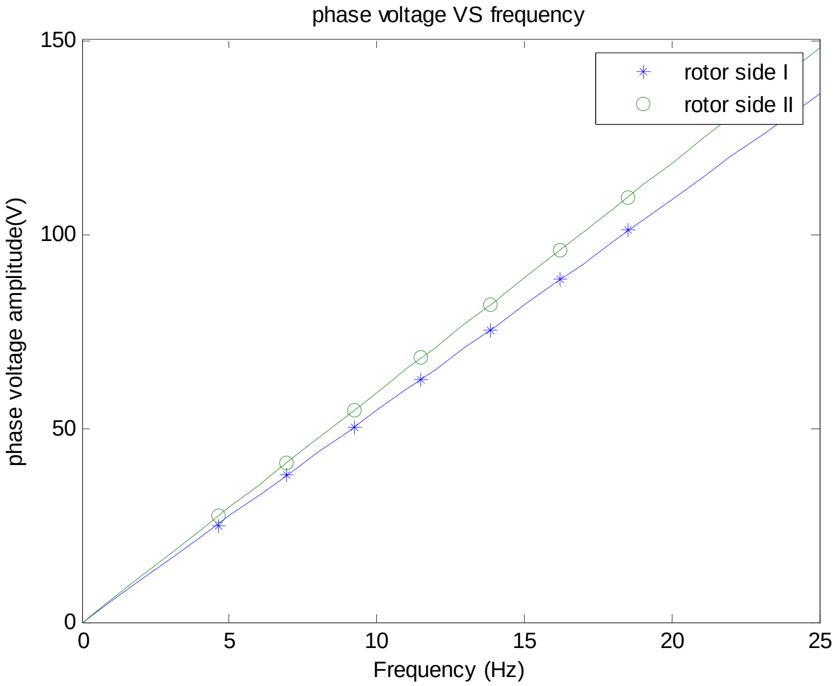

Figure 4.12 Rotor open circuit V-f curve

The slope for rotor side I is 5.44V/Hz and the slope for rotor side II is 5.91V/Hz. Therefore, the flux linkage for rotor I is 0.866Vrad^{-1}s and the flux linkage for rotor II is 0.941Vrad^{-1}s. The average flux linkage of power rotor is 0.903Vrad^{-1}s.

4.3 Static experiment

The static experiment is done with the prototype machine stationary. Then 60Hz voltage is applied to the terminals of the machine. This experiment is to measure the parameters of the prototype, such as the resistance and subtransient inductance at 60Hz and then is compared with the result of from Section 3.2.3 and 3.3.3 to verify the validity of the model of machine.

Stator static experiment

With the power rotor winding open and machine stationary, 60Hz voltage is applied to one phase of the stator winding using a transformer. Through the measured voltage and current, the inductance and resistance can be known. Besides, the DC resistance of stator winding was measured using a digital multimeter. The result is shown in Table 4.1, compared with the result of Section 3.2.

Table 4.1 Comparing the stator parameters from the experiment with from simulation

Three phases		**Phase A**	**Phase B**	**Phase C**
DC resistance (ohm)	**Measured**	0.144	0.142	0.142
	Calculated	0.1		
Subtransient resistance at 60Hz (ohm)	**Measured**	0.177	0.174	0.177
	Calculated	0.144		
Subtransient inductance at 60Hz (uH)	**Measured**	254.1	245.6	245.6
	Calculated	209.0		

The phase difference between A and B is about 124.6^0. Phase difference between B and C is about 124.8^0. Phase difference between C and A is about 110.6^0. The mutual inductance should satisfy

$$M_{ab} = L\cos\alpha_{ab}, M_{bc} = L\cos\alpha_{bc}, M_{ac} = L\cos\alpha_{ac}.$$

where L is the total subtransient inductance, which is 209uH. Using the above equation, the calculated mutual inductance is compared with the measured value, as shown in Table 4.2.

Table 4.2 Stator phase to phase mutual inductance

Mutual inductance between phases	Phase A-B	Phase A-C	Phase B-C
Measured value (uH)	133.2	71.4	133.4
Calculated value (uH)	118.7	73.5	119.3

In this experiment, the induced voltage in the power rotor winding is hard to observe. At 60Hz, the skin depth of aluminum is $\delta = \frac{1}{\sqrt{\pi f \mu\sigma}} \approx 10.5mm$. The PM aluminum plate is

24mm thick. So it is rather reasonable that there is very little field that can penetrate the PM rotor plate. From the comparison, it can be seen that difference between the simulation results and the experiment results is within the tolerance.

Rotor static experiment

The same experiment is done to both of the power rotors. The result is shown in Table 4.3 with comparison of the results from Section 3.3.

Table 4.3 Comparing the rotor parameters from the experiment with from simulation

Rotor terminal #		Measured subtransient Lr (mH)	Calculated subtransient Lr (mH)	Measured subtransient Rr (ohm)	Calculated subtransient Rr (ohm)
Rotor I	1	3.83	3.6	2.96	2.74
	3	3.88		3	
	5	3.74		3	
Rotor II	2	3.79		2.93	
	4	3.66		2.96	
	6	3.96		2.93	

It can be seen from the Table, the theoretical result is good enough for the estimation of the parameters of the prototype machine. Moreover, the contact resistance between the brushes and slip rings are relatively large, around 2.5ohms to 4ohms (The resistance between any two terminals measured from brushes is usually more than 10ohms). Therefore, to be able to drive the prototype machine, a set of better slip rings and brushes should be made.

4.4 *V-curve experiment*

The v-curve experiment is to determine the synchronous impedance of the prototype machine. This is a plot showing the current going in to the terminals of the machine as a function of internal voltage when the machine is run unloaded. Normally, the internal voltage of the machine is adjusted by varying field current. But for PM machines, the field is fixed by the PM. To do this experiment, our v-curve is generated by varying the voltage on the terminals through a transformer. An ideal v-curve is shown in the Figure 4.13.

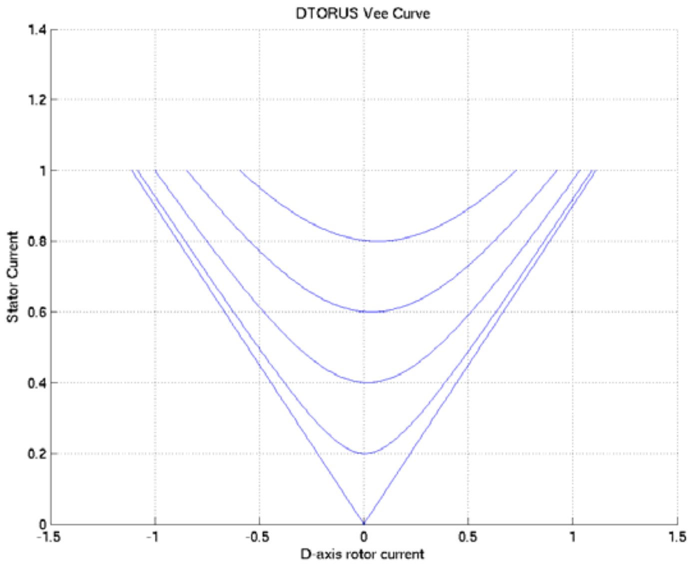

Figure 4.13 Ideal vee curve (Source: J. Kirtley, Final Report to National Renewable Energy Laboratory)

The experiment was done by shorting the power rotor winding and synchronous the machine to the power system through a transformer. Then the machine was run as a motor without load. In the experiment, the neutral points of the stator winding and the transformer are isolated. The experiment v-curve is shown in Figure 4.14.

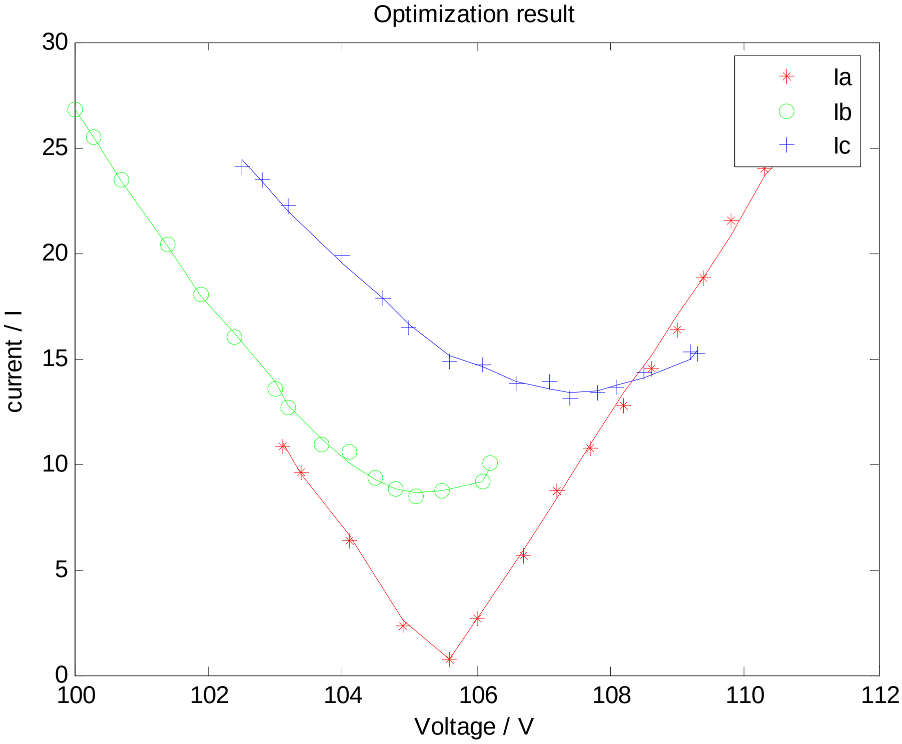

Figure 4.14 Experiemental v-curve data with fitting curve

The experiment result deviates from the idea v-curve quite a lot. The main reason is that the three phase open circuit voltage of the stator winding is not 120 degrees phase spaced, which is shown in Section 4.1. To interpret the v-curve, an optimization method is used. Start with the machine model, which is shown in Figure 4.15 of the stator equivalent circuit of phase A converted to the stator side.

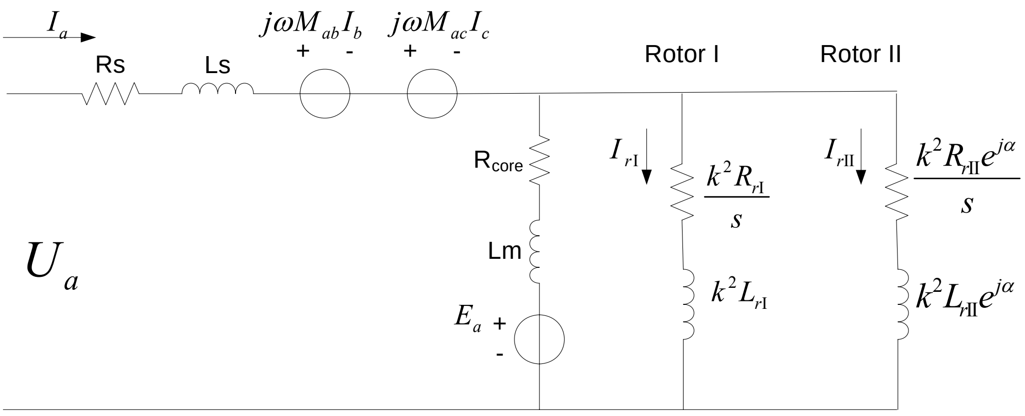

Figure 4.15 Figure Equivalent circuit of phase A converted to the stator side

This is a special equivalent circuit for this prototype machine. Because the asymmetry of the phases, the mutual inductance M_{ab}, M_{ac} are not incorporated into L$_s$. Also $e^{j\alpha}$ takes into account the misalignment of the two power rotors, where $\alpha = 32.8^0$. In the Figure, E_a is the internal voltage, k is the voltage ratio between the stator and the power rotor, which is $k = \frac{10}{48} \approx 0.208$ and s is the slip speed. Core loss resistance R$_{\text{core}}$ should be very small. L_s, L_m and $L_{r\text{I,II}}$ can be derived from the self inductance and mutual inductance in Chapter 3.

$$L_m = \frac{3}{2} M_{sr} k = 0.0547 mH \, ,$$

$$L_s = L_{Sself} - L_m \approx 0.250 mH$$

$$L_{r\text{I,II}} = \frac{3}{2}(L_{Rself} - M_{sr} / k) \approx 5.60 mH$$

In the experiment, rotor is unloaded, therefore the slip speed should be very small, (It must be smaller than 0.01, because in experiment it is observed that the speed change of the drive shaft is only about 10RPM, which corresponds to a slip speed of 0.0077). Therefore, $\frac{R_r}{s}$ will be very large. So the rotor circuit can be omitted. Because the neutrals are isolated, then we have

$$U_a - Z_a I_a - Z_{ab} I_b - Z_{ac} I_c - E_b - E_n = 0$$

$$U_b - Z_{ab} I_a - Z_b I_b - Z_{bc} I_c - E_b - E_n = 0$$

$$U_c - Z_{ac} I_a - Z_{bc} I_b - Z_c I_c - E_c - E_n = 0$$

$$I_a + I_b + I_c = 0$$

Where E_a, E_b, E_c are the internal voltage, E_n is the neutral voltage and U_a, U_b, U_c are the terminal voltage from the transformer output.

From the above four equations, I_a, I_b, I_c and E_n can be represented by the other variables. From the energy point of view, the machine is run as a motor without load or has only friction load. Therefore, no power or only a very small amount of power is delivered from the stator. Thus,

$$P = real(E_a I_a^* + E_b I_b^* + E_c I_c^*)/2 = 0 \text{ or } P_{loss},$$

where P_{loss} is the friction loss of the machine.

Given the amplitude of terminal voltage U_a, U_b, U_c, internal voltage E_a, E_b, E_c and the winding impedances, the phase of the terminal voltage can be solved so does the three phase current I_a, I_b, I_c. However, the above nonlinear equations must be solved numerically in Matlab by the function “fzero”.

Once the three phase current I_a, I_b, I_c is solved, they can be compared with the measured value. The optimization used here is to optimize the winding impedance so that the residual between the calculated current and measured current is minimized. Also, other parameters such as the phase difference between internal voltages and the magnitude of these voltages can also be incorporated and optimized.

However, it is very important to have a reasonable scope in which the parameters are optimized. The results from Section 3.2 will help setting this scope. In Section 3.2, it is estimated that the total self inductance per phase is $L_s = 0.304mH$ and the resistance is $R_s = 0.135ohm$. From the open circuit test, it is known that the phase difference of the stator voltage is $\alpha_{ab} = 124.6^0, \alpha_{bc} = 124.8^0, \alpha_{ca} = 110.6^0$. Therefore, the mutual inductance is:

$$M_{ab} = L_s \cos\alpha_{ab} = -0.173mH,$$

$$M_{bc} = L_s \cos\alpha_{bc} = -0.174mH$$

$$M_{ca} = L_s \cos\alpha_{ca} = -0.107mH.$$

The *rms* value of the internal voltages are $|E_a| = 107.0V, |E_b| = 107.1V$ and $|E_c| = 107.0V$. The optimization curve is shown in Figure 4.14, which fits the experiment data. The optimization result is shown in Table 4.4 with comparison to the theoretical estimation.

Table 4.4 v-curve results compared with simulation result

Parameters	Optimization result	Theoretical estimation
Ra / ohm	0.177	0.135
Rb / ohm	0.168	
Rc / ohm	0.089	
La / mH	0.340	0.304
Lb / mH	0.489	
Lc / mH	0.520	
M_{ab} / mH	-0.199	-0.173
M_{ac} / mH	-0.037	-0.107
M_{bc} / mH	-0.237	-0.174
P_{loss} / W	430	

The phase angle between the internal three phase voltages from the optimization is quite close to the result from the Section 4.1, which is compared in the Table 4.5.

Table 4.5 Stator phase angle from v-curve fitting result compared with open circuit experiment result

	V-curve fitting result	Open circuit experiment
α_{AB} **/ degree**	124.66	124.6
α_{CA} **/ degree**	110.27	110.6

In the experiment, the phase angles between three voltages determined the shape of the curve. Due to the unbalanced three phase current, the voltage trop on the impedance of the transformer will cause the output three phase voltages of the transformer not 120 degree apart. In the experiment, not all the variac output voltage phases are measured. Thus in the optimization, at all the data points, only one set of the variac output voltage phases are used and optimized, which is therefore the averaged phases. So this will induce error in the simulation. But from the comparison in the above Table, it can be concluded that the experiment data match with the theoretical data, which further verifies the validity of the theoretical model.

4.5 *Flux sensor experiment*

To measure the flux density produced by the PM rotor near the surface of the stator winding, a flux sensor is made. The sensor is a 10 turn coil with a diameter of 51mm.

This sesnsor is inserted into the air gap through the slot in the body of the housing. The induced voltage in the coil is recorded in Figure 4.16.

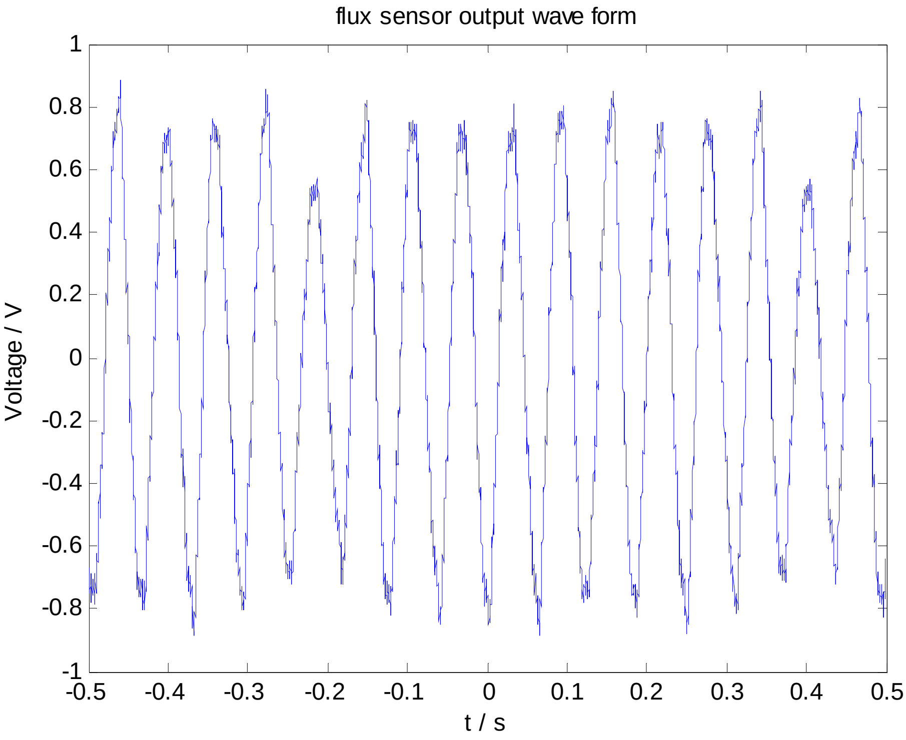

Figure 4.16 Flux sensor output voltage wave form

Every peak in the wave form represents a magnet of the PM rotor therefore one period of the wave form has 20 peaks. It can be seen that there are two magnets which are obviously weaker than the other ones, results two voltage sags in the wave form. An averaged wave form is recorded as in Figure 4.17.

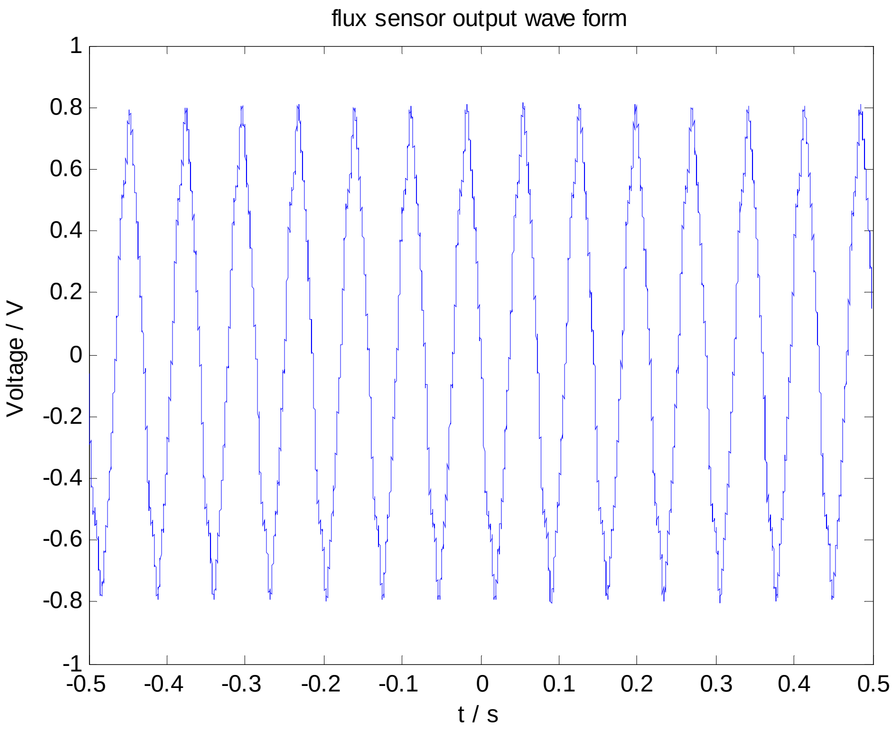

Figure 4.17 Averaged output voltage of the flux sensor

The averaged voltage amplitude is 0.7133V at the frequency of 13.94Hz. As in Section 3.1, assuming the wave length of the air gap flux is 194.78mm and using formula $|V| = 2\pi fn\phi = 2\pi fn\int_S Bds$, the average amplitude of the air gap flux density can be estimated, which is 0.435T.

Chapter 5

5 Control

Machine control constitutes a vast topic. It includes the converter design, control methods design and estimation. For a doubly-fed induction machine, the most frequently used converter is the back-to-back converter. In [10], it is demonstrated that the back-to-back voltage fed current regulated converter is superior for the Scherbius DFIG system compared with the current-fed DC-link converter or cycloconverer. Our doubly-fed PM machine will employ the same configuration as of the DFIG system. This chapter mainly focuses on the development of the control method and explores its stability.

5.1 Overview of vector control

Vector control is widely used in the induction motor drives due to its high performance by decoupling the flux into d axis and q axis and thus the induction motor can be controlled as a dc motor. Our machine is a hybrid of a doubly-fed induction machine and a PM synchronous machine. The presence of the PM simplifies the vector control because the d axis field is produced by the PM. Therefore, we will implement a vector control scheme to our machine.

The idea of vector control is to transform the three phase quantities into a rotating orthogonal frame, dq0 frame. The transformation is

$$\begin{bmatrix} S_d \\ S_q \\ S_0 \end{bmatrix} = \frac{2}{3}\begin{bmatrix} \cos\theta & \cos(\theta-120^0) & \cos(\theta+120^0) \\ -\sin\theta & -\sin(\theta-120^0) & -\sin(\theta+120^0) \\ 0.5 & 0.5 & 0.5 \end{bmatrix}\begin{bmatrix} S_a \\ S_b \\ S_c \end{bmatrix},$$

Where θ is the position of rotational frame referenced to the stationary three phase frame. Usually, the transformation is decomposed into two transformations.

The Clarke Transformation,

$$\begin{bmatrix} S_\alpha \\ S_\beta \\ S_0 \end{bmatrix} = \frac{2}{3}\begin{bmatrix} 1 & \cos(-120^0) & \cos 120^0 \\ 0 & -\sin(-120^0) & -\sin 120^0 \\ 0.5 & 0.5 & 0.5 \end{bmatrix}\begin{bmatrix} S_a \\ S_b \\ S_c \end{bmatrix}$$

And Park Transformation,

$$S_d = S_\alpha \cos\theta + S_\beta \sin\theta$$

$$S_q = -S_\alpha \sin\theta + S_\beta \cos\theta$$

The difference between $\alpha\beta 0$ and dq0 is that α, β is stationary and dq is rotating and usually, α axis is aligned with the axis of phase A.

5.2 Control scheme development

Because the flux is produced by the PM, it is quite simple for the control of the machine. Rotor d axis current i_{dr} can be set to zero and q axis current i_{qr} is controlled for the torque. Setting d axis on the pole of PM rotor, then we have the following equations.

$$\phi_{dr} = \phi_f, \phi_{qr} = L_{qr} i_{qr}$$

$$u_{dr} = -\omega_{sl} L_{qr} i_{qr}$$

$$u_{qr} = i_{qr} R_r + L_{qr} \frac{di_{qr}}{dt} + \omega_{sl} \phi_f$$

$$T_r = \frac{3}{2} p \phi_f i_{qr}$$

where p is the number of pole pairs and ω_{sl} is the slip frequency.

Note that in the above equations, the mutual inductance between the stator winding and rotor winding is neglected, which is a reasonable assumption. From Chapter 3, it is calculated that the mutual inductance between the stator and the power rotor is only 0.174mH, while from the open circuit experiment, the magnetic flux linkage is 0.398weber and 0.94weber for stator and rotor winding respectively. At the stator rating current, 30A rms, the mutual flux linkage is only 0.005weber. According to the above equations, the control block diagram for a voltage regulated voltage fed inverter is shown in Figure 5.1.

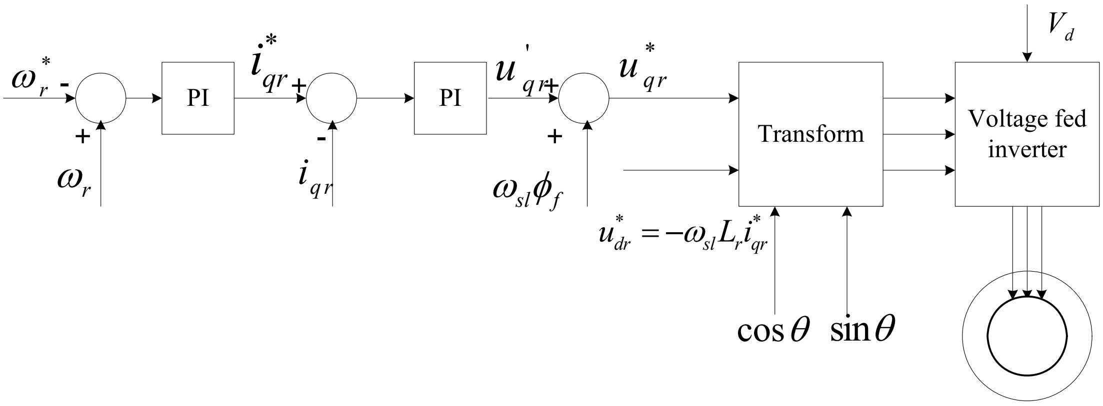

Figure 5.1 Control block diagram for a voltage regulated voltage fed converter

However, a current controlled scheme is much simpler and has a lower order as shown in Figure 5.2. This control scheme can be implemented using the back-to-back PWM voltage fed inverter with current regulation as is discussed in [10]. The following analysis is based on this model.

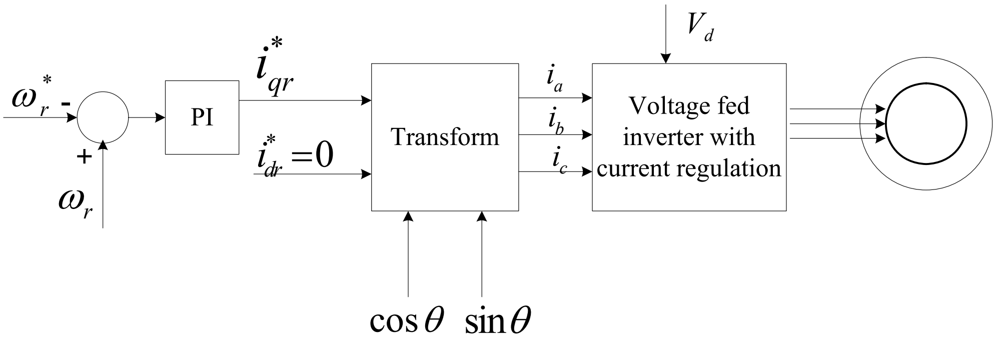

Figure 5.2 Control block diagram for a current regulated voltage fed converter

5.3 Control Stability Analysis

Before building the real drive for the machine, running simulation is very important which is to examine the stability of the control scheme and determine the control parameters such as the PI controller parameters.

This machine has two sets of rotors, a set of PM rotors and a set of power rotors. It can be split into two kinds of the machines. The interaction between PM rotor and the stator is a PM synchronous machine, while the interaction between the power rotor and PM rotor is a doubly-fed induction machine.

The control of the machine is performed by adjusting the current in the power rotor windings to produce the demanding torque. Because the PM rotor is an intermedia of the torque transmission between the power rotors and the stator winding, the stability of the PM rotor is very crucial to the dynamics of the machine.

5.3.1 PM rotor stability analysis without damping coil

Unlike the doubly fed induction machine, there is nearly no power rotor reactance due to the low mutual inductance. Isolating the PM rotor and stator from the power rotor, it is a PM synchronous machine and the torque between the power rotor and PM rotor can be seen as the external load. The following simulation of the stability of PM rotor does not consider the affection of the aluminum PM rotor plate, which is the equivalent damping coil.

Parameter Derivation

The PM rotor plate is made of aluminum with a diameter of 740mm. The aluminum plate has 20 pockets for the permanent magnets. The density of the Neodymium-Iron-Boron permanent magnetic material is 7.5×10^3kg/m^3 and the density of aluminum is 2.7×10^3kg/m^3. Therefore, the mass of the two magnetic rotors is

$$m_m = 2(\frac{\pi}{4} d_{Al}{}^2 t_m \rho_{Al} + 20\pi(r_o{}^2 - r_i^2) t_m \frac{12}{360}(\rho_m - \rho_{Al})) \approx 73kg \, .$$

The rotational inertial of the two magnetic rotors is

$$J_{PM} = 2(\frac{\pi}{4} d_{Al}{}^2 t_m \rho_{Al} \frac{d_{Al}{}^2}{8} + 20\pi(r_o{}^2 - r_i^2) t_m \frac{12}{360}(\rho_m - \rho_{Al}) \frac{r_o{}^2 + r_i^2}{2}) \approx 5.6kgm^2$$

Stator winding parameters used in the simulation is from Section 3.2. The unbalanced phases of the stator winding are not considered. Stator resistance is Rs = 0.14ohm. Stator winding self inductance is $L_s = 0.304mH$. The flux linkage of the stator winding is ϕ_{s0}= 0.398weber.

Simulation Formulation

The interaction of power rotor and PM rotor is simplified as an external torque T_L acting on PM rotor. The stator winding of the machine is “Y” connected and is connected to the power system with neutral isolated. The dynamic of the PM rotor can be described as the following equations:

$$v_a = \omega_{PM}\phi_{s0}\sin\theta + i_a R_s + 1.5L_s\frac{di_a}{dt} + v_n$$ **Equation 5.1**

$$v_b = \omega_{PM}\phi_{s0}\sin(\theta - 120^0) + i_b R_s + 1.5L_s\frac{di_b}{dt} + v_n$$ **Equation 5.2**

$$v_c = \omega_{PM}\phi_{s0}\sin(\theta + 120^0) + i_c R_s + 1.5L_s\frac{di_c}{dt} + v_n$$ **Equation 5.3**

Where $v_a = 155.56\sin\omega_e t$, $v_b = 155.56\sin(\omega_e t - 120^0)$, $v_c = 155.56\sin(\omega_e t + 120^0)$, ω_{PM} is the angular velocity of the PM rotor and $\theta = \int_0^t \omega_{PM}dt$ is the position of PM rotor; V_n is the neutral voltage of the stator winding. For the symmetric winding, $V_n = 0$.

Because the neutral is isolated, $i_a + i_b + i_c = 0$, by Clarke transformation,

$$i_\alpha = i_a, i_\beta = (2i_b + i_a)/\sqrt{3}$$

By Park transformation, aligning d axis with ϕ_{0s}

$$i_d = i_\alpha\cos\theta + i_\beta\sin\theta$$

$$i_q = -i_\alpha\sin\theta + i_\beta\cos\theta$$

The electromagnetic torque is

$$T_e = \frac{3}{2}pi_{qs}\phi_{0s}.$$ **Equation 5.4**

Where p is the number of pole pairs.

The dynamic equation of the PM rotor is

$$T_L + T_e = J_{PM}\frac{d\omega_{PM}}{dt}$$ **Equation 5.5**

Where T_L is the load, positive for generator mode, negative for motor mode.

The system described by these equations is a second order nonlinear system. Converting Equations 5.1, 5.2 and 5.3 into d-q axis (d axis is aligned with pole of PM rotor).

$$\frac{di_{ds}}{dt} = \frac{v_{ds}}{L_{ds}} - \frac{R_s}{L_{ds}}i_{ds} + \frac{L_{qs}}{L_{ds}}p\omega_{PM}i_{qs}$$ **Equation 5.6**

$$\frac{di_{qs}}{dt} = \frac{v_{qs}}{L_{qs}} - \frac{R_s}{L_{qs}} i_{qs} - \frac{L_{ds}}{L_{qs}} p\omega_{PM} i_{ds} - \frac{\phi_{s0} p\omega_{PM}}{L_{qs}}$$ **Equation 5.7**

Because this machine is nonsalient, $L_{ds} = L_{qs} = \frac{3}{2} L_s = 0.456mH$.

The simulation procedure is:

1. Transform Va, Vb, Vc into d-q coordinates using Clarke and Park transformation. Set the PM rotor initial position is $\theta_{initial} = 0$, which is aligned with phase A.
2. Solving the differential Equations 5.5, 5.6 and 5.7.
3. Output $i_a, i_b, i_c, i_d, i_q, \theta, \omega_{PM}$

The stator is assumed to be connected to a stiff system which has constant magnitude of voltage.

Simulation Result

The following simulation is run at the initial external torque of 10Nm with a torque increase of 10Nm at t = 0.

For the Rs = 0.14ohm, the PM rotor is not stable.

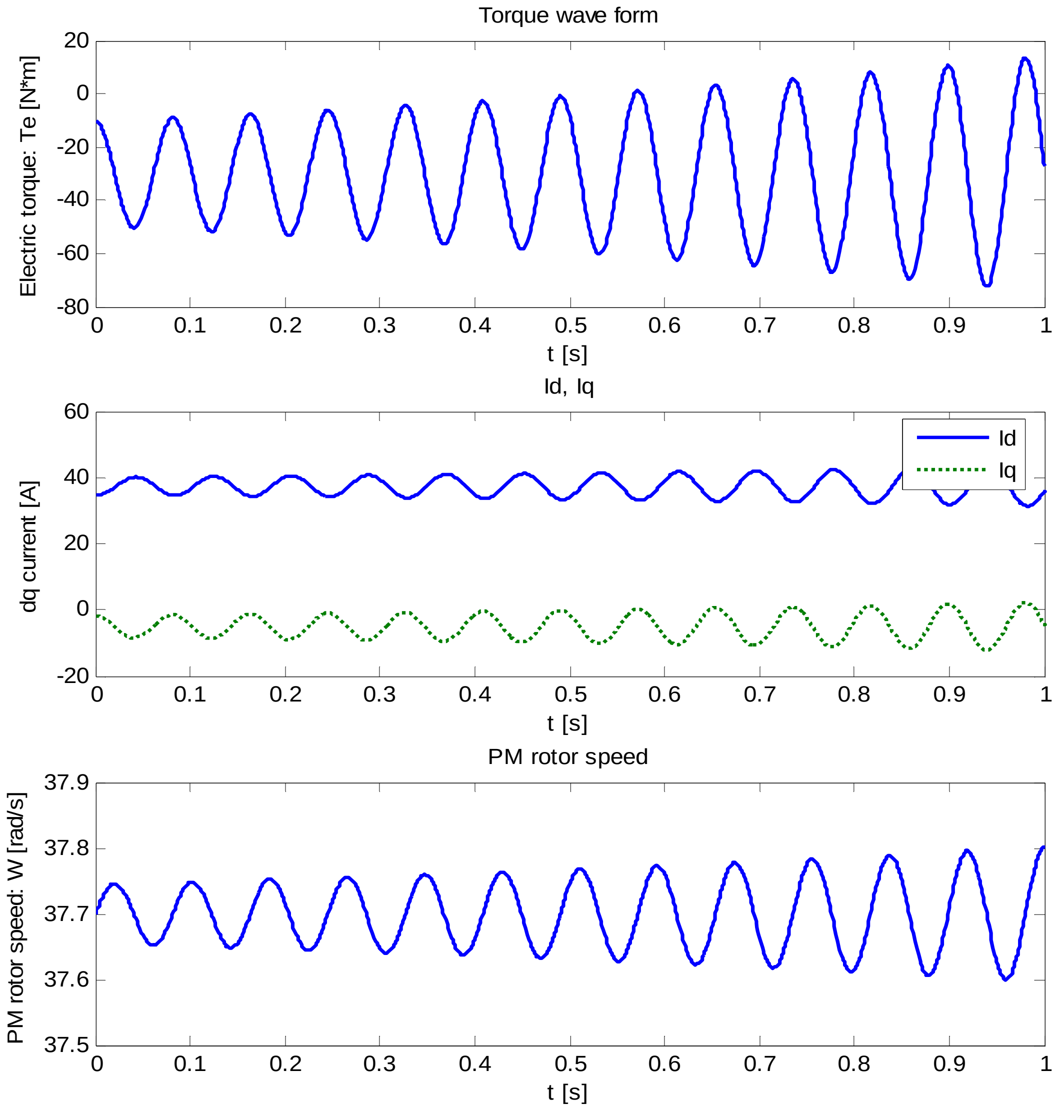

Figure 5.3 PM rotor dynamics for 0.14 ohm stator winding resistance

Increasing the stator resistance, the machine is stable. Figure 5.4 is the result when the resistance of the stator winding is 0.5ohm.

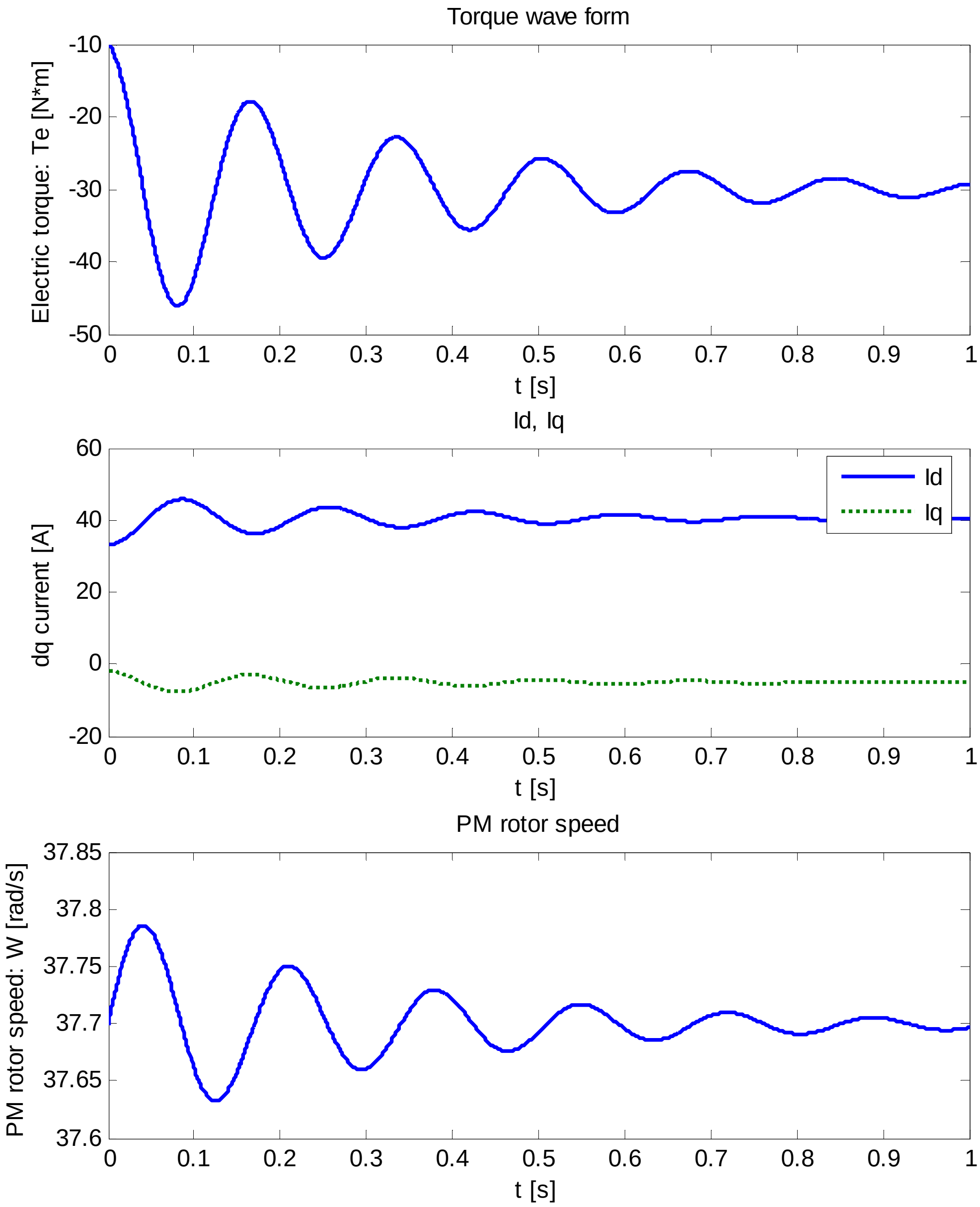

Figure 5.4 PM rotor dynamics for 0.5ohm stator winding resistance

Without the damping coil, it turns out that the resistance of the stator winding can help with the stability of the PM rotor. The larger is the resistance, the more stable the PM rotor. The resistance damps the vibration of the PM rotor. This is result is expected because without any control from the stator winding, a PM synchronous machine is prone to be unstable. However, it is undesirable to increase in the resistance of the stator winding which will lower the efficiency of the machine.

5.3.2 PM rotor stability analysis with damping coil

In this section, the effect of the PM rotor plate is considered, which is modeled as an additional damping coil. As shown in Section 3.5, the parameters of the equivalent damping coil has been estimated. The time constant is $\tau_k = \frac{L_k}{R_k} \approx 0.0188s$ and another parameter is $\frac{M_{sk}^2}{R_k} \approx 1.76\times10^{-6} H\bullet s$, where M_{sk} is the mutual inductance between the stator winding and damping coil.

Through Park transformation, the stator three phase windings are transformed into d and q axes coils with inductance of $L_d = L_q = 1.5L_s$. Because the d axis is aligned with one pole of the PM rotor, the d, q axes stator windings are stationary with the PM rotor. Corresponding to the stator d, q coils are the d, q damping coils in PM rotor plate, which can be modeled the same as in Section 3.5 with L_{s0} replaced by L_d, L_q which is 1.5 times L_{s0}. Therefore, the equations in Section 3.5 will become

$$1.5R = \frac{\omega^2 M_{dsk}^2 R_k}{R_k^2 + \omega^2 L_{dk}^2}$$

$$1.5L = 1.5L_{s0} - \frac{\omega^2 M_{dsk}^2 L_{dk}}{R_k^2 + \omega^2 L_{dk}^2}$$

The same equations apply to q axis coil. So the time constant for the d, q damping coil is

$$\tau_{dk} = \tau_{qk} = 0.0188s$$

Which is unchanged while the other parameter is 1.5 times the one derived in Section 3.5.

$$\frac{M_{qsk}^2}{R_k} = \frac{M_{dsk}^2}{R_k} = 1.5\times1.76\times10^{-6} = 2.64\times10^{-6} H\bullet s.$$

Incorporating the d axis and q axis damping coils, the state equations can be written as

$$L_{ds}\frac{di_{ds}}{dt} = v_{ds} - R_s i_{ds} + p\omega_{PM}(L_{qs}i_{qs} + M_{qsk}i_{qk}) - M_{dsk}\frac{di_{dk}}{dt}$$

$$L_{qs}\frac{di_{qs}}{dt}=v_{qs}-R_s i_{qs}-p\omega_{PM}(L_{ds}i_{ds}+M_{dsk}i_{dk})-\phi_{s0}p\omega_{PM}-M_{qsk}\frac{di_{qk}}{dt}$$

$$\frac{di_{dk}}{dt}=-\frac{R_k}{L_{dk}}i_{dk}-\frac{M_{dsk}}{L_{dk}}\frac{di_{ds}}{dt}$$

$$\frac{di_{qk}}{dt}=-\frac{R_k}{L_{qk}}i_{qk}-\frac{M_{qsk}}{L_{qk}}\frac{di_{qs}}{dt}$$

Note that there is not speed emf term in the damping coil state equations, because no current will be induced when stator d, q axes current are constant.

With dynamic equations,

$$T_{eS}=\frac{3}{2}p(i_{qs}(\phi_{0s}+M_{dsk}i_{dk})-i_{ds}M_{qsk}i_{qk})$$

$$T_L+T_{eS}=J_{PM}\frac{d\omega_{PM}}{dt}$$

Where T_{eS} is the electromagnetic torque between the PM rotor and the stator.

To solve the above ordinary differential equations, the mutual inductance M_{dsk}, M_{qsk} is not known but needn't to be known either. Instead, the d, q axes mutual flux linkage, $M_{dsk}i_{dk}$ and $M_{qsk}i_{qk}$, are treated as independent variables. With the same simulation condition in Section 5.3.1, that is the initial external torque is 10Nm, with a change of 10Nm at t = 0. The simulation result is shown in Figure 5.5.

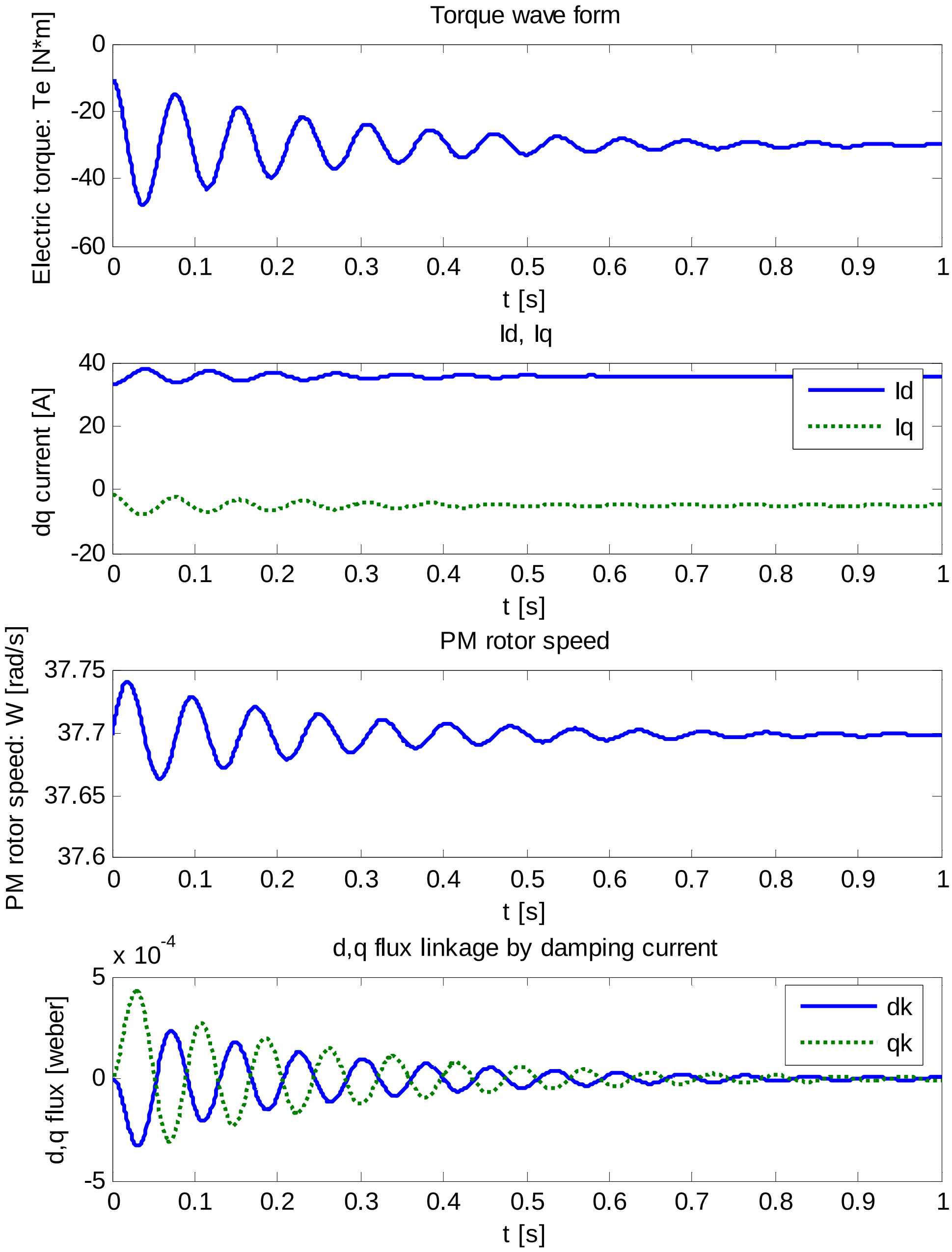

Figure 5.5 PM rotor dynamics with damping coil

It can be seen that considering the damping effect of the PM rotor plate, the PM rotor is damped compared with the result of Section 5.3.1. The PM aluminum plate is very effective in damping the vibration of PM rotor.

5.3.3 Power rotor stability analysis without damping coil

This section is to examine the stability of the control scheme developed above in Figure without the damping effect of PM rotor plate. Besides, the parameters of the voltage fed inverter are not included in the simulation either.

Parameters

The power rotor aluminum plate is of 1.75 inch thick with a diameter of 740mm. The mass of the rotor aluminum plate is

$$m_{Al} = V\rho = \frac{\pi}{4} d^2 t_{Al} \rho \approx 51.6kg$$

The rotational inertial of the aluminum plate is

$$J_{Al} = \frac{m_{Al} r_{Al}^{\ 2}}{2} = \frac{m_{Al} d_{Al}^{\ 2}}{8} \approx 3.5kgm^2 .$$

The steel core of power rotor is of 16.5mm thick with inner radius of 270mm and outer radius of 350mm. The material is M-19 lam steel with the density of 7700kg/m^3. So the mass of the steel core is

$$m_{core} = \pi(r_o^{\ 2} - r_i^2) t_{core} \rho \approx 19.8kg$$

The rotational inertial of the steel core is

$$J_{core} = \frac{1}{2} m_{core} (r_i^2 + r_o^{\ 2}) \approx 1.9kgm^2 .$$

The total length of one phase of the winding is about 198.6m. The #16 AWG wire is 0.0197kg/m. Therefore, the mass of the three phase winding is

$$m_w = 3l\rho_l \approx 11.7kg$$

The rotational inertial of the winding is

$$J_w = m_w (\frac{r_i + r_o}{2})^2 \approx 1.13kgm^2$$

The total rotational of the two power rotors is

$$J_r = 2(J_{Al} + J_{core} + J_w) = 13.1kgm^2$$

Power rotor flux linkage is $\phi_{r0} = 0.94 weber$ for each rotor. From the result of Section 3.3, the resistance of rotor winding is R_r = 2.6ohm. The contact resistance of the brushes and slip rings is not considered. The inductance of the active winding side is $L_{r0} = 3.57 mH$ and the end turn leakage inductance is $L_{rl} = 1.2 mH$.

Simulation Establishment

The control of power rotor is by current. In the reference frame of power rotor, the q axis rotor current i_{qr} is controlled while maintaining $i_{dr} = 0$. Both of the power rotor windings are “Y” connected and neutral isolated. They are parallel to each other. State equations for each rotor winding are

$$\frac{di_{dr}}{dt} = (u_{dr} + \omega_{sl} L_{qr} i_{qr} - R_r i_{dr}) / L_{dr}$$

$$\frac{di_{qr}}{dt} = (u_{qr} - i_{qr} R_r - \omega_{sl} \phi_{0r} - \omega_{sl} L_{dr} i_{dr}) / L_{qr}$$

$$T_{eR} = \frac{3}{2} p \phi_{0r} i_{qr} \times 2 \text{ (a pair of power rotors)}$$

Because the rotor is nonsalient, $L_{dr} = L_{qr} = \frac{3}{2} L_{r0} + L_{rl} \approx 6.56 mH$.

The dynamic equation for the pair of power rotors is

$$T_L - T_{eR} = J_r \frac{d\omega_r}{dt},$$

where T_{eR} is the electromagnetic torque on the power rotors by the PM rotors.

The dynamic equation for the PM rotor is

$$T_{eR} + T_{eS} = J_{PM} \frac{d\omega_{PM}}{dt},$$

where T_{eS} is the electromagnetic torque on the PM rotors by the stator winding.

Because $i_{dr} = 0$, the above equations can be simplified as:

$$u_{dr} + \omega_{sl} L_{qr} i_{qr} = 0$$

$$\frac{di_{qr}}{dt} = (u_{qr} - i_{qr}R_r - \omega_{sl}\phi_{0r}) / L_{qr}$$

In the simulation, it is assumed that the position of the PM rotor in the reference frame of power rotor is known to us. The estimation of PM rotor position is not concerned. Therefore, the PI control can be described as

$$i_{qr} = k_1(\omega_r - \omega_r^*) + k_2\int_0^t (\omega_r - \omega_r^*)dt$$

Where ω_r^* is the command angular velocity and ω_r is the feedback velocity.

Since the parameters of the converter is not known, the reaction of power rotor winding to the converter cannot be described. A rather simple way is just to assume that the reaction is instant, which means that the current of power rotor can be controlled instantly as wanted. Therefore, the rotor current is not governed by its state equations but by the PI controller, which is described by the following differential equations:

$$\frac{d\omega_r}{dt} = (T_L - T_{re}) / J_r = (T_L - 1.5p\phi_{0r}i_{qr}) / J_r$$

$$\frac{di_{qr}}{dt} = k_1\frac{d\omega_r}{dt} + k_2(\omega_r - \omega_r^*)$$

Combined with the differential equations of the stator described in Section 5.3.1, the simulation of the control of the machine can be performed. In this simulation, the damping coil is not considered either.

Simulation Result

In the load torque TL is kept at 40 Nm and the speed of power rotor is controlled from 37.32 rad/s to 34.32 rad/s. The PI parameters are: k1 = 3, k2 = 6.5.

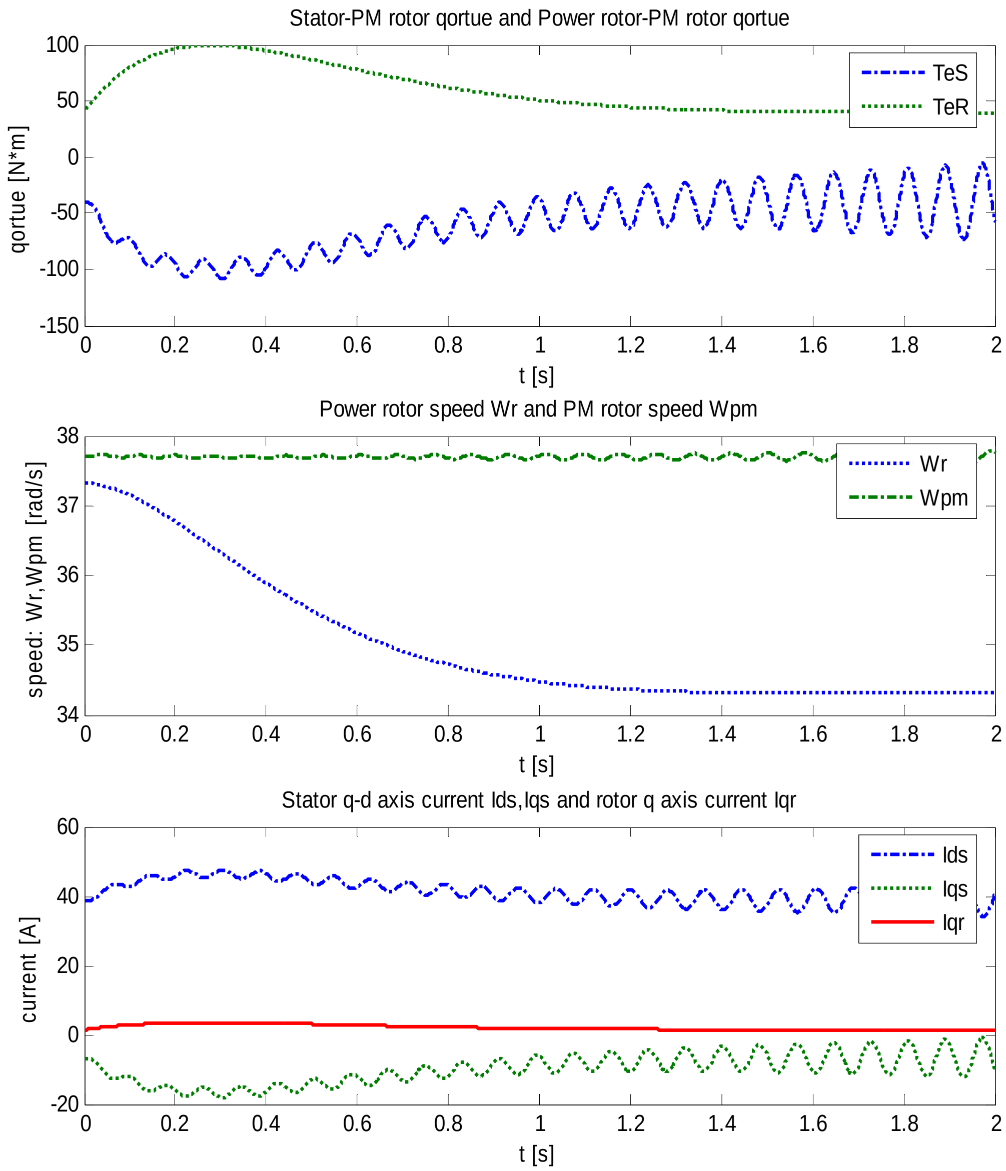

Figure 5.6 Power rotor and PM rotor dynamics using vector control (damping coil is not considered)

It can be seen that rotor tends to be stable while the PM rotor is vibrating. This phenomenon is due to the unrealistic assumption for the converter. However, through this simulation, the property of the PI controller is examined. The parameters of the PI controller determine the overshooting and response speed.

5.3.4 Power rotor stability analysis with damping coil

The section is similar to Section 5.3.2. The effect of PM rotor plate is taken into the simulation. As in the Section 5.3.2, the PM rotor plate is modeled as damping coils in d, q axes, with the parameters of $\tau_k = \frac{L_k}{R_k} \approx 0.0188s$ and $\frac{M_{rk}^2}{R_k} \approx 2.14\times10^{-5} H\bullet s$. Note that unlike the case in Section 5.3.2, the parameters are only for each of the power rotors. Transforming into d-q axes, then

$$\tau_{dk} = \tau_{qk} = 0.0188s$$

And

$$\frac{M_{qrk}^2}{R_k} = \frac{M_{drk}^2}{R_k} = 1.5\times2.14\times10^{-5} = 3.21\times10^{-5} H\bullet s$$

The rotor state equations are

$$L_{dr}\frac{di_{dr}}{dt} = u_{dr} - R_r i_{dr} + \omega_{sl}(L_{qr}i_{qr} + M_{qrk}i_{qk}) - M_{drk}\frac{di_{dk}}{dt}$$

$$L_{qr}\frac{di_{qr}}{dt} = u_{qr} - i_{qr}R_r - \omega_{sl}(\phi_{0r} + M_{drk}i_{dk}) - M_{qrk}\frac{di_{rk}}{dt}$$

As in Section 5.3.3, the back-to-back voltage fed current regulated converter is assumed to be ideal and the current is controlled instantly as commanded. So the i_{dr} is controlled to be zero and i_{qr} is controlled by PI controller

$$i_{qr} = k_1(\omega_r - \omega_r^*) + k_2\int_0^t(\omega_r - \omega_r^*)dt$$

So,

$$\frac{di_{qr}}{dt} = k_1\frac{d\omega_r}{dt} + k_2(\omega_r - \omega_r^*).$$

Setting $i_{dr} = 0$, the dynamic equations are

$$T_{eR} = \frac{3}{2}pi_{qr}(\phi_{r0} + M_{drk}i_{dk})\times 2 \text{ (a pair of power rotors)}$$

$$T_L - T_{eR} = J_r\frac{d\omega_r}{dt},$$

$$T_{eR}+T_{eS}=J_{PM}\frac{d\omega_{PM}}{dt},$$

$$T_{eS}=\frac{3}{2}p(i_{qs}(\phi_{0s}+M_{dsk}i_{dk})-i_{ds}M_{qsk}i_{qk})$$

Where T_{eR} is the electromagnetic torque between the power rotor and PM rotor. The positive torque is in the PM rotor rotating direction.

The state equations for the damping coil are

$$\frac{di_{dk}}{dt}=-\frac{R_k}{L_{dk}}i_{dk}-\frac{M_{dsk}}{2L_{dk}}\frac{di_{ds}}{dt}$$

$$\frac{di_{qk}}{dt}=-\frac{R_k}{L_{qk}}i_{qk}-\frac{M_{qsk}}{2L_{qk}}\frac{di_{qs}}{dt}-\frac{M_{qrk}}{L_{qk}}\frac{di_{qr}}{dt}$$

The factor of ½ in the equations is to convert the total mutual inductance M_{dsk},M_{qsk} into one of the PM rotors.

Combining with the stator equations

$$L_{ds}\frac{di_{ds}}{dt}=v_{ds}-R_s i_{ds}+p\omega_{PM}(L_{qs}i_{qs}+M_{qsk}i_{qk})-M_{dsk}\frac{di_{dk}}{dt}$$

$$L_{qs}\frac{di_{qs}}{dt}=v_{qs}-R_s i_{qs}-p\omega_{PM}(L_{ds}i_{ds}+M_{dsk}i_{dk})-\phi_{s0}p\omega_{PM}-M_{qsk}\frac{di_{qk}}{dt}$$

The simulation result is shown in Figure 5.7 with the same condition as in Section 5.3.3.

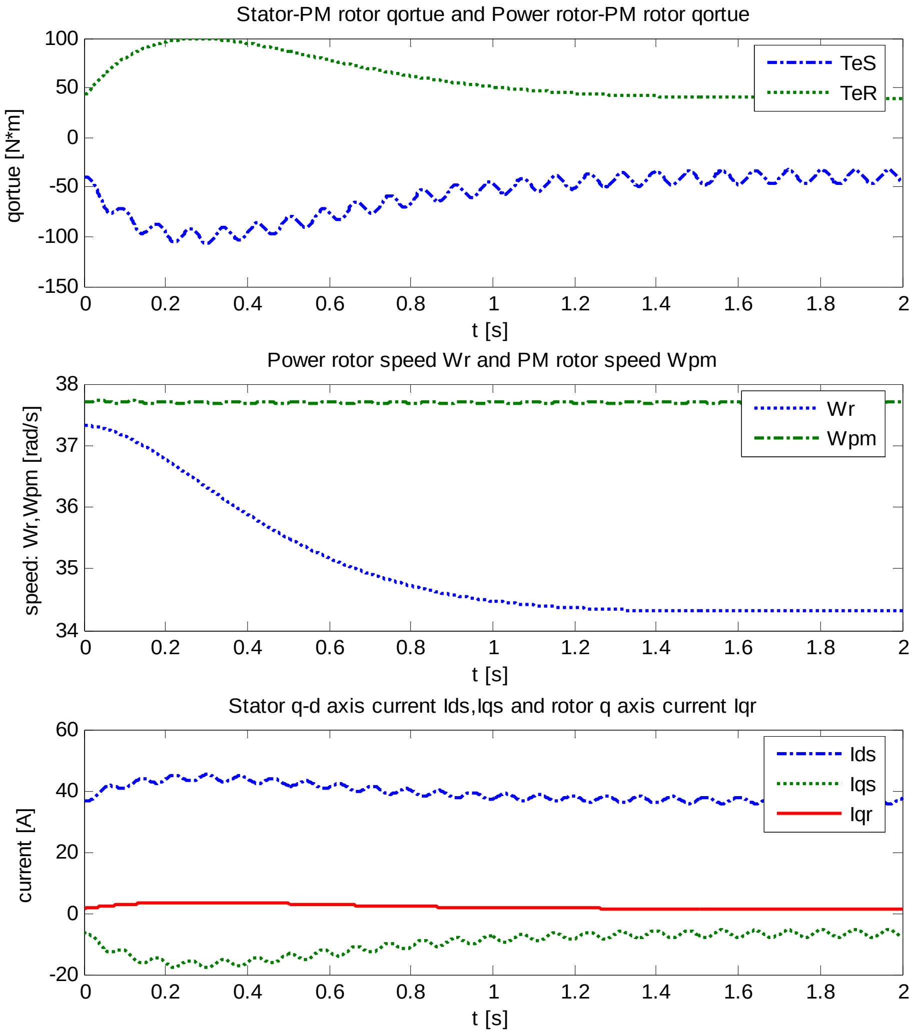

Figure 5.7 Power rotor and PM rotor dynamics using voltage control (damping coil is considered)

With the damping of PM rotor plate, the stability of the machine is improved compared with the result in Section 5.3.3. However, the ripples are still obvious and not decaying as fast as in Section 5.3.2. This is because the impact of the back-to-back voltage fed current regulated converter is ignored in the simulation. Instead, the control is assumed to be ideal so that the power rotor d, q axes current responds instantly to the command value, which is obvious not the case in reality. Therefore, this simulation only shows the response and performance of the PI controller. To examine the full performance of the control for the machine, the converter circuit parameters need to be incorporated into the power rotor state equations so that the transient response of the power rotor can be simulated with the PM rotor and stator winding.

5.4 Sensorless control

Vector control relies on the esitimation of the position of the dq0 frame referenced to the A,B,C frame. Traditionally, a speed sensor is imbedded in the machine but it will add the costs of the machine and also have reliability problems. Therefore, sensorless vector control is desirable.

In the vector control of our machine, the positions of both power rotor and PM rotor are needed. However, the mounting of position sensors for both rotors will be difficult and not economical. Therefore, for the control our machine, it is very necessary to develop a sensorless vector control.

Development of sensorless control

The main task of this section is to develop a method for the estimation of PM rotor position both in the stator frame, θ_{PM} , and in the power rotor frame, θ_{slip} . The rotor speed ω_r is also need to be estimated.

In the frame of the stator,

$$L_{ds}\frac{di_{\alpha s}}{dt}+\frac{d\phi_{0\alpha s}}{dt}+R_s i_{\alpha s}=v_{\alpha s}$$

$$L_{qs}\frac{di_{\beta s}}{dt}+\frac{d\phi_{0\beta s}}{dt}+R_s i_{\beta s}=v_{\beta s}$$

$$\phi_{0s\alpha}=\phi_{0s}\cos\theta_{PM}$$

$$\phi_{0s\beta}=\phi_{0s}\sin\theta_{PM}$$

Therefore,

$$\frac{d\phi_{0\alpha s}}{dt}=-p\omega_{PM}\phi_{0s}\sin\theta_{PM}=v_{\alpha s}-R_s i_{\alpha s}-L_{ds}\frac{di_{\alpha s}}{dt}$$

$$\frac{d\phi_{0\beta s}}{dt} = p\omega_{PM}\phi_{0s}\cos\theta_{PM} = v_{\beta s} - R_s i_{\beta s} - L_{qs}\frac{di_{\beta s}}{dt}$$

So

$$\tan\theta_{PM} = -\frac{v_{\alpha s} - R_s i_{\alpha s} - L_{ds}\frac{di_{\alpha s}}{dt}}{v_{\beta s} - R_s i_{\beta s} - L_{qs}\frac{di_{\beta s}}{dt}}$$

$$\omega_{PM} = \frac{1}{p}\frac{d\theta_{PM}}{dt}$$

Where $v_{\alpha s}, v_{\beta s}, i_{\alpha s}$ and $i_{\beta s}$ can be calculated through Clarke transformation.

The position of the PM rotor in the power rotor frame can be estimated by the same method as above.

$$\tan\theta_{slip} = -\frac{v_{\alpha r} - R_r i_{\alpha r} - L_{dr}\frac{di_{\alpha r}}{dt}}{v_{\beta r} - R_r i_{\beta r} - L_{qr}\frac{di_{\beta r}}{dt}}$$

$$\omega_{slip} = \frac{1}{p}\frac{d\theta_{slip}}{dt}$$

Therefore the power rotor speed is

$$\omega_r = \omega_{PM} - \omega_{slip}$$

Further discussion

The problem with this method of position estimation is that the PM rotor must be rotating in the reference frame. But in our machine, the PM rotor will always rotate around the synchronous speed. So the estimation of PM rotor position in the stator reference frame should not be a problem.

In the reference frame of power rotor, when the speed of power rotor is very close to the speed of PM rotor, the position of PM in this frame can not be estimated correctly by this method. Hopefully, the PI control loop in the power rotor can correct this error.

Chapter 6

6 Conclusion

The purpose of the thesis is to verify the design of the DFPM generator through experiments. The tasks constitute three parts: prototype machine construction, modeling and simulation, and experiment. All these tasks have been finished in the past a year. It is demonstrated that the model of the machine is successful. Section 6.1 summarizes the results from the simulation model and experiments for the prototype machine. Future work is suggested in Section 6.2. Finally, the status of the project is concluded in Section 6.3.

6.1 Overview of the prototype machine

The experiments and the simulation model reveal the prototype machine parameters. The results are summarized below.

Permanent Magnet

Experiment Result:	**Stator**	**Power rotor I**	**Power rotor II**
Average flux density (T)	0.421	0.370	0.408
Flux linkage (Weber)	0.398	0.866	0.941

Note: There are one or two permanent magnets which is weaker than the other ones.

Simulation Result:

Flux density (T)	**0.446**

Stator Winding

Simulation Result:	**Active winding**	**End turn winding**
Inductance (mH)	0.257	0.047
Total self-inductance (mH)	0.304	

Experimental DC resistance: 0.14ohm

Experimental 60Hz subtransient resistance: 0.18ohm

Phase difference (Degree)	α_{AB}	α_{BC}	α_{CA}
	124.6	124.8	110.6

Rotor Winding

Simulation Result:	**Active winding**	**End turn winding**
Inductance (mH)	3.57	1.202
Total self-inductance (mH)	3.60	

Experimental 60Hz subtransient resistance: 2.9ohm

Phase difference between rotor I and rotor II: 32.8 degrees.

Stator-Rotor Mutual inductance

Simulation Result: **0.175mH**

PM rotor equivalent damping coil

Stator winding-damping coil	
$\frac{M_{d,qsk}^{2}}{R_k}\ (H \bullet s)$	2.64×10^{-6}
Rotor winding-damping coil	
$\frac{M_{d,qrk}^{2}}{R_k}\ (H \bullet s)$	3.21×10^{-5}
Time constant (s)	0.0188

6.2 Future work

The control simulation in Section 5 is preliminary. It explores the basic stability problem of the machine but doesn't include the impact of the convert, which actually plays an important role in stabilizing the machine. Therefore, it is highly recommended that the parameters of the converter be incorporated into the simulation, which should be based on a detailed design of the converter. A drive system may be built for the prototype machine to demonstrate the control strategy. Besides the proposed microchip in [6], there are commercialized DSP systems designated for motor control such as *TMS320C2000* from *TI*. Moreover, Due to the significant contact resistance, the brushes and slip ring should be replaced with better ones.

The machine was originally designed for wind turbine. But due to the low mutual inductance between the stator and power rotor, the generator will have a poor voltage regulation capacity. However, it is possibly a good motor, a DFPM motor. It has the benefit of PM motor and also the doubly-fed motor. Only a slip fraction power needs to be handled through the power electronic devices so that the cost can be decreased dramatically. However, the control strategy for the DFPM motor should be tricky. At low speed, it can be control with DC current in the stator and the total power delivered through power rotor, which will very efficient. At high speed mode, it is desired that only a slip fraction power is through the power electronic devices of the power rotor while the other is delivered from stator directly from the power system. However, how to switch this low speed mode to high speed mode is challenging.

6.3 Summary

The thesis has demonstrated that the finite element model of the machine is very successful. It can be used for designing the DFPM machine in the future. The parameters of the prototype machine gained from both the experiment data and the finite element model provide us the insight into the performance of the machine. They form the basis for developing motor drive for the prototype in the future. We are hoping that the DFPM machine can provide a cost-effective, efficient solution to ship propulsion.

Appendix A

Structure drawings

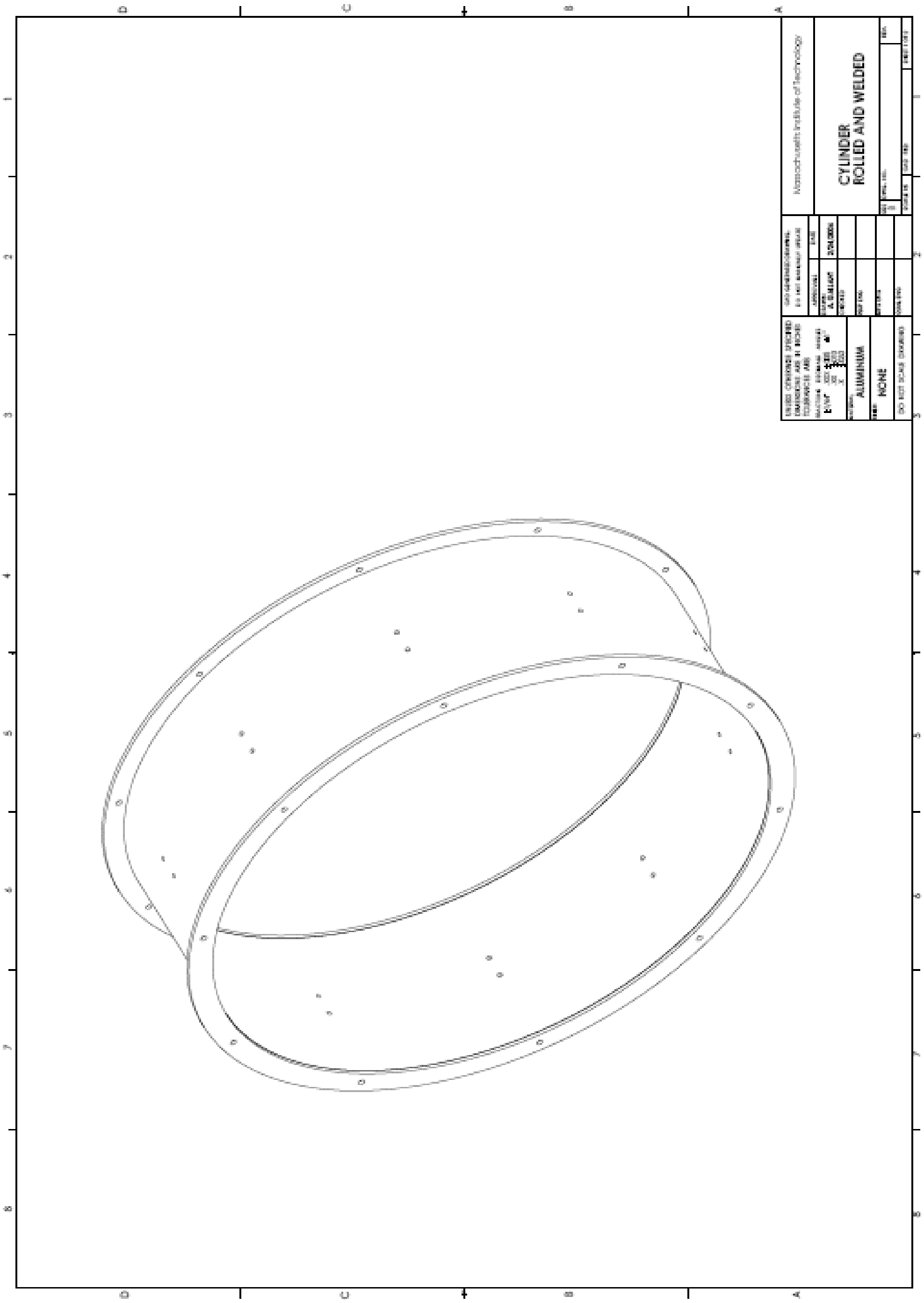

Figure A.0.1 Solid work impression of the new housing

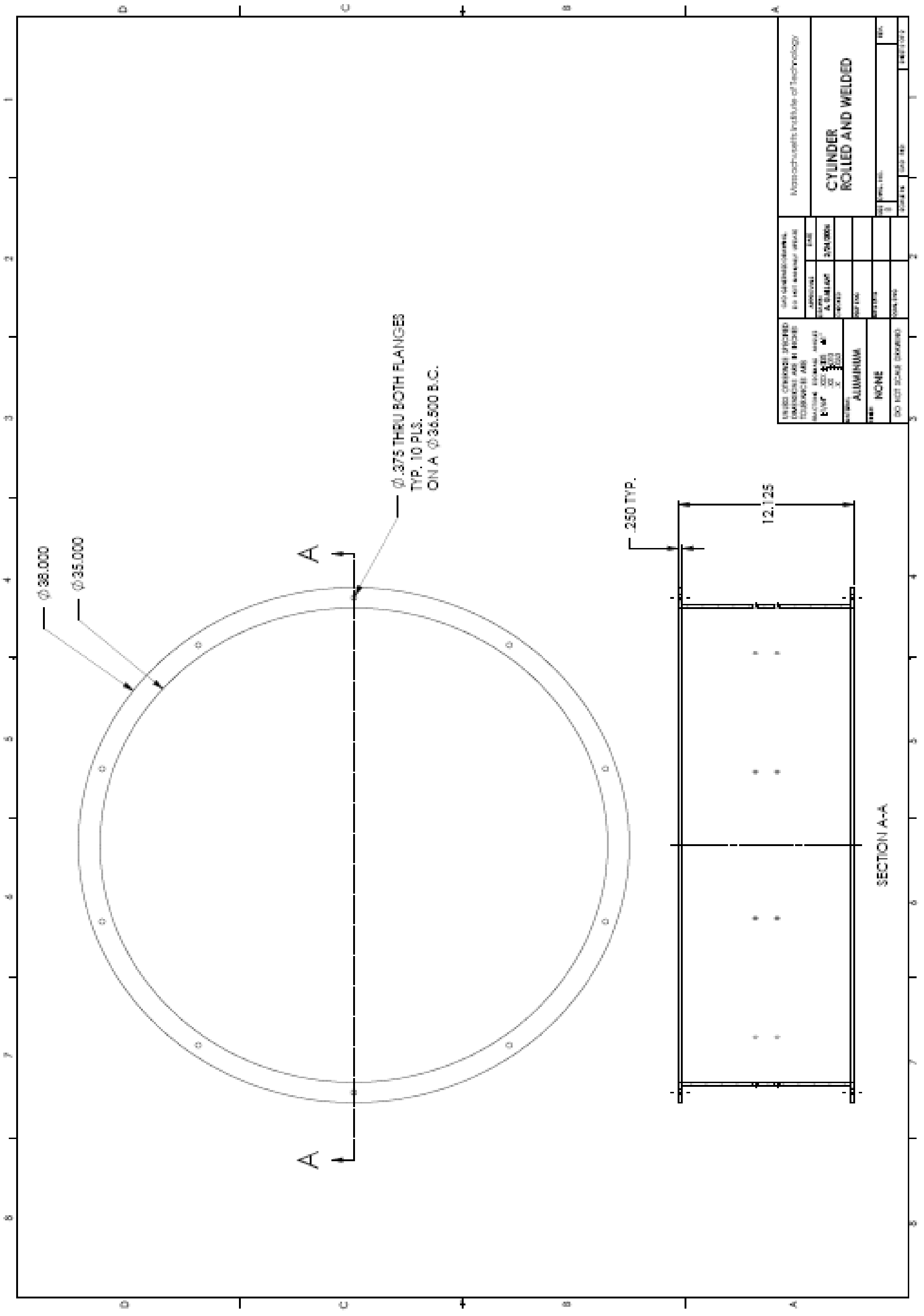

Figure A.0.2 New housing drawing

Appendix B

Matlab codes

v-curve optimization

main function

```
%%%% neutral isolated test
% % Optimization main function
close all
clear all
clc
%% initial value: result given by static test
wo=2*pi*60;
Rs=0.135;%%ohm
Ls=0.304;%%mH

Ra0=Rs;
La0=Ls;
Rb0=Rs;
Lb0=Ls;
Rc0=Rs;
Lc0=Ls;

Mab0=-.173;%mH
Mac0=-.107;
Mbc0=-.174;

A=load('V_I.txt');
Va0=A(:,1);Vb0=A(:,2);Vc0=A(:,3);%+0.5;
Ia0=A(:,4);Ib0=A(:,5);Ic0=A(:,6);

alpABE=124.6;alpBCE=124.8;alpCAE=110.6;
alpABV=123.72;alpBCV=123.38;alpCAV=112.9;
X0=[Ra0,La0,Rb0,Lb0,Rc0,Lc0,Mab0,Mac0,Mbc0,alpABE,alpCAE,300,alpABV,alpCAV];
LB=[.08,.2,.08,.2,.08,.2,-.25,-.25,-.25,124,109,0,119,111];
UB=[.3,.55,.3,.55,.3,.55,-.02,-.02,-.02,126,111,800,125.5,121];
options = optimset('TolFun',1e-8,'MaxFunEvals',5000,'TolX',1e-7);
[Xr,resnorm]=lsqnonlin(@opt_syntest,X0,LB,UB,options);

% % Xr10 nd Xr11 are in degrees.
alphaAB=Xr(10)/180*pi;
alphaCA=Xr(11)/180*pi;

Ea=107.0;
Eb=107.1*exp(-i*alphaAB);
Ec=107.0*exp(i*alphaCA);

Za=Xr(1)+Xr(2)*wo/1000*i;
Zb=Xr(3)+Xr(4)*wo/1000*i;
Zc=Xr(5)+Xr(6)*wo/1000*i;

ZAB=Xr(7)*wo/1000*i;
ZAC=Xr(8)*wo/1000*i;
ZBC=Xr(9)*wo/1000*i;

Ua=Va0';Ub=Vb0';Uc=Vc0';
for j=1:length(Ua)
    x=fzero(@(x) fun_synch_opt(x,Ua(j),Ub(j),Uc(j),Za,Zb,Zc,ZAB,ZBC,ZAC,...
        Ea,Eb,Ec,Xr(12),Xr(13),Xr(14)),0,optimset('TolX',1e-5));
    alpha(1,j)=x;
end
UA=Ua.*exp(i*alpha);
UB=Ub.*exp(i*(alpha-Xr(13)/180*pi));
```

```
UC=Uc.*exp(i*(alpha+Xr(14)/180*pi));

Ia=(-UC*Zb+UC*ZAB+Ec*Zb-Ec*ZAB+UA*Zb-Ea*Zb+ZBC*UB-ZBC*Eb-2*ZBC*UA+2*ZBC*Ea...
    -ZAB*UB+ZAB*Eb+ZAC*UB-ZAC*Eb-UB*Zc-ZAC*UC-ZBC*Ec+ZBC*UC+ZAC*Ec-
Ea*Zc+UA*Zc+Eb*Zc)...
    /(-2*ZAC*Zb+Zc*Zb-ZBC^2-ZAB^2-ZAC^2+2*ZBC*ZAC+2*ZAC*ZAB-2*Za*ZBC-
2*Zc*ZAB+2*ZBC*ZAB+Zc*Za+Za*Zb);

Ib=-(-Ec*Za+Za*Eb-Ea*Zc-Za*UB-Ea*ZAB-UB*Zc+Eb*Zc+UC*Za+ZAC*Ec+UA*Zc-
2*ZAC*Eb+ZBC*UC...
    -ZBC*UA-ZAC*UC+Ec*ZAB+UA*ZAB-ZBC*Ec-ZAC*UA+2*ZAC*UB-UC*ZAB+ZBC*Ea+ZAC*Ea)...
    /(-2*ZAC*Zb+Zc*Zb-ZBC^2-ZAB^2-ZAC^2+2*ZBC*ZAC+2*ZAC*ZAB-2*Za*ZBC-
2*Zc*ZAB+2*ZBC*ZAB+Zc*Za+Za*Zb);

Ic=(UC*Zb-2*UC*ZAB+UC*Za-Ec*Za+ZBC*UA-Ec*Zb+2*Ec*ZAB-Ea*ZAB-
UA*Zb+UA*ZAB+Ea*Zb+ZBC*Eb...
    -Za*UB+Za*Eb-ZBC*UB+ZAB*UB-ZAB*Eb+ZAC*Ea-ZBC*Ea-ZAC*Eb-ZAC*UA+ZAC*UB)...
    /(-2*ZAC*Zb+Zc*Zb-ZBC^2-ZAB^2-ZAC^2+2*ZBC*ZAC+2*ZAC*ZAB-2*Za*ZBC-
2*Zc*ZAB+2*ZBC*ZAB+Zc*Za+Za*Zb);

plot(Va0,Ia0,'* r',Vb0,Ib0,'o green',Vc0,Ic0,'+ blue')
legend('Ia','Ib','Ic')
hold
plot(Ua,abs(Ia),'r',Ub,abs(Ib),'green',Uc,abs(Ic),'b')
xlabel('Voltage / V')
ylabel('current / I')
title('Optimization result')
```

subfunction

```
function f=opt_syntest(X)
wo=2*pi*60;
A=load('V_I.txt');
Va0=A(:,1);Vb0=A(:,2);Vc0=A(:,3);%+0.5;
Ia0=A(:,4);Ib0=A(:,5);Ic0=A(:,6);

alphaAB=X(10)/180*pi;%%%convert to rad
alphaCA=X(11)/180*pi;

Ea=107;
Eb=107.1*exp(-i*alphaAB);
Ec=107.0*exp(i*alphaCA);

Za=X(1)+X(2)*wo/1000*i;
Zb=X(3)+X(4)*wo/1000*i;
Zc=X(5)+X(6)*wo/1000*i;

ZAB=X(7)*wo/1000*i;
ZAC=X(8)*wo/1000*i;
ZBC=X(9)*wo/1000*i;

Ua=Va0';Ub=Vb0';Uc=Vc0';

for j=1:length(Ua)
    x=fzero(@(x) fun_synch_opt(x,Ua(j),Ub(j),Uc(j),Za,Zb,Zc,ZAB,ZBC,ZAC,...
        Ea,Eb,Ec,X(12),X(13),X(14)),0,optimset('TolX',1e-5));
    alpha(1,j)=x;
end
UA=Ua.*exp(i*alpha);
UB=Ub.*exp(i*(alpha-X(13)/180*pi));
UC=Uc.*exp(i*(alpha+X(14)/180*pi));

Ia=(-UC*Zb+UC*ZAB+Ec*Zb-Ec*ZAB+UA*Zb-Ea*Zb+ZBC*UB-ZBC*Eb-2*ZBC*UA+2*ZBC*Ea...
    -ZAB*UB+ZAB*Eb+ZAC*UB-ZAC*Eb-UB*Zc-ZAC*UC-ZBC*Ec+ZBC*UC+ZAC*Ec-
Ea*Zc+UA*Zc+Eb*Zc)...
    /(-2*ZAC*Zb+Zc*Zb-ZBC^2-ZAB^2-ZAC^2+2*ZBC*ZAC+2*ZAC*ZAB-2*Za*ZBC-
2*Zc*ZAB+2*ZBC*ZAB+Zc*Za+Za*Zb);


Ib=-(-Ec*Za+Za*Eb-Ea*Zc-Za*UB-Ea*ZAB-UB*Zc+Eb*Zc+UC*Za+ZAC*Ec+UA*Zc-
2*ZAC*Eb+ZBC*UC...
```

```
    -ZBC*UA-ZAC*UC+Ec*ZAB+UA*ZAB-ZBC*Ec-ZAC*UA+2*ZAC*UB-UC*ZAB+ZBC*Ea+ZAC*Ea)...
    /(-2*ZAC*Zb+Zc*Zb-ZBC^2-ZAB^2-ZAC^2+2*ZBC*ZAC+2*ZAC*ZAB-2*Za*ZBC-
2*Zc*ZAB+2*ZBC*ZAB+Zc*Za+Za*Zb);

Ic=(UC*Zb-2*UC*ZAB+UC*Za-Ec*Za+ZBC*UA-Ec*Zb+2*Ec*ZAB-Ea*ZAB-
UA*Zb+UA*ZAB+Ea*Zb+ZBC*Eb...
    -Za*UB+Za*Eb-ZBC*UB+ZAB*UB-ZAB*Eb+ZAC*Ea-ZBC*Ea-ZAC*Eb-ZAC*UA+ZAC*UB)...
    /(-2*ZAC*Zb+Zc*Zb-ZBC^2-ZAB^2-ZAC^2+2*ZBC*ZAC+2*ZAC*ZAB-2*Za*ZBC-
2*Zc*ZAB+2*ZBC*ZAB+Zc*Za+Za*Zb);

f=[abs(Ia)-Ia0',abs(Ib)-Ib0',abs(Ic)-Ic0'];
```

Subfunction

```
function f=fun_synch_opt(x,Ua,Ub,Uc,Za,Zb,Zc,ZAB,ZBC,ZAC,Ea,Eb,Ec,P0,X13,X14)
UA=Ua*exp(i*x);
UB=Ub*exp(i*(x-X13/180*pi));
UC=Uc*exp(i*(x+X14/180*pi));

Ia=(-UC*Zb+UC*ZAB+Ec*Zb-Ec*ZAB+UA*Zb-Ea*Zb+ZBC*UB-ZBC*Eb-2*ZBC*UA+2*ZBC*Ea...
    -ZAB*UB+ZAB*Eb+ZAC*UB-ZAC*Eb-UB*Zc-ZAC*UC-ZBC*Ec+ZBC*UC+ZAC*Ec-
Ea*Zc+UA*Zc+Eb*Zc)...
    /(-2*ZAC*Zb+Zc*Zb-ZBC^2-ZAB^2-ZAC^2+2*ZBC*ZAC+2*ZAC*ZAB-2*Za*ZBC-
2*Zc*ZAB+2*ZBC*ZAB+Zc*Za+Za*Zb);

Ib=-(-Ec*Za+Za*Eb-Ea*Zc-Za*UB-Ea*ZAB-UB*Zc+Eb*Zc+UC*Za+ZAC*Ec+UA*Zc-
2*ZAC*Eb+ZBC*UC...
    -ZBC*UA-ZAC*UC+Ec*ZAB+UA*ZAB-ZBC*Ec-ZAC*UA+2*ZAC*UB-UC*ZAB+ZBC*Ea+ZAC*Ea)...
    /(-2*ZAC*Zb+Zc*Zb-ZBC^2-ZAB^2-ZAC^2+2*ZBC*ZAC+2*ZAC*ZAB-2*Za*ZBC-
2*Zc*ZAB+2*ZBC*ZAB+Zc*Za+Za*Zb);

Ic=(UC*Zb-2*UC*ZAB+UC*Za-Ec*Za+ZBC*UA-Ec*Zb+2*Ec*ZAB-Ea*ZAB-
UA*Zb+UA*ZAB+Ea*Zb+ZBC*Eb...
    -Za*UB+Za*Eb-ZBC*UB+ZAB*UB-ZAB*Eb+ZAC*Ea-ZBC*Ea-ZAC*Eb-ZAC*UA+ZAC*UB)...
    /(-2*ZAC*Zb+Zc*Zb-ZBC^2-ZAB^2-ZAC^2+2*ZBC*ZAC+2*ZAC*ZAB-2*Za*ZBC-
2*Zc*ZAB+2*ZBC*ZAB+Zc*Za+Za*Zb);

f=real(Ea*Ia'+Eb*Ib'+Ec*Ic')-P0;
```

Power rotor stability analysis with damping coil

Main function

```
%%% machine simulation %%%
%%== sign convention===
%% The positive rotation direction is the stator electric angular velocity.
%% The positive direction of torque is in the same direction
%% of the positive rotation direction.
%% The positive direction of power rotor electric angular velocity is the
%% same of the stator.

%% current Iqr control, Iqd=0 %%
clear all
close all
clc

%%%===rotor parameters=====
Ldr=6.56e-3;Lqr=Ldr;%H
Jr=13.1;%kgm^2 two power rotor
Rr=2.6;%ohm
lamdaR=0.94;%V/rad*s
%%-------------------------

%%%%===Stator parameters====
Lds=456e-6;Lqs=Lds;%H
Jpm=5.6;%kgm^2
Rs=0.14;%ohm
lamdaS=0.398;%V/rad*s
%%--------------------------
Vs0=155.56;%system voltage amplitude
```

```
p=10;%pole pairs
W0=2*pi*6;

%%%damping coil parameters===
tk=0.0188;
tms=1.5*1.76e-6;
tmr=3.21e-5;

%%==input value ===========
s=0.01;%rating slit
Wr0=(1-s)*W0;%power rotor initial mechanical speed
TL=40;%External torque magnitude
k1=3;k2=6.5;%PI controller parameter, k1+k2/s
dWr=-3;
dTL=0;
%%---------------------------

%%%% steady state calculation
Wpm0=2*pi*6;%PM rotor speed at steady state
[Ids0,Iqs0,thetaPM0,Iqr0]=fun_SteadyStat(Rs,Lds,Lqs,Jpm,...
    lamdaS,lamdaR,p,TL,Vs0,Wpm0)
TeS0=1.5*p*lamdaS*Iqs0
TeR0=1.5*p*lamdaR*Iqr0*2
%%initial status
Y0=[Ids0,Iqs0,Wpm0,thetaPM0,Wr0,Iqr0, 0, 0, 0, 0];
tspan=[0 2];

% % machine(t,y,Rs,Lds,Lqs,lamdaS,lamdaR,Jpm,Jr,p,TL,Wr0,Vs0,k1,k2,tk,tms,tmr)
% %
% y(1)=ids;y(2)=iqs;y(3)=Wpm;y(4)=thetaPM,y(5)=Wr,
% y(6)=Iqr,y(7)=Mdks,y(8)=Mqks,y(9)=Mdkr,y(10)=Mqkr
options = odeset('RelTol',1e-5);
[t,Y]=ode45(@machine,tspan,Y0,options,Rs,Lds,Lqs,...
    lamdaS,lamdaR,Jpm,Jr,p,TL+dTL,Wr0+dWr,Vs0,k1,k2,tk,tms,tmr);

%%== output values =========
Ids=Y(:,1);
Iqs=Y(:,2);
Wpm=Y(:,3);
thetaPM=Y(:,4);
Wr=Y(:,5);
Iqr=Y(:,6);
Mdks=Y(:,7);
Mqks=Y(:,8);
Mdkr=Y(:,9);
Mqkr=Y(:,10);
TeS=1.5*p*(Iqs.*(lamdaS+Mdks)-Ids.*Mqks);
TeR=1.5*p*Iqr.*(lamdaR+Mdkr)*2;
Wslit=Wpm-Wr;
% [ia,ib,ic]=InvParkTran(Ids,Iqs,thetaPM);

%%%%%%%%%%%%%%%%%%%%%%%%%%
figure(1)
subplot(3,1,1)
plot(t,TeS,'-.',t,TeR,':','LineWidth',2)
xlabel('t [s]'),ylabel('qortue [N*m]')
legend('TeS','TeR')
title('Stator-PM rotor qortue and Power rotor-PM rotor qortue')

subplot(3,1,2)
plot(t,Wr,':',t,Wpm,'-.','LineWidth',2)
xlabel('t [s]'),ylabel('speed: Wr,Wpm [rad/s]')
title('Power rotor speed Wr and PM rotor speed Wpm')
legend('Wr','Wpm')

subplot(3,1,3)
plot(t,Ids,'-.',t,Iqs,':',t,Iqr,'-','LineWidth',2)
xlabel('t [s]'),ylabel('current [A]')
legend('Ids','Iqs','Iqr')
title('Stator q-d axis current Ids,Iqs and rotor q axis current Iqr')
```

```
figure(2)
subplot(2,1,1)
plot(t,Mdks,'-',t,Mqks,':','LineWidth',2)
xlabel('t [s]'),ylabel('d,q flux [weber]')
legend('dks','qks')
title('Stator d,q damping flux linkage')

subplot(2,1,2)
plot(t,Mdkr,'-',t,Mqkr,':','LineWidth',2)
xlabel('t [s]'),ylabel('d,q flux [weber]')
legend('dkr','qkr')
title('rotor d,q damping flux linkage')
```

subfunction

```
function dy = machine(t,y,Rs,Lds,Lqs,lamdaS,lamdaR,Jpm,Jr,p,...
    TL,Wr0,Vs0,k1,k2,tk,tms,tmr)
dy = zeros(10,1);
%% y(1)=ids;y(2)=iqs;y(3)=Wpm;y(4)=thetaPM,y(5)=Wr,y(6)=Iqr
% % y(7)=Mdks,y(8)=Mqks,y(9)=Mdkr,y(10)=Mqkr
Va=Vs0*sin(2*pi*60*t);
Vb=Vs0*sin(2*pi*60*t-2*pi/3);
Vc=Vs0*sin(2*pi*60*t+2*pi/3);

[Vds,Vqs]=ParkTran(Va,Vb,Vc,y(4));

%% Power rotor
TeR=1.5*p*y(6)*(lamdaR+y(9))*2;%%two power rotors
dy(5)=(TL-TeR)/Jr;
dy(6)=k1*dy(5)+k2*(y(5)-Wr0);%%PI controller

%% y(1)=ids;y(2)=iqs;y(3)=Wpm;y(4)=thetaPM,y(5)=Wr,y(6)=Iqr
% % y(7)=Mdks,y(8)=Mqks,y(9)=Mdkr,y(10)=Mqkr
%% Stator and PM rotor
dy(1)=(Vds-Rs*y(1)+p*y(3)*(Lqs*y(2)+y(8))+y(7)/tk)/(Lds-tms/tk/2);
dy(2)=(Vqs-Rs*y(2)-p*y(3)*(Lds*y(1)+y(7)+lamdaS)+y(8)/tk...
    +sqrt(tms*tmr/tk^2)*dy(6))/(Lqs-tms/tk/2);
TeS=1.5*p*(y(2)*(lamdaS+y(7))-y(1)*y(8));
dy(3)=(TeR+TeS)/Jpm;
dy(4)=y(3)*p;

%%%% damping coil
dy(7)=-y(7)/tk-tms/tk/2*dy(1);
dy(8)=-y(8)/tk-tms/tk/2*dy(2)-sqrt(tms*tmr/tk^2)*dy(6);
dy(9)=-y(9)/tk-sqrt(tms*tmr/tk^2)/2*dy(1);
dy(10)=-y(10)/tk-sqrt(tms*tmr/tk^2)/2*dy(2)-tmr/tk*dy(6);
```

subfunction

```
%%% stator and PM rotor simulation %%%
%%%% steady state calculation
function [Ids0,Iqs0,thetaPM,Iqr0]=fun_SteadyStat(Rs,Lds,Lqs,Jpm,...
    lamdaS,lamdaR,p,TL,Vs0,Wpm0);

Iqr0=TL/1.5/p/lamdaR/2;
thetaPM=fzero(@(thetaPM) zerofun_SteadyStat(thetaPM,Rs,Lds,Lqs,p,...
    lamdaS,Wpm0,TL,Vs0),-2,optimset('TolX',1e-5));

Va=Vs0*sin(2*pi*60*0);
Vb=Vs0*sin(2*pi*60*0-2*pi/3);
Vc=Vs0*sin(2*pi*60*0+2*pi/3);

[Vds,Vqs]=ParkTran(Va,Vb,Vc,thetaPM);
Is0=[Rs -Lqs*p*Wpm0;Lds*p*Wpm0 Rs]\[Vds;Vqs-lamdaS*p*Wpm0];
Ids0=Is0(1);Iqs0=Is0(2);
```

subfunction

```
function f=zerofun_SteadyStat(x,Rs,Lds,Lqs,p,lamdaS,Wpm0,TL,Vs0)
Va=Vs0*sin(2*pi*60*0);
```

```
Vb=Vs0*sin(2*pi*60*0-2*pi/3);
Vc=Vs0*sin(2*pi*60*0+2*pi/3);

[vd,vq]=ParkTran(Va,Vb,Vc,x);
Is=[Rs -Lqs*p*Wpm0;Lds*p*Wpm0 Rs]\[vd;(vq-lamdaS*p*Wpm0)];
Ids=Is(1);Iqs=Is(2);
f=1.5*p*lamdaS*Iqs+TL;
```

subfunction

```
function [d q]=ParkTran(A,B,C,x)
a=5.5/180*pi*0;
b=10.3/180*pi*0;
d=2/3*(cos(x).*A+cos(x-2*pi/3-a).*B+cos(x+2*pi/3-b).*C);
q=2/3*(-sin(x).*A-sin(x-2*pi/3-a).*B-sin(x+2*pi/3-b).*C);
```

subfunction

```
function [A,B,C]=InvParkTran(d,q,x)
a=5.5/180*pi*0;
b=10.3/180*pi*0;
A=cos(x).*d-sin(x).*q;
B=cos(x-2*pi/3-a).*d-sin(x-2*pi/3-a).*q;
C=cos(x+2*pi/3-b).*d-sin(x+2*pi/3-b).*q;
```

Biblyography

[1] Kirk G. Pierce, Paul G. Migliore. *Maximizing Energy Capture of Fixed-Pitch Variable-Speed Wind Turbines.* National Renewable Energy Laboratory, NREL/CP-500-27551, July 2000.

[2] L.H. Hnsen, L. Helle, F. Blaabjerg, E. Ritchie, S. Munk-Nielsen, H. Bindner, P. Srensen and B. BakJensen. *Conceptual survey of generators and power electronics for wind turbines.* ISBN 87-550-27438. Ris National Laboratory, Roskilde, Denmark, Tech. Rep., 2001

[3] S. Muller, M. Deicke, R.W. De Doncker. *Doubly fed induction generator systems for wind turbines*. In *IEEE Industry Applications Magazine*, volume 8, issue 3, 2002.

[4] E. Spooner, B.J. Chalmers. *'TORUS': A slotless, toroidal-stator, permanent-magnet generator.* In *IEE Proceedings B,* Vol. 139, No. 6, Nov. 1992.

[5] A.J. Thomas. *A doubly-fed permanent magnet generator for wind turbines.* Master's thesis, Massachusetts Institute of Technology, June 2004.

[6] S.K. Reddy. *Operational behavior of a doubly-fed, permanent magnet generator for wind turbines.* Master's thesis Massachusetts Institute of Technology, June 2005.

[7] J.L. Kirtley Jr., *Dual rotor, constant frequency, variable speed generator,* Final Report to the National Renewable Energy Laboratory, Subcontract XCX-2-32227-06, MIT Laboratory for Electromagnetic and Electronic Systems, June, 24 2005.

[8] A.E. Fitzgerald, Charles Kingsley, Jr., Stephen D. Umans. *Electric Machinery*. McGraw-Hill, 2003.

[9] M.S. Vicatos, J.A. Tegopoulos. *Steady State Analysis of a Doubly-fed Induction Generator under Synchronous Operation*. IEEE Transactions on Energy Conversion, Vol. 4, No. 3, September 1989.

[10] R. Pena, J.C. Clare, G.M. Asher. *Doubly fed induction generator using back-to-back PWM converters and its application to variable speed wind-energy generation,* IEE Proc. Electr. Power Appl., Vol. 143, No. 3, May 1996

[11] Bimal K. Bose, *Modern Power Electronics and AC drives.* Prentice Hall, 2002